1st Conference on Sustainable Process Systems Engineering (SPSE-2021) and 1st Pakistan Congress on Membranes and Membrane Processes (PCOM-2021)

21st October 2021

Conference Proceedings

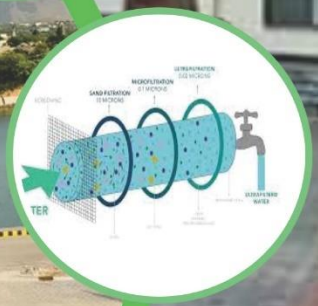

Organized by:
Department of Chemical and Energy Engineering &
Pakistan Membrane Society (PMS)

Pak-Austria Fachhochschule: Institute of Applied Sciences and Technology (PAF-IAST), Haripur

Design by:
AZ Printing Services
0345-9404148/0302-9339184

Preface

The 1st Conference on Sustainable Process Systems Engineering (SPSE-2021) and 1st Pakistan Congress on Membranes and Membrane Processes (PCOM-2021) were held on 21st October 2021 at Pak-Austria Fachhochschule: Institute of Applied Sciences and Technology (PAF-IAST), Haripur. The conference was organized by the Dept. of Chemical & Energy Engineering, PAF-IAST in collaboration with Pakistan Membrane Society (PMS) and Pakistan Scientific and Technological Information Center (PASTIC). A large number of faculty members, research students and professionals from various institutes participated in the conference. Prof. Sandra Kentish from University of Melbourne, Australia presented an inspiring plenary lecture on emerging membrane processes for applications in bio-gas separation and dairy industry. There were four technical sessions in the conference, where participants shared and discussed their research works. An idea workshop was also organized in one of the conference sessions. The objective of workshop was to provide an opportunity to create research proposals and networking among participants.

In his address to participants, Prof. Dr. Mohammad Mujahid (Rector, PAF-IAST) emphasized the need of interdisciplinary and applied research. He informed the participants that PAF-IAST is developing a technology park and several research centers in collaboration with Chinese and Austrian universities. These centers will be opened for collaborative research works that have potential of developing commercial products. Participants were also addressed by Dr. Fazal Ahmad Khalid (Rector, GIKI), Prof. Dr. Muhammad Akram Shaikh (DG, PASTIC) and Prof. Dr. Mohammad Younas (President PMS).

Putting SPSE and PCOM 2021 together was a team effort by members of Executive Council of Pakistan Membrane Society, PASTIC focal persons, faculty members of Department of Chemical and Energy Engineering and the administrative staff of PAF-IAST. I would like to thank everyone involved in organizing and making this conference successful.

Dr. Amir Muhammad
Conference Secretary
Email: amir.muhammad@fcm3.paf-iast.edu.pk

Acknowledgement

We are thankful to all the participants who provided contents of these conference proceedings in the form of abstract and full-length papers. We are also grateful to plenary speaker and the session mentors. These valuable talks and suggestions can and will guide us to a better understanding of sustainable processes and membrane technology.

We would like to thank the host organization, PAF-IAST, Haripur and collaborators PMS, PASTIC and Rizvi and Co. (Pvt) Ltd. Without their support it would not be possible to hold this conference.

We are grateful to all organizers, who worked hard in order to make this conference successful.

Organizing Committee

Patron-in-Chief:
Prof. Dr. Mohammad Mujahid
(Rector, PAF-IAST)

Conference Chair:
Prof. Dr. Arshad Hussain
(Dean, Faculty of Mechanical, Chemical, Materials and Mining Engineering, PAF-IAST)

Conference Co- Chair:
Prof. Dr. Mohammad Younas
(President PMS)

Conference Secretaries:
Dr. Amir Muhammad
Dr. Asim Laeeq Khan

Members Organizing Committee

Ms. Ghazala Ali Khan

Dr. Rizwan Ahmad

Dr. Fida Hussain

Dr. Muhammad Muqeet

Dr. Imran Ullah Khan

Dr. Sadia Mehmood

Dr. Abdul Mateen

Dr. Asif Khan

Dr. Zahid Ullah

Dr. Ayaz Muhammad Haneef

Dr. Fazal Wahab

Engr. Muhammad Imad

Engr. Maryam Khalid

Mr. Mubashir Saeed

Editorial Board

Organizers Profile

1. Pak-Austria Fachhochschule: Institute of Applied Sciences & Technology (PAF-IAST):

PAF-IAST is a collaborative venture with selected Austrian and Chinese Universities. PAF-IAST is unique in its concept, approach, and methodology. The institute concept stems from the slogan "Skilling Pakistan" and envisages creating highly credible technical education infrastructure both at tertiary and hi-tech industry levels. With this twin-aim concept, the project is a quantum leap forward in the fast burgeoning knowledge-based economy, far beyond a mere educational program.

We aim to raise the standards of technical education in Pakistan at par with those of most advanced industrial economies, notwithstanding the problems confronting developing nations in trying to achieve standards in advanced countries: standards that are constantly on the rise at a pace much faster than the economic capacity of a developing country. At the same time, we are fully conscious of and alive to the need of linking employment with education by harnessing high-quality manpower produced by such projects to induce, not only an inward flow of technology investment into Pakistan but also enable the generation of local hi-tech industry. The technology park integrated into the scheme of Pak-Austria Fachhochschule is a cardinal feature of this holistic concept.

Fulfilment of this novel concept, however, will remain an elusive dream without creating a critical mass of high-quality engineers and a hi-tech industry base. The whole spectrum of hi-tech industrial base in the country, therefore, needs to grow fast to develop an industrial infrastructure capable of supporting the progress of a diverse array of growing industrial companies. From this perspective, this unprecedented initiative in Pakistan supported by several universities based in Austria and China for awarding degrees to our students assumes enormous importance of its kind. The institute is comprised of academic departments and research centers covering the areas of process engineering, design, and media technologies, applied computer sciences, medical technologies, energy, and environmental engineering, electrical engineering, civil engineering, transportation engineering, mineral resource engineering, extraction metallurgy, and agriculture and forestry.

PAF-IAST boasts the latest teaching and practical laboratories equipped at par with partner universities. Effective plans are in hand to keep pace, through a process of monitoring by their accreditation bodies, with the highest standards of the curricula, teaching resources, and the learning outcomes adopted by the foreign partners. On completion of the initial establishment phase, the quality and output will be gauged, and programs accredited, using internationally-recognized criteria.

Visit www.paf-iast.edu.pk for more information.

2. Pakistan Membrane Society (PMS):

Pakistan Membrane Society (PMS) aims to be the nexus of membrane science and technology activities in Pakistan. PMS vision is to promote collaborative engagements across the community to disseminate membrane technology to end users. PMS provides an open forum for transferring and sharing technologies as well as capabilities within the members, industries and high education organizations. PMS is the representation body to promote the activities in membrane science and technology both in the research and industrial sectors.

PMS was founded in 2014 as an outcome of a national seminar on membrane technology organized by the Membrane Group of COMSATS University Islamabad, Lahore Campus. The society has since grown very fast with a number of membrane groups becoming its part. In the past few years, a number of successful international events have been organized by PMS that include International Conference on Separation Processes (2017), Sustainability in Process Industries (2016/2018) and GCRF Workshop on Membrane Technology (2019). PMS welcomes the researchers, students, industrial professionals and entrepreneurs involved in the membrane research and development to become members of society.

Website: www.pakmembrane.com/
Email: pakmembrane@gmail.com

3. Pakistan Scientific and Technological Information Centre (PASTIC):

Information plays a fundamental role for Scientific, Technological and Economic development of a country. Realizing the importance of potential role that Scientific Information plays, government of Pakistan with the assistance of UNESCO established (1957) Pakistan National Scientific and Technical Documentation Centre (PANSDOC) under the Pakistan Council of Scientific & Industrial Research (PCSIR), Karachi to cater to the Scientific Community needs such as Procurement of Documents, Compilation of Bibliographies, Abstracting, Indexing and Technical Translations. An expanded project namely Pakistan Scientific and Technological Information Centre (PASTIC) was launched (1974) around the nucleus of PANSDOC and was transferred from PCSIR to Pakistan Science Foundation (PSF), Islamabad. Presently, PASTIC is functioning as subsidiary of PSF, an autonomous organization under Ministry of Science & Technology. PASTIC is the premier organization in the field of S&T Information and is serving thousands of researchers and other professionals through its specialised information services. Scopes and facilities of PASTIC were expanded after transferring to PSF. PASTIC National Centre (Headquarter) is located in the premises of Quaid-i- Azam University Campus, Islamabad whereas its six Sub-Centers are located at Karachi, Lahore, Fasilabad, Peshawar, Muzaffarabad and Quetta. PASTIC is currently offering wide ranging services such as supply of full-text S&T Documents, publication of primary (Pakistan Journal of Computer and Information System-PJCIS) and Secondary Journals (Pakistan Science Abstracts in Ten(10) Disciplines), Patent Information Service, Bibliographic Information Service, development of indigenous S&T databases, compilation of Union Catalogues and Directories, National Science Reference Library, Printing Services (Reprographic) ranging from Mimeographing, Photocopying and Microfilming to printing. PASTIC is dedicated to fulfil the ever-growing needs of information community in the field of Science, Engineering and Technology for research and development activities at national level.

Website: www.pastic.gov.pk
Office Address:
PASTIC National Centre,
QAU Campus, Islamabad.
051-9248103-04
Email: psc-peshawar@pastic.gov.pk

Table of Contents

Abstracts

Treatment of Pharmaceutical wastewater through green synthesized nanocomposites

Waqar-Un-Nisa[1,*], Maria Ashfaq[1] , Talat Ara[2]
[1]*Center for Interdisciplinary Research in Basic Sciences, International Islamic University Islamabad 46000*
[2]*Department of Environmental Sciences, International Islamic University Islamabad 46000*
**Corresponding author*
Email: *waqarunnisa@iiu.edu.pk*

ABSTRACT

Contamination of water due to release of antibiotics which are non-biodegradable in nature from pharmaceuticals is the emerging problem. Antibiotics in wastewater are of particular concern and pose a serious threat to humans and environment. This study aims to synthesize Ni nanoparticles from grapefruit for the removal of antibiotics from pharmaceutical wastewater. Ni NPs were synthesized by making orange peel powder. Characterization of synthesized nanoparticles were done through XRD, SEM and FTIR. Green synthesized nanoparticles were used as adsorbent for removal of antibiotics. The crystallinity of NPs was determined through XRD, sharp peaks for Nickel suggest the presence of crystalline nature, Surface morphology of NPs were determined through SEM and it shows rough surface with discrete patterns. Functional group presence in NPs were determined through FTIR and it shows the presence of -COOH, -COH, -OH groups. NPs at contact time 30 minutes at 35°C more efficiently remove antibiotics from pharmaceutical wastewater. Removal of antibiotics from pharmaceutical waste water by using nanoparticles synthesized from green waste. Eco Friendly approach for pharmaceutical wastewater remediation.

Keywords: Pharmaceutical wastewater, Green Nanoparticles, Adsorption, Antibiotics.

Synthesis of Mixed Matrix Polymeric Membrane using a novel filler for enhanced CO_2 Separation

Alisha Tariq[1*], Sikander Rafiq[1] , Ali Raza Afzal[1]
[1]*Department of Chemical, Polymer and Composite Material Engineering, University of Engineering and Technology, Lahore, New Campus, Pakistan.*
Email: *alishatariq000@gmail.com*

ABSTRACT

Membrane technology have more advantages over other techniques like low cost and higher efficiency. The proposed research based upon the synthesis of membrane by the incorporating organic fillers in polysulfone to synthesis mixed matrix membranes . The presence of amino groups and carboxyl groups in the fillers of synthesized membrane matrixes has greater affinity for the CO2 and thus possess higher performance in-terms of permeability and selectivity. Hence, the Mixed Matrix Membrane (MMM's) will increase the selectivity and permeability of CO2 which is the inherent trade off in membranes and will overcome Robeson's upper bound limit 2008 and the membrane will help to increase the calorific value of the natural gas by the separation of CO2 as well as it plays its role to save environment from the Green House Gas Emissions.

The membranes are characterized by scanning electron microscope (SEM), Fourier transform infrared Spectroscopy (FTIR), and it has also been tested by XRD (X-Ray Diffraction). The overall strength of the MMMs was found to be improved with filler loadings.

Keywords:
Scanning electron microscope (SEM), Fourier transform infrared Spectroscopy (FTIR), X-Ray Diffraction (XRD).

Preparation of novel Zn (II)-imidazole based mixed matrix membrane for the removal of heavy metals from drinking water by forward osmosis

Aneeza Naz[a], NoamanUl–Haq[b], AsimLaeeqKhan[b], Muhammad WaqasIshaq[c], ZahidAli[a,d],

[a]*Department of Chemistry, University of Lahore, Defense road, Lahore,*
[b]*Department of Chemical Engineering, COMSATS University Islamabad – Lahore Campus, Pakistan,*
[c]*Department of Chemical Physics, University of Science and Technology of China, Hefei, Anhui 230026, China.*
[d]*State key laboratory of Organic-Inorganic Composites (Beijing University of Chemical Technology) Ministry of Education, Beijing 100029, China.*

**Corresponding author*
Email: pchem01201014@student.uol.edu.pk

ABSTRACT

The presence of heavy metals in drinking water is a major problem especially for developing countries. These heavy metals cause serious diseases like cancer and even lead to death. Recently, Interfacial polymerization was used for the fabrication of thin film nanocomposite forward osmosis membrane by using microfiltration support. For this purpose Zn-based MOF was incorporated into polymeric membrane as nanofillers and the membrane was modified for the removal of heavy metals as well as for the rejection of salt. Different characterization techniques like SEM, EDS and X-ray diffraction analysis was used for the evaluation of morphology, composition and crystallinity of the prepared FO membrane. It was observed that synthesized Zn-MOF based FO membrane exhibit high water flux by increasing the porosity of the membrane. In addition to this, this particular FO membrane was tailored for lower reverse salt flux and concentration polarization which ensures minimum withdrawal of salt from the draw solution to the feed solution. So, the prepared Zn-MOF based FO membrane produce synergistic results for the removal of heavy metals and this strategy can be used as novel option for future FO application.

Keywords: Zn-based MOF, heavy metals removal, Interfacial polymerization, thin film composite membrane,

In Situ Incorporation of Zwitterionic Metal-Organic Framework in Thin Film Membranes for Enhanced Water Permeability and Antifouling Property

Anfal Sajid[1*], Asim Laeeq Khan[1], Noaman Ul –Haq[2]

[a]*Department of Chemistry, University of Lahore, Defense road, Lahore,*
[b]*Department of Chemical Engineering, COMSATS University Islamabad – Lahore Campus, Pakistan,*
[c] *Department of Chemical Physics, University of Science and Technology of China, Hefei, Anhui 230026, China.*

[d]*State key laboratory of Organic-Inorganic Composites (Beijing University of Chemical Technology) Ministry of Education, Beijing 100029, China.*
Email: anfalsajid05@gmail.com

Abstract

In the field of water reuse and desalination, modulation of the polyamide structure is vital for reverse osmosis performance of thin-film composite (TFC) membranes. The interfacial polymerization approach was used to create zwitterionic nanoparticles of Zr-based Metal organic framework-66 (PZ@UIO-66) and introduce them into the polyamide active layer. Due to the modified diffusion rate of m-phenylenediamine (MPD) from the aqueous phase into the organic phase during the interfacial polymerization process, a hydrophilic, zwitterionic ring structure was generated on the surface of polyamide thin-film nanocomposite (TFN) membranes. Surface

characterization demonstrated that the ring structure increased the amounts of water transport channels on the membrane surface and the intrinsic pores of PZ@UIO-66 maintained the salt rejection. The bacterial-"defending" and bacterial-"attacking" behavior of hydrophilic zwitterionic groups from PZ@UIO-66 significantly improved the antifouling and bactericidal activities of TFN membranes. This research could pave the way for zwitterion polymer with MOFs to be used to improve the bio/organic fouling resistance of TFN membranes with high water permeability and salt rejection.

Keywords: UIO-66, DMAPS, mixed matrix membrane, water desalination, antifouling, Zwitterionic UIO-66

Flexible Electroactive Membranes explore Separator-Free High-performance Batteries

Aqsa Yasmin*, Muhammad A. Shehzad, ChunHua Chen, Liang Wu, and Tongwen Xu

*DADA Laboratories for Water, Energy, and Environment Technologies, Punjab Small Industrial Estate Kasur, Punjab Pakistan

Email: ayasmin@mail.ustc.edu.cn

Abstract: The concept of flexible recharge energy storage batteries is broadened to prepare advanced separator-free flexible batteries. Generally, the conventional batteries consist of an electrode, a separator, and a cathode as three basic parts (as shown in Fig). Contact resistance among the three parts is unavoidable and largely lowers the charge transfer rate in such conventionally assembled batteries. In this context, an effectual alternate battery design is proposed, which has negligible contact resistance between anode and separator due to the replacement of the conventional independent separator with "anode-cum-separator", a unified design. In the proposed anode-cum-separator or ACS design, brominated polyphenylene oxides (BPPO) is systematically phase-separated into membranes in such a way as to prepare an asymmetric membrane morphology containing a non-conductive porous surface supported by an electroactive porous anode. The use of ACS structural electrode design was employed in coin cells, which showed significantly lower charge transfer resistance (~64.5 Ω cm^2, 3.7× less) than the resistance of conventionally assembled cells (~236.4 Ω cm^2), containing the same electroactive material but the use of independent separator. Consequently, the ACS-NTP exhibits comparatively high discharge capacities such as 123 mA h/g at 0.2C and 89 mA h/g at 30C compared with the NTP with conventional cell design (discharge capacities of 116 mA h/g at 0.2C and 70 mA h/g at 30C). This is the first report on the anode-cum-separator design, which after further improvements, can be envisioned as a potential strategy to prepare ultra-lightweight, flexible, and high-performance batteries.

Perhaps Monomer Seeding is the Requisite to Grow Biomimetic Nanostructures?

Muhammad A. Shehzad*, Aqsa Yasmin, Asif A. Qaiser, Michael D. Guiver, Liang Wu, and Tongwen Xu

*Advanced Materials & Membrane Technology Centre Department of Polymer & Process Engineering, University of Engineering and Technology Lahore-54890, Punjab Pakistan

aamirshehzad@uet.edu.pk

Abstract: The effectual permselective transport of ions is a critical issue in membrane-integrated separation processes for seawater desalination, chlorine-alkali production, and the treatment of high salinity effluents due to the tradeoff between ions permeability and their selectivity. However, we found that careful membrane engineering, particularly biomimetic structuring, can help to circumvent the issues of the conventional ion-exchange membrane. In biological systems, conical-shaped pores enable selective unidirectional ion permeation across lipid bilayers and thus serve as a biomimetic model for the highly selective separation of cations using synthetic membranes. Here, we propose a radically novel and simple "monomer seeding" approach to grow electro-ionically conductive nanostructures (in general) such as conical-shaped nanopores (in particular) at the surface of acid-functionalized membranes. Such readily scalable biomimetic nanocone membranes enable ultra-fast cation permeation (Na^+ = 8.4× vs. Mg^{2+} = 1.4×) due to negligible surface resistances and simultaneously boost ion charge selectivity (Na^+/Mg^{2+} = 6×) owing to the positively charged conical walls, compared with state-of-the-art permselective membrane (CSO, Selemion™, Japan).

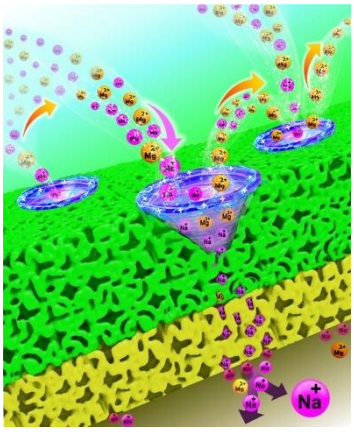

An Energy Nexus Study on Stress Analysis of Buried Fuel Pipelines under Railway Tracks to find Safe Depth

Hamza Sajid[1*], Gul Haider[2]

[1]*Mechanical Engineering, University of Engineering and Technology Peshawar, Peshawar 29000, University Town*

[21]*Mechanical Engineering, University of Engineering and Technology Peshawar, Peshawar 29000, University Town*

**Corresponding author*

Email: hamza913114@gmail.com

ABSTRACT

Every year, the world's energy demands rise, but the finite natural resources used to fuel industrial society deplete. These natural resources are in short supply and scarce. While they do arise naturally, replenishment can take hundreds of thousands of years. As a result, it is critical that we make the best use of all available resources and avoid their wastage. Pipelines are one of the primary means of transporting these resources, primarily fuels, from the point of supply to the point of consumption. Pipelines offer a less expensive, safer, and faster means to transfer energy throughout the country. Fuel transportation is critical to the country's economy. Fuel pipes are often buried underground at a greater depth to protect them from damage and keep them away from humans.

This research paper provides a study to determine a safe depth for underground pipes beneath railway tracks. A variety of stresses and loads, including static, dynamic, fatigue, and internal stresses, were investigated and assessed on pipelines at various depths. Proper experiments under the railway track were conducted through an Arduino based load cell system at varying depths and were compared with analytical calculations based on different techniques such as Spangler's, Direct Earth Load Method, Timoshenko's, Bousinessq's, Westergaard's and PCA, etc. Results showed that pipelines experience static loading due to soil weight when there is no traffic on the track as static load depends on soil density, stone concentration and compaction of soil. Both static and dynamic load act on the pipe when train passes. Static loading is responsible for Creep failure and Dynamic loading is responsible for Fatigue failure of the buried pipeline.

The primary objective of this research and effort was to analyze the buried pipeline for load distribution due to static and dynamic loads and then suggest the safe depth for the buried pipeline to avoid failure. It was concluded that for low pressure pipelines 4 ft. was the critical length as it results in a Fatigue Factor of Safety greater than 2 while 7 ft. was concluded as the safest depth as below this point the dead load surpasses the live load.

Assessing Potential of Warm Mix Asphalt Technology Adoption in Pakistan

Hamza Shehzad[1,*],Muhammad Waseem[2] ,Abdullah[3] , Junaid Shafiq[4]

Civil Engineering, University of Engineering and Technology Peshawar Jalozai Campus, Mardan 23200, Pakistan.

Civil Engineering Department, University of Engineering and Technology Peshawar Jalozai Campus, Charsadda 24420, Pakistan.

Civil Engineering, University of Engineering and Technology Peshawar Jalozai Campus, Charsadda 23200, Pakistan.

**Hamza Shehzad*

Email: *hsmkhan460@gmail.com*

ABSTRACT

The traditional Hot Mix Asphalt (HMA) technology is to blame for a significant amount of greenhouse gases and other hazardous compounds being released into the environment. As a result, many studies on global warming attempt to introduce new innovative technologies that are produced at lower temperatures than conventional HMA. Warm Mix Asphalt (WMA) Technology is one of these new technologies, which is produced at a temperature 20-40°C lower than HMA. This new technology uses a variety of techniques to reduce production temperatures, therefore, to reduce the environmental impact of conventional HMA. These techniques are divided into three categories: organic additives, chemical additives, and foaming techniques (water-based and water-containing foaming). This study used a natural zeolite (clinoptilolite) as a foaming technology (water-containing foaming) to reduce the viscosity of the bitumen, which improves workability and creates a better coating ability for bitumen and aggregates.

This study compares the feasibility of using WMA containing natural zeolite to that of HMA. The bitumen samples were made from 60/70 penetration grade bitumen with varying amounts of natural zeolite ranging from 3 to 7 percent by weight of bitumen. Using traditional bitumen test methods, the fundamental physical properties of bitumen samples with varying zeolite content were determined. Marshall specimens were cast for HMA after physical properties were assessed, and the optimum binder content was calculated and was 4.53 percent. Using this optimum binder content, specimens were cast for bituminous concrete modified with zeolite at various contents ranging from 3 to 7 percent. Marshall tests were conducted to determine the stability and flow values.

Based on the findings of this study, the ductility and penetration values of bitumen decreases while the softening

point value increases as zeolite content increases. When zeolite was introduced to the bituminous mix and the stability values were computed, the stability values improved with an increase in zeolite content. For a zeolite content of 7%, the stability value increased by 20.53 percent. As a result, when compared to HMA mixes, the overall performance of WMA mixes is superior.

Keywords: Warm-mix asphalt, Natural zeolite, Foaming technology, Marshall test,Stability value

PVA/Zeolite Mixed Matrix Membranes for Pervaporation: Effect of Polyaniline Deposition on Permeation Performance

Muhammad Hassan Haqnawaz, Asif Ali Qaiser, Nida Abid

Department of Polymer and Process Engineering, University of Engineering and Technology, Lahore 54890 Pakistan

Key words: Polyaniline, Poly vinyl alcohol, Mixed Matrix Membranes, Pervaporation.

ABSTRACT

Electroactive polyaniline (PANI) has been used as a surface layer on polyvinyl alcohol (PVA)/ZSM-5 (Zeolite Socony Mobil-5) membranes to affect pervaporation performance. PVA/ZSM-5 membranes were synthesized by solution casting method whereas PANI was deposited on the surface using in situ polymerization technique by varying time. The performance of these membranes was tested on lab scale pervaporation unit for the ethanol-water mixture at different feed temperatures. These PANI modified MMMs were characterized by using various characterization techniques such as Fourier transform infrared spectroscopy (FTIR), thermogravimetric analysis (TGA), and optical microscopy (OM) and swelling index. FTIR showed the crosslinking of PVA and polymerization dependent deposition extent of PANI on base membranes surface. TGA thermograms indicated multistep degradation mechanism involving PANI that improved thermal stability of base membranes. Optical microscopy indicated that prolonged aniline polymerization deposited a compact PANI layer at the surface, progressively.

In pervaporation of water-ethanol mixture, PANI affected both permeation flux and separation factor through its film hindrance, modifying surface hydrophilicity and electrostatic interactions. PANI deposition also influenced thermal activation energy of these composite membranes that were computed using Arrhenius Law. This study showed effects of PANI layering on PVA mixed matrix membranes on structural and pervaporation performance in a systematic manner to improve readers understating of such membranes systems.

Mxene Nano Composite Nanofiltration Membrane or Water Desalination

Hikmatullah[1*], Mansoor Ul Hasan Shah[1], Waheed Ur Rehman[2], Mohammad Younas[1*]

[1] Department of Chemical Engineering, University of Engineering and Technology, Peshawar, 25120, Pakistan

[2] PCSIR laboratories, Peshawar, 25120, Pakistan

Email: * *hikmatullah.che@uetpeshawar.edu.pk*, m.younas@uetpeshawar.edu.pk

ABSTRACT

MXene is a new type of highly hydrophilic and negatively charged two-dimensional (2D) nanosheets material, especially its supernatant has good dispersibility and stability. The MXene supernatant containing several layers was treated as aqueous solvent for interfacial polymerization, consequently the prepared MXene nanocomposite membrane could maintain high permeselectivity even under low pressures required for low carbon. MXene nanocomposite membrane had better hydrophilicity and higher negative charge. Na_2SO_4 rejection and the pure

water flux was improved as compared with the pristine membrane. The MXene nanocomposite membrane also showed the better antifouling property and good stability [1].

Hydrophilic and negative MXene supernatant had better dispersibility and stability. Substituting MXene supernatants of different concentrations for deionized water in aqueous phase, MXene nanocomposite membranes are generally prepared by interfacial polymerization. It was observed that few-layers Ti_3C_2Tx acted a crucial role in membrane surface modification, so that it improved the hydrophilicity and negative charge of membranes surface and increased surface roughness. Few-layers MXene nanosheets with excellent hydrophilicity, negative charge and mechanical properties provided an academic basis for the preparation of low-carbon and durable NF membranes with outstanding performance.

Keywords: MXene, Nano filtration (NF) membranes, Nano composite membrane.

Mathematical Modeling and Analysis of Harmonic Filter to Reduce Total Harmonic Distortion due to Nonlinear Load

Hina Zaheer[1,*], Mamoon Javed[2], Tahir Mehmood[3], M. Tanveer Riaz[4], Maria Tariq[5], Misha Urooj Khan[6]

[1*,3,5,6]*University of Engineering and Technology, Taxila, Pakistan*

[2]*School of Electronics Engineering, Chang'an University, China*

[4]*University of Engineering and Technology, Lahore (FSD-Campus), Pakistan*

**Hina Zaheer*

Email: *electricalengineer1019@gmail.com*

ABSTRACT

With the advancement in technology, power electronics has become a vital part of the power sector. Almost every electrical device is based on power electronics due to its tremendous advantages but, these devices offer some major power quality issues. Among these power quality issues, harmonics are the most crucial ones caused mainly due to the nonlinear load. and need urgent mitigation. This research is being conducted for mitigation of harmonics, that mainly comprises of mathematical modeling and analysis of harmonic filters to reduce total harmonic distortion. In other words, it is an application of mathematics in the field of electrical engineering. In which, a filter will be designed based on a synchronous reference frame (SRF-Theory), harmonic analysis will be conducted with the help of Fourier and Fast Fourier transform which will reduce total harmonic distortion up to 3.81% in accordance with the standard harmonic limits provided by IEEE-519. Finally, the proposed research will establish the highly improved total harmonic distortion and will significantly improve the power quality.

Keywords: Harmonics, Active Filter, FFT, SRF- theory, THD, Power Quality, IEEE Standard, Fourier Analysis.

Next Generation Mixed Matrix Membranes for the dehydration of bio-alcohols

Hira Naveed*, Asim Laeeq Khan

[1]*Chemical Engineering Department, COMSATS University, Lahore, Pakistan*

**Hira Naveed*

Email: *hiranaveed931@gmail.com*

ABSTRACT

Pervaporation is an advanced technique which is used for liquid mixture separation. Metal-organic framework (MOF) based mixed matrix membrane (MMMs) are one of the most advanced materials used for bio-alcohols dehydration using pervaporation. In this study ZIF-67 will be used as the inorganic filler material to fabricate MMMs. In order to make the filler solution processable it will be used as a porous liquid. These types of

membranes are expected to provide good selectivity and permeability due to better polymer-filler interface. Polydimethylsiloxane (PDMS) will be used as polymer matrix for MMMs

Keywords: Porous Liquids, Pervaporation, Mixed Matrix Membranes

Synthesis of low-cost Si-O2/PVC composite ultrafiltration membrane and its antifouling performance

Mamoona Alam,* Humna Azim

Department of Chemistry, Shaheed benazir Bhutto Women University of Peshawar, Main Campus, Landay Sarak, Charsadda road, Larama, District Peshawar.

**Corresponding author*

Email: oxacine@gmail.com

ABSTRACT

By the separation or phase inversion method the different low cost SiO_2/PVC membrane with different concentration by weight ratio of SiO_2 particles was prepared. The most desirable SiO_2 dosage was determined based on the casting solution composition and mechanical properties. The SiO_2/PVC membranes have various application in the municipal water waste treatment for their low price and good antifouling performance.

Keywords: SiO_2/PVC membranes

Synthesis of Carbon Nanofiber for the Application of Water Purification

Tariq Jamil[1,*], Gul Jamil Shah[1] , Muhsina Jamil[1], Qamar Wali[3]

[1]Materials Research Laboratory, Department of Physics, University of Peshawar, Peshawar 25120, Pakistan

[2]School of Applied Sciences & Humanities, National University of Technology, 44000, Islamabad, Pakistan.

**Corresponding author*

Email: *tjamilshah@gmail.com*

ABSTRACT

A novel approach to synthesis carbon nanofibers for the application of water purification is presented in this study. For this purpose, the commercially available polyvinyl alcohol (PVA) and tetraethyl orthosilicate (TEOS) were mixed with green tea solution under different concentrations. The composite and carbonized nanofibers samples were prepared via electrospinning technique. The structural properties of the composite and carbonized nanofibers were studied via X-ray diffraction (XRD). X-ray spectroscopy showed that the overall structure of nanofibers are amorphous but little crystallinity peaks arose after the heat treatment of nanofibers. The effect of heat and different concentrations of PVA and TEOS on the morphology of nanofibers were studied through Scanning electron microscope (SEM). SEM showed the nanofibers diameter ~500 nm, which decrease almost 50% after carbonization. The behavior of nanofibers chemically revealed through Fourier transform infrared spectroscopy (FTIR). For water purification test synthesized the carbon nanofibers filter under the same condition. The prepared filter morphology and elemental behavior studied through SEM and Energy dispersive x-ray (EDX), respectively before and after the filtration of water. Carbon nanofibers filter successfully performed the purification of water.

Keywords: Carbon Nanofibers; Polyvinyl alcohol; Electrospinning; Electrospun nanofibers.

Cellulose Blended Membranes for High-Salinity Water Pervaporation Desalination

Jawad Fareed[1], Muhammad Zafar[2], Mohsin Saleem[3], Rizwan Ahmed Malik[4], Muddassir Ali[5,*]

[1]*Department of Mechanical Engineering, University of Engineering and Technology, Taxila 47080, 7-km N-125 National Highway*

[2]*Institute of Energy and Environmental, University of the Punjab, Lahore 54590, Canal Bank*

[3]*School of Chemical and Materials Engineering, National University of Sciences and Technology, Islamabad 44000, H-13*

[4]*Department of Metallurgy and Materials Engineering, University of Engineering and Technology, Taxila 47080, 7-km N-125 National Highway*

[5]*Department of Energy Engineering, University of Engineering and Technology, Taxila 47080, 7-km N-125 National Highway*

**Corresponding author*

Email: *muddassir.ali@uettaxila.edu.pk*

ABSTRACT

Water scarcity has recently emerged as one of the significant global crises in recent times. To address water scarcity, membrane-based desalination is one of the most promising candidates to improve freshwater availability. Recently, pervaporation desalination has been projected as an emerging membrane-based technique to overcome membrane distillation limitations in handling high-salinity water. The development of exceptional membranes is the primary focus in pervaporation desalination by enhancing water flux rates through the matrix of the polymers whereas keeping a high degree of salt selectivity. In the current study, cellulose acetate (CA)/cellulose triacetate (CTA) nanocomposite membranes blended with zirconium dioxide (ZrO_2) are prepared via phase inversion for pervaporation desalination performance. ZrO_2 nanoparticles are added to enhance the hydrophilicity and porosity of the nanocomposite membranes. The fabricated nanocomposite membranes are characterized by SEM, FTIR, TGA, DSC, and tensile strength to study the surface morphology, chemical composition, thermal stability, mechanical properties and strength. Nanocomposite membranes' performance for pervaporation desalination is assessed as a function of feed temperature, flow rate, and concentration. Pervaporation results revealed that the nanocomposite membrane consisting of 2% ZrO_2 achieved a maximum water flux of 6.5 kg/m^{2}h, whereas the salt rejection was about 99.8%. This indicates that the fabricated CA/CTA/ZrO_2 nanocomposite membranes are appropriate for salt removal from high-salinity water.

Keywords: Cellulose acetate, Desalination, Nanocomposite membranes, Pervaporation, Zirconium dioxide (ZrO_2).

Catalytic Conversion of Used Cooking Oil (UCO) Into High-Grade Chemicals

Muhammad Kashif[1,*], Naseer Ahmed Khan[1], Hayat Khan[1]

[1]*Department of Chemical Engineering,University of Engineering & Technology, Peshawar 25120, (KP),*

**M. Kashif*

Email: kashifkhan15291@gmail.com

ABSTRACT

The development of renewable energy sources will decrease our dependency on the usage of fossil fuels; also, will safeguard the green environment from the harmful effects of the produced greenhouse gases.

In this study we investigated the catalytic conversion of used cooking oil (UCO) with the objectives to examine the catalytic activity of the proposed metal oxide catalysts (CaO, TiO_2, CaO/TiO_2 (hybrid)) to obtain maximum

yield of the produced products (high grade chemicals), in addition to study the influence of the reaction parameters (reaction temperature, heat rate, reaction time and catalyst load) for the selectivity of the product and process optimization. The catalysts were characterized by X-ray diffraction (XRD) and X-ray fluorescence (XRF) and the produced products were evaluated by gas chromatography (GC-MS).

The experimental results showed that for hybrid catalyst (CaO/TiO_2); 4 wt. % catalyst, 10 °C/min heat rate, 500 °C reaction temperature, and 120 min reaction time gives the maximum product (biofuel) yield of 79 % compared to 63 % and 68 % for TiO_2 and CaO, respectively. It was also observed that the hybrid catalyst showed better activity on repeated recycle turns illustrating that it is a potential choice for the conversion of UCO into high grade chemicals.

Keywords: UCO, metal oxide catalysts, catalytic cracking, bio-fuel.

Amino-modified ZIF based mixed matrix membrane

Zarrar Salahuddin[1,*], Sarah Farrukh[1] , Arshad Hussain[2] , Tayyaba Noor[1] , Witold Kwapinski[3]

[1]*School of Chemical and Materials Engineering (SCME), NUST, Sector H-12, Islamabad, Pakistan*

[2] *Department of Chemical Engineering, Pak-Austria Fachhochschule Institute of Applied Sciences and Technology, Haripur, Hazara, Pakistan*

[3] *Department of Chemical Sciences, School of Natural Sciences, Faculty of Science and Engineering, Bernal Institute, University of Limerick, Limerick, Ireland*

**Corresponding author*

Email: sarah.farrukh@scme.nust.edu.pk

ABSTRACT

Dense and translucent CA/PEG 1000/ZIF membranes were synthesized in acetone, utilizing solution casting. Membrane characterization was carried out using FT-IR, SEM and tensile testing. SEM proved presence of dense membranes and increase in the filler amount may have formed voids, raising the permeability of both gases. Single and mixed gas (CO2/CH4) permeation testing showed an increased permeability, on addition of more filler, which is probably due to formation of nano-gaps. A maximum selectivity of 39.49 and 34.86 for single and mixed gases respectively, and maximum permeabilities of 49.7685 and 1.41 barrers were observed. Tensile testing showed that strength peaked then decreased on increased loading, due to agglomeration on adding more ZIF, which introduced defects in structure. To conclude, selectivity of higher loaded membranes is favourable whereas tensile strength of lower loaded membrane is superior, but we have a trade-off between selectivity and tensile strength, so a higher-loaded membrane is most suitable.

Keywords: Mixed Matrix Membranes, Metal-organic Frameworks, Selectivity, Mixed Gases, Gas Separation

Synthesis Of Inorganic Membrane Through Geopolymerization to Treat Wastewater

Usman Khan*, Kashif Khan, Ahsan Khan, Minhas Tariq, Saeed Gul

Department of Chemical Engineering, University of Engineering & Technology Peshawar

25120, Pakistan.

*Email: chemicalengr.usmankhan@gmail.com

ABSTRACT

In recent years, inorganic membranes have drawn prominent recognition because of their high mechanical strength, durability, and excellent chemical resistance. Still, their application is limited due to the heat-intensive synthesis steps and expensive source material. Geopolymerization is an efficient technique used for the synthesis of inorganic membranes. It is a two-step mechanism; the first step involves the chemical activation of fly ash. The

second step comprises of hydrothermal treatment of geopolymer paste under specified conditions. In this work, geopolymer membrane is synthesized using the Geopolymerization process. The chemical activator solution consists of 12M NaOH solution stirred with sodium silicate in a ratio of Na_2SiO_3/NaOH=2.5. Chemical activation of fly ash was done using fly ash/chemical activator =1.5. Geo-polymer membrane was synthesized after the hydrothermal treatment of geopolymer paste at 70ºC in a closed environment. XRF analysis of fly ash revealed an optimum ratio of Si/Al of 2.4. Scanning Electron Microscopy was used to examine the membranes' surface morphology. For crossflow filtration mode, the flux for the membrane was 45.88, 64.51, and 70.25 l/hr.m^2 at 1,2, and 3 bars, pressure respectively. Before and after treatment, parametric analysis of carwash wastewater was conducted, and the overall rejection for the membrane was 59%.

Keywords: Chemical activation, hydrothermal treatment, Crossflow filtration.

Effective Thin Film Membranes Incorporated with UiO-66 Zr-MOF for Cadmium, Copper and Mercury Removal from Aqueous Medium

Seema Gul[1*], Maliha Asma[1], Aamir Malik[2], Maryam Latif[2], Muhammad Nouman[3]

[1]Department of Environmental Sciences (FC), International Islamic University Islamabad, H-10 Sector, Pakistan.
[2]Department of Materials Science and Engineering, Institute of Space Technology (IST), Islamabad, Pakistan.
[3]Institute of Environmental Sciences and Engineering (IESE), School of Civil and Environmental Engineering (SCEE), National University of Science and Technology (NUST), Islamabad, Pakistan.

**Corresponding author:*
Email: seemagul23@gmail.com

ABSTRACT

UiO-66 Zirconium MOF based thin film nanocomposite (TFN) membranes were fabricated via interfacial polymerization method for the removal of Cd (II), Cu (II) and Hg (II) from aqueous medium. Various weight percentages of UiO-66, metal organic framework (MOF) were incorporated in TFNs to get high permeability and selectivity of membranes. XRD proves that fine TFN membranes with finger-like nano-channels and uniform distribution of MOF particles were obtained with 0.2 wt% of MOF. Adsorption capacities of TFN membrane with 0.2 wt% of UiO-66 MOF were 419 mg/g for Cd (II) and Cu (II) and 414 mg/g for Hg (II), respectively at 25°C and pH-6. Both equilibrium isotherms and kinetic orders for adsorption were investigated. Kinetic and isotherms data calculated with different time intervals have been analyzed by pseudo first order, pseudo second order, intraparticular diffusion equations, and Langmuir, Freundlich isotherms. The experimental data fitted well to both Langmuir and Freundlich isotherms and also followed a kinetic model of pseudo second order for Cd (II), Cu (II) and Hg (II). The mechanism was confirmed generally as a monolyer physical adsorption and coordination interaction between metal ions and TFNs adsorption system.

Keywords: Adsorption, Zirconium MOF, Thin Film Nanocomposite Membranes, Interfacial polymerization.

Full Length Papers

Removal of COD and Color from MBR treated distillery effluent spent wash through Moringa oleifera coagulant

BAHADUR ALI[1*], ZUBAIR AHMED[2], MARYAM ARAIN[3]

[1]Institute of environmental engineering and management Mehran University of Engineering and Technology (MUET) Jamshoro, 76020, Pakistan

[2]US-Pakistan Center of Advanced Studies in Water Mehran University of Engineering and Technology (MUET) Jamshoro, 76020, Pakistan

abbaci.bahadur@gmail.com, zahmed.uspcasw@faculty.muet.edu.pk, ms.maryam@faculty.muet.edu.pk

*Corresponding author

Email: abbaci.bahadur@gmail.com

Abstract

The COD and color of distillery effluent (spent-wash) results in critical environmental issues when discharged without any treatment into the natural water resources. In this research study, we used Moringa oleifera seeds as an activated carbon in the form of powered activated carbon (PAC). The synthesized material is characterized by Scanning Electron Microscope (SEM) and Brunauer Emmett Teller (BET), SEM and BET results clearly shows that the pore structure and size of Moringa oleifera affected the capability of adsorption. Batch experiments were conducted for the removal of COD and color at different doses (0.4, 0.6, 0.8, 1.0, 1.2, 1.4, 1.6 g/100ml). From results, it was observed that at 1.6 g/100ml dose of PAC material the maximum removal of COD was 96.6% and 99.4% of distillery effluent spent-wash decolonization. The experimental data was found to be the excellent coagulant.

Key words: Distillery, Spent wash, Decolorization, Moringa oleifera, Powered Activated Carbon (PAC).

1 Introduction

Distillery industry is the key sources of contaminants to surface water bodies and the adverse effects of sugar mills effluents are well known. Distilleries are among the greatest polluting industries with reference to bulk water contamination. (R. Kirishna Parsad, 2009, Bernardo et al., 1997) The distilleries wastewater is categorized by its brown color, high BOD, COD, temperature, low pH, total solids, odour, and high level of dissolved organic and inorganic matter (Methodologies et al., 2016). The dark color given by melanoidin and anaerobic microbial mass in municipal solid waste (MSW) exceed to reduce sunlight penetration in watercourses, ponds and river in this manner decreasing the photosynthetic activity affecting damage to aquatic life. Dumping on land because decrease in soil manganese, alkalinity availability and prevents seed maturing. (R. Kirishna Parsad, 2009)

Several studies have been carried out regarding the removal of color from waste water through different methods like coagulation, sedimentation, electrochemical, adsorption, degradation, ion-floatation and photocatalysis. The application of electrochemical technique to treat wastewaters. This method assurances great treatment efficiency, but its effectiveness be influenced by nature of electrodes, the manufacturing of electrocoagulators and the form under which the method is run.

Coagulation has keep on the greatest practiced process of removing particulate and organic matter in wastewater treatment. Conventional coagulants in waste water treatment are sodium aluminate, ferric chloride ($FeCl3{\cdot}6H2O$), alum ($Al2(SO4)3{\cdot}14H2O$),ferric sulphate and aluminium chloride. Conventional coagulants are mainly salts of a strong acid ($H2SO4$ or HCl) and a weak base ($Fe(OH)3$ or $Al2(OH)3$); therefore they are a combination of cation and anion, an anion (from an acid)and a cation (from a base). However current research have pointed out many serious disadvantages of using aluminum salts, such as the difficulties of reaction of alum with natural alkalinity existing in the water

leading to a decrease of pH. At this time more active trivalent aluminum coagulants are poly aluminum silico sulphate and poly aluminum chloride have been established. While these new coagulants have improved the coagulation process significantly but they have not improved all the problems mentioned previous. Therefore it is beneficial that other low cost and more environmentally satisfactory alternative coagulants be developed to present a feasible alternative. Some natural coagulants of mineral 5 origin and vegetable similar Prosopisjuliflora, Moringaoleifera and Cactus latifaria were in use in water treatment before the advent of chemical salts, but have succumbed gradually under innovation and survived only in remote areas of some developing countries. (M. P. Wagh et al., 2015, R. Kirishna Parsad, 2009)

Presence of great scope for Moringaoleifera coagulant in removal of color of distillery spent wash. The decolorization of distillery wastewater is difficult and needs sequential treatment via different techniques such as electrocoagulation, ozonation, and adsorption. In this series Moringaoleifera coagulant can be presented as natural coagulant to remove portion of color from spent wash. (Abdulrazak et al., 2015, R. Kirishna Parsad, 2009)

M. oleifera seeds have 1% dimeric and closely charged cationic proteins, isoelectric pH, 10–11 and molecular mass, 6–16 KDa, which can remove the wastewater contaminations by electrostatic interface between cationic protein and colloidal present in wastewater. The latest research shown that the cationic proteins presented in seeds can be extracted through several chemical and physical procedures like precipitation, delipidation, salt-based extraction, ion exchange, centrifugation, lyophilization, and membrane-based separation i.e., dialysis. A limited studies founded on usage of crude seed powder as coagulant, very limited works have been done regarding the size special effects of powder on coagulation effectiveness of textile wastewaters. (Hirendrasinh Padhiyara et al. 2020)

As we know the Moringa Oleifera tree is the natural coagulant and so much effective on water treatment with its different parts (drumsticks, leaves, seed pods, seeds and seed oil) so that's why I wanted to use its seeds but as Activated carbon in the form of PAC (Powered Activated Carbon).

Problem Statement

The COD and color of distillery effluent (spent-wash) results in critical environmental issues when discharged without any treatment into the natural water resources. Even after treatment from the membrane bioreactor (MBR), the spent-wash effluent has a COD of 30% and a dark brown color, which threatens the aquatic life.

Methods

Source water (MBR treated distillery spent wash)

In this research study, distillery industry wastewater selected as a source water. The sample were collected from distillery industry located at Matiari. The distillery wastewater consisting a particularly combination of effluents generated from different processes. Spent wash samples were collected after membrane bio reactor MBR treated wastewater from distillery industry and delivered to the pilot scale wastewater laboratory at USPCASW, Mehran university engineering and technology, Jamshoro.

Synthesis activated carbon from natural material Moringa oleifera MO

Collected moringa oleifera from the garden at MUET, Jamshoro. Delivered the moringa oleifera samples to pilot scale laboratory at USPCASW. Wash the MO samples with DI water, oven dried samples at 120°C for 24 hours. Once the MO samples get completely dried then manually outer shell were removed from seeds. Filled the crucible with MO seeds and covered with Aluminium foil after that place the

covered crucible in muffle furnace for carbonization at 400°C for 2hours then increased the temperature upto 800°C for 45 minutes for making activated carbon. When procedure have been done then cool down the sample (activated carbon) from this sample made powdered activated carbon PAC. For making PAC crushed the activated carbon in crusher further processed in ball mill machine for granules after that granules were grind in grinder until granules change in powder form which is PAC. After synthesis PAC then characterized by SEM technique (JSM-6490).

Physicochemical parameters

Analysis the physicochemical parameters from MBR treated spent wash effluent initially checked the pH through (HANNA HI 8424) pH meter.

Color

For checking color very first selected the color method 122 in DR 900 HACH then filtered the sample with syringe filter size 0.22 µm, Wash the glass vial with DI water and Inserted a vial in blank value cell (DI water) and pressed zero, Inserted the sample filled vial in cell and pressed Measure in the last record the reading.

Chemical Oxygen Demand (COD)

Added 1.5ml from each samples in prepared COD vials (HR 0-1500 mg/L range, Lovibond) tightly cap vials and invert each several times to mix completely. Placed COD Vials in block digester preheated to 150°C and reflux for 2 hrs. Behind a protective shield. After Heating let it be cooled down at room temperature. Used COD photometer Lovibond MD 200measured the amount of COD present in a Sample, firstly set the mode of reading high range (Hr) and used the reference vials press zero/test, then placed the sample and press test.

Coagulation and Flocculation

In this study, we selected natural coagulant moringa oleifera PAC and observed for their efficiency of color removal and COD reduction. Batch study test have been done. This process was taken on the Jar Test Apparatus to optimize and compare different doses and contact times for removal efficiency. A jar test is conducted on spent wash samples with coagulants. VELP Scientific jar test apparatus (Model JLT6, France) were used. Six one liter samples were taken in six one liter beakers and fast mixed at 100 rpm for 5 minutes followed by slow mixing at 60 rpm for 25 minutes. After suitable settling time varying from 30 to 300 minutes, taken a supernatant of samples for additional analysis. Optimum dose was found out by varying dose of coagulant over a wide range.

Results

Physicochemical parameters

Analysis of COD, color and pH from distillery Spent wash sample. Distillery Spent wash effluent pH was 14. We did not change the pH throughout the research, we worked on original pH. Initially COD concentration were 4500 mg/l and amount of color were 37200 mg/l after the treatment of distillery Spent wash sample through different coagulant and different doses COD and color were decrease. Detail result listed in table1.

Table 1. Physicochemical parameters of distillery effluent Spent wash by using natural coagulant PAC at different doses for removal of color and COD.

Coagulant	PAC different Doses g/100ml	Color removal rate	COD removal rate
Moringa Oleifera powdered activated carbon (PAC)	0.4	5130	1500 5130
	0.6	3120	1210
	0.8	1660	900
	1.0	810	600
	1.2	350	210
	1.4	200	150
	1.6	120	80

Scanning electron micrographs (SEM) result

The scanning electron micrographs (SEM) of the PAC Moringa oleifera. The morphology of this material shown a heterogeneous and relatively porous matrix. This structure facilitates the processes of ion adsorption, due to the interstices and, more importantly, to the presence of the protein component of the seed. Thus, based on these characteristics, it can be concluded that this material has an adequate morphological profile. (JSM-6490) figure 1.

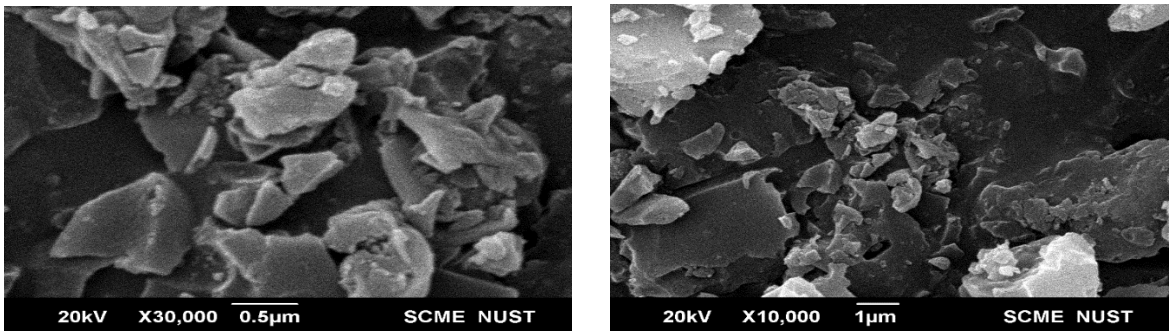

Figure 1. SEM micrograph shown synthetic Moringa Oleifera PAC coagulant characteristics at 10,000x-30,000x. Material is look like high porous through in through pores and Plates like shapes.

Removal efficiency of COD and color through natural coagulant MO PAC

As we selected natural coagulants moringa oleifera PAC for the removal of COD and color. Different doses were applied as follows, 0.4, 0.6, 0.8, 1.0, 1.2, 1.4, 1.6 g/100ml. Results shown that, at 0.4g/100ml PAC dose were observed very low removal percentage of color 86.1% and COD 66.6% from distillery spent wash effluent. Moderate removal efficiency were recorded at 0.8g/100ml PAC dose for color 95.5% and COD 80% removed. The highest removal efficiency of PAC dose at 1.6 g/100 ml and achieved 96.6% of COD reduction and 99.4% of color removal from distillery spent-wash effluent figure 2.

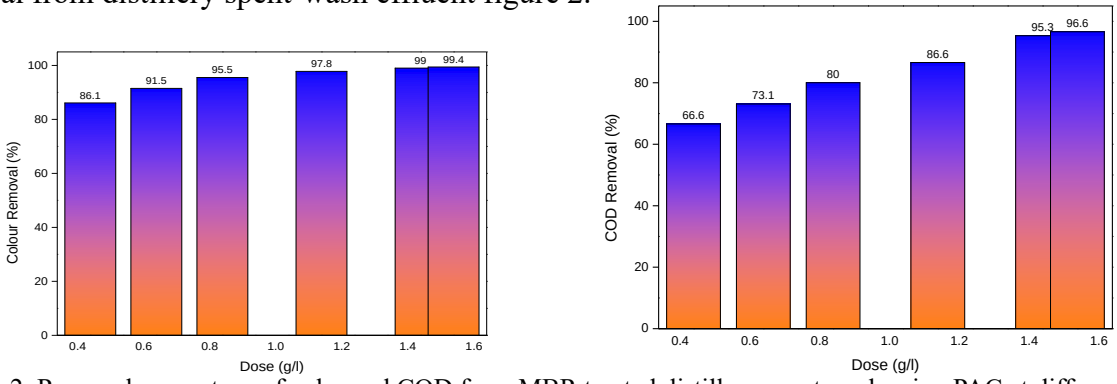

Figure 2. Removal percentage of color and COD from MBR treated distillery spent wash using PAC at different coagulate doses.

Conclusions

In this research, we synthesised natural coagulant from Moringa oleifera seeds as an activated carbon in the form of powered activated carbon (PAC). The synthesized material is characterized by Scanning Electron Microscope (SEM) and Brunauer Emmett Teller (BET), SEM and BET results clearly shows that the pore structure and size of Moringa oleifera affected the capability of adsorption. Batch experiments were conducted for the removal of COD and color Moreover, Different doses were applied as follows (0.4, 0.6, 0.8, 1.1, 1.4, 1.5 g/100ml) of PAC coagulant. From results, it was observed that at 1.6 g/100ml dose of PAC material the maximum removal of COD was 96.6% and 99.4% of distillery effluent spent-wash decolonization. The experimental data was found Moringa oleifera Powered Activated Carbon (PAC) were excellent coagulants for removal of COD and color from distillery effluent spent-wash.

Further study, Moringa olifera seeds can be an effective alternative to the use of activated carbons in the form of Granular Activated Carbon (GAC) and Powered Activated Carbon (PAC) for removal of color and COD from other industries waste waters.

References

Abdulrazak, S., Sulyman, Y. I., Bello, H. I., Akanni, A. S., Oniwapele, Y. A., & Muktari, M. (2015). Tannery Wastewater Treatment Using Activated Carbon From Moringa Oleifera Pods. *IOSR Journal of Environmental Science, Toxicology and Food Technology*, *9*(12), 96–99. https://doi.org/10.9790/2402-091219699

Bernardo, E. C., Egashira, R., & Kawasaki, J. (1997). Decolorization of molasses' wastewater using activated carbon prepared from cane bagasse. Carbon, 35(9), 1217– 1221. https://doi.org/10.1016/S0008-6223(97)00105-X

Methodologies, E., David, C., Arivazhagan, M., Hariram, J., & Sruthi, P. (2016). Spent wash Decolorization using Granular and Powdered Activated Carbon : Taguchi's Orthogonal Array design and ANN approach. 229(1), 224–229.

R. Krishna Prasad∗, (2009) Color removal from distillery spent wash through coagulation using Moringa oleifera seeds: Use of optimum response surface methodology, Journal of Hazardous Materials 165, 804–811, doi:10.1016/j.jhazmat.2008.10.068

Hirendrasinh Padhiyara, Arti Thankib, Nitin Kumar Singhc,*, Siddhartha Pandeyd, Manish Yadave,(2020) Tara Chand Yadavf, Parametric and kinetic investigations on segregated and mixed textile effluent streams using Moringa oleifera seed powders of different sizes, Journal of Water Process Engineering 34,101159, https://doi.org/10.1016/j.jwpe.2020.101159

Wagh, M. P., & Nemade, P. D. (2015). Treatment of Distillery Spent Wash by Using Chemical Coagulation (CC) and Electro - coagulation [EC]. *American Journal of Environmental Protection, Vol. 3, 2015, Pages 159-163*, *3*(5), 159–163. https://doi.org/10.12691/ENV-3-5-1

Integration of f-CNTs into Glass fiber by Solution Dip Coating and Characterization via Nano-indentation

Misbah Ullah Qureshi[1*], Nehar Ullah[1], Muhammad Sulaiman[2]

[1]*Department of Chemical Engineering, M.Sc. student, University of Engineering and Technology Peshawar, Pakistan*

[2] *Department of Chemical, Polymer & Composite Materials Engineering, University of Engineering & Technology, Lahore, (New Campus), Kala Shah Kaku-39020, Pakistan.*

Email: 14PWCHE0910@uetpeshawar.edu.pk

Abstract

Functionalized Carbon Nano tubes-Glass fiber composite is manufactured by different methods, however, each method possess several flaws. In this paper *F-CNTs* are deposited on glass fiber via a novel technique; Solution Dip Coating. The concentration of *F*-CNTs, temperature, agitation rate, Soaking time played key roles in making a strengthened composite material during the Dip coating phase. Secondly, the processed Glass fibers were joined via Epoxy. Once the composite was prepared then different tests were conducted in order to know about the properties of the composed material. The result manifested that increasing the *F-CNTs* concentration increased the properties up to great extent. Similarly, the Nano indentation ensured the impressive strength of the material. The composite can be utilized in different industries i.e. aerospace, sports goods, Automobile, Wind Turbine Blades.

Key words: Functionalized Carbon nanotubes (*F-CNTs*), Glass fiber, Epoxy, Nano-indentation.

1. Introduction

Carbon nanotubes (CNTs) are thin sheets of graphene which were discovered in 1991. The rolling of graphene sheets in single walled CNTs exist in various forms i.e. Armchair, Zigzag, and Chair shaped. The CNTs can be wrapped into different forms that results in changing its structure and electronic properties. The CNTs exist in single sheet-Single Walled nanotubes (SWNT) or multiple sheets-multi Walled nanotubes (MWNTs) form. SWNT possess single cylindrical structure that ranges in diameter of 0.5-0.2 nm, having length in the range of 50-150µm .Similarly, it possess micro-porous surface with surface area that ranges up to 1300 m^2/g(outer surface).SWNTs have strong mechanical and electrical behaviors. The electrical properties depends on two factors: Tube diameter, Helicity. The presence of Electrical conductivity, surface curvature make the CNTs different than Activated carbon. MWNTs are formed by placing several SWNTs concentric. The concentric spacing of the wall is kept 0.34nm. Similarly, MWCNTs possess an outer diameter of 2-100nm which depend on the number of coaxial tubes present in it. As compare to SWNTs, MWNTs are more stable [1]. Carbon nanotubes are prepared by number of ways. Different methods used to manufacture the composite include; Electric Arc discharge, Laser Ablation, and Chemical vapor deposition. Electric Arc discharge is the most efficient method used to manufacture CNTs. In this method, current is passed between two electrodes of graphite. The anode possess metallic oxide catalysts (Ni, Co, Fe, -oxides). Helium, Argon or Methane is provided for making the environment cold for synthesis of CNTs. The nature of electrodes, Current amount, and Catalyst quality of CNTs. In Laser ablation, graphite rod is hit by Laser in an inert gas environment that sublimes the graphite where the vapors are recollected to get CNTs. Pyrolysis of Hydrocarbons (Propane, Butane, Hexane, Benzene, and Toluene) is the most used

method for getting CNTs. It is also known to be Chemical Vapor Deposition method. In this method CNTs are produced in enormous quantity at temperature range of 500-1300 C˚ in presence of catalysts (Ni, Co, Fe).In this process, initially, the vapors are dissociated and saturated in metal nano-particles. Afterwards, the vapors are precipitated. The catalysts used in this process act as a nucleation sites. Metallic catalysts not only provide space for deposition of vapors but also play role in decomposition of hydro-carbon. The vapors are deposited on the catalyst in Root Growth manner or Tip growth manner [2].

1.2.Functionalization of CNTs

CNTs possess a variety of impurities, catalyst particles, that need a separate step of purification which not only make the process more complex but also less economical [3]. In addition to it, In order to improve the interaction of the Carbon nanotubes, CNTs are treated either physically (Covalent) or chemically (non-covalent) in order to improve its surface which is known as Functionalization.

1.3.Non Covalent functionalization

This method involve adsorption or wrapping of polymer to CNT surface. The polymer and the CNTs interact via π-π-interaction [4]. Non-covalent functionalization does not affect the structure of the aromatic ring of CNTs. Beside polymer surfactants, sodium dodecyl benzene sulfonate are also used for non-covalent functionalization. This method effects the side walls but it does not oxidize CNTs up to great extent.

1.4.Covalent Functionalization

Covalent functionalization oxidizes CNTs up to greater extent as compare to Non-covalent functionalization. As the end caps of CNTs are more reactive than the side walls, therefore, the side walls need proper treatment, in order, to improve its reactivity. For this purpose, CNTs are treated with chemicals having functional groups: -COOH, $-NO_2$,-OH, -H,=O,HNO_3,H_2SO_4 as they change the sp^2 hybridization into sp^3 [3]. However the major concerns of this method includes the surface damage of CNTs during Ultra-sonication and its length breakage, resulting in degradation of its mechanical properties. Similarly, the chemicals damage the surface as they are either not easy to be used, or they may have a weak interaction with polymer matrix or may have a re-agglomeration with the matrix [5].

1.5.Carbon nanotube and Glass fiber composites

Glass fibers are widely used as reinforcement material because of their low cost, more reliabilities and availabilities in manufacturing composites like shopped strand mat, and woven fiber because of its high stiffness, strength, good chemical and thermal resistance [6, 7]. Such fibrous materials are usually doped with nano-fillers and reinforced with polymeric matrix as it result in high strength, good electrochemical behavior [8]. Functionalized Carbon Nano-tubes are efficient fillers in this regard as they possess strength of 22GPa and Young modulus of 1TPa [9]Various conventional techniques are used for manufacturing the *F-CNTs* nano-composites. As, In Melt processing the polymer is blended with CNTs .Shear mixing is carried out in order to disperse the nano-fillers on substrate efficiently. Similarly, In Situ polymerization the changes are brought at the monomer level resulting in a nano-composite material [5]. Bin Hai, and Peng-Cheng Mai used Electrophoretic deposition to manufacture a composite of CNTs , graphene and Glass fibers by depositing the nano-fillers on the substrate using electric current and electrodes[1]. Delong, Benue, and Hang experimented by depositing CNTs on Glass fiber by Chemical Vapor deposition (CVD) [10]. Similarly, Solution mixing method was carried out to embed CNTs into polymeric matrix [11].Furthermore, Rapid Nano welding of carbon nanotubes by electrical and thermal shocks witness coating of CNTs on Glass fiber [12]. However, all the conventional techniques have various drawbacks that effect the factors responsible for efficient functioning of the composite materials, including Improper alignment, interaction and dispersion of CNTs on the substrate material resulting in malfunctioning of

the composite including; Delamination, micro-cracking, and fiber breaking of the composite material [1, 10, 13-18]. Therefore, to overcome the flaws associated with conventional techniques, the solution Dip coating method is an appropriate method to follow for manufacturing *F-CNTs* and epoxy (Glass fiber) composite. These *F-CNTs* based Glass fibers have the potential to be utilized in light weight, automotive product, Fuel cells, Satellite, Armor, Sports.

2. Methodology

Initially, Carbon nano tubes were treated with different chemicals(Benzene-ticarbo-oxallic acid(BTC), Poly-phosphoric acid(PPA), Phosphorus penta oxide(P_2O_5) in order to carryout its Fnctionalization which increases its interaction and dispersion abilities.Secondly, Solution Dip Coating method was used for fabricating the Glass fiber with the Functionalized Carbon nanotubes. The treated carbon nano tubes were fabricated onto the glass fiber surface by manupulating different experimental variables; Agitation speed, Concentration of Functionalized Carbon nanotubes (*F*-CNTs) , Soaking time, and Temperature. The processed glass fiber sheets were cut into different laminates form .Different number of laminates were selected. They were joind via resin inorder to form a strong composite. The composite was cured for some time .Once the product samples were ready they were tested via different tests which showed the improved abilities of the composite.

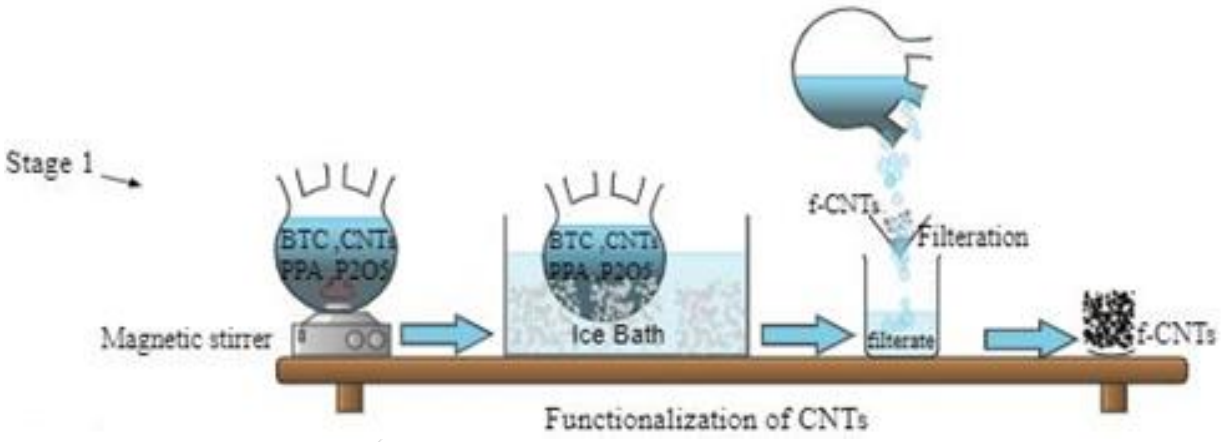

Figure2a) Functionalization of CNTs

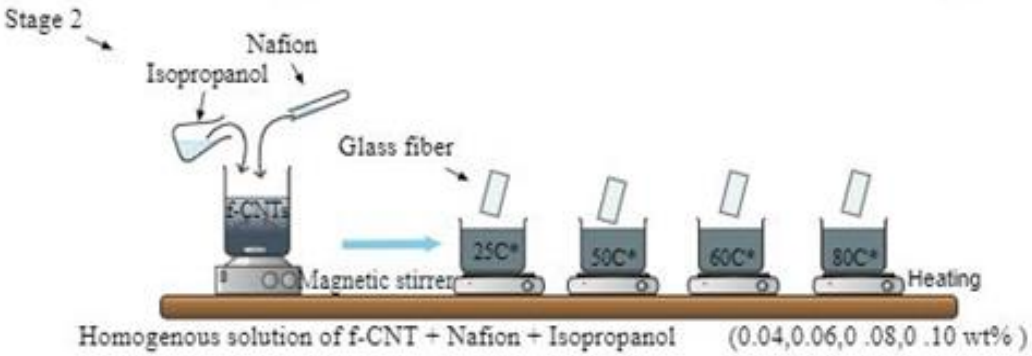

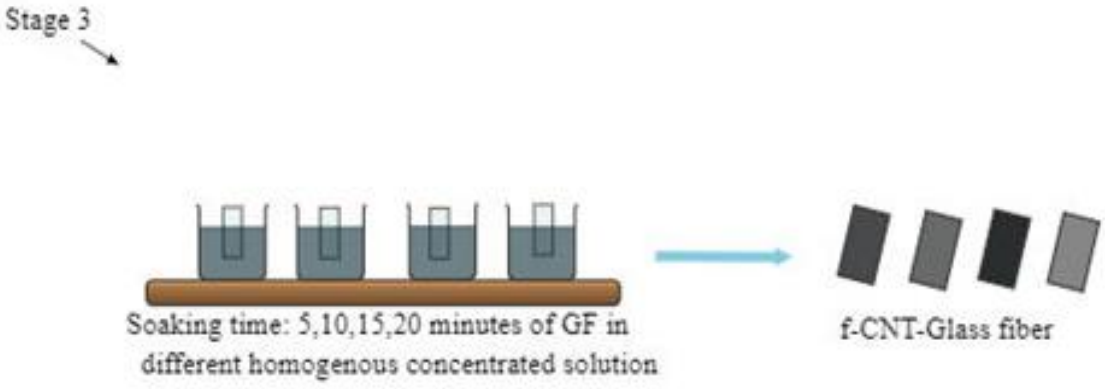

Figure2b). Solution Dip Coating Process(stage 2, stage 3)

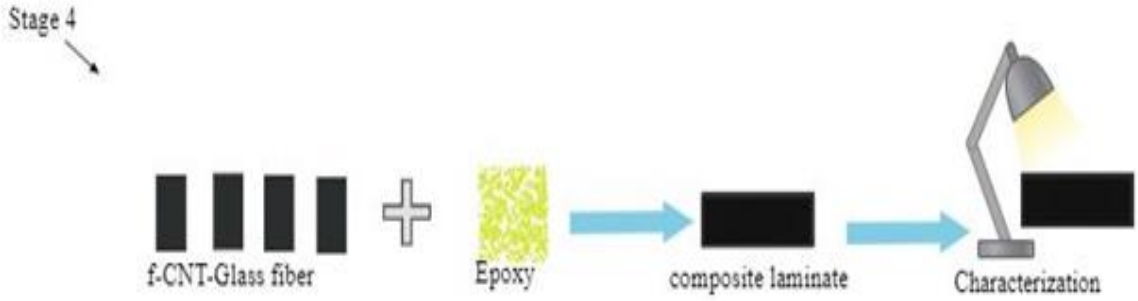

Figure2c) Characterization of the composite

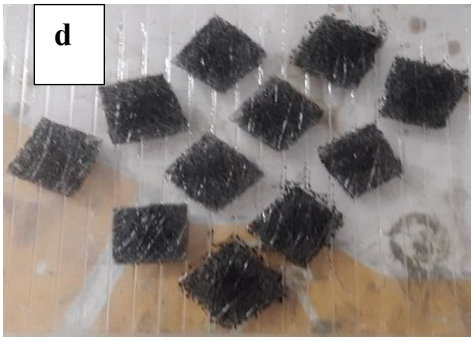

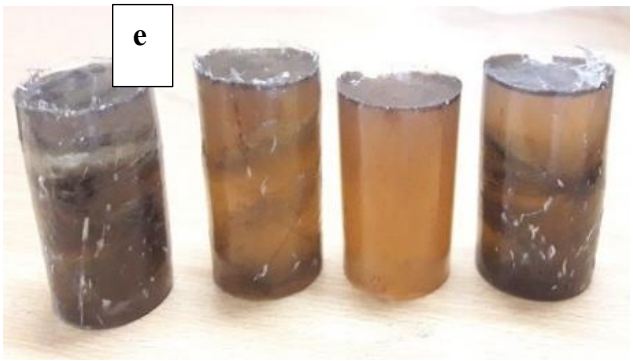

Figure 2d) Functionalized Carbon Nano tubes 2e) *f*-CNT-Glass fiber composite

Results

Cylindrical Samples with requirements of Length and diameter to be 1cm and 2cm inches were prepared for crushing test. The samples were tested via Universal testing machine (model number UH-200A, Capacity of 200tons).The pinnacle plate of UTM was impacted at different impact rate on the sample. Loading impact was continued over the sample till it crashed/fractured. On such occasion the UTM machine showed the maximum value of compressive load at which the sample fractured. The UTM analysis shows the increasing strength of the composite material as mentioned in the graph given below.

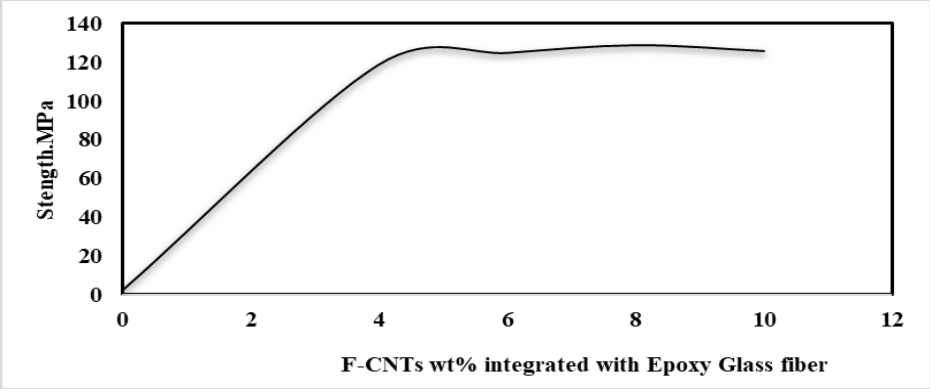

Figure 3a). Strength of the *F-CNTs* glass fiber composite

The instrument used for nanoindentation was Nanoscope IIIa scanning probe microscope equiped with a dimension 3100 AFM head and with a Hysitron TriboScope nanoindentor head. The nanoindentor samples were glued on a steel stage where a particullar load was applied for a particullar span of time . With the help of Berkovich indenter the load was applied over the sample for a particular period of time. The Nano indentation manifested the improved Modullus of the composite as mentioned below in the graph.

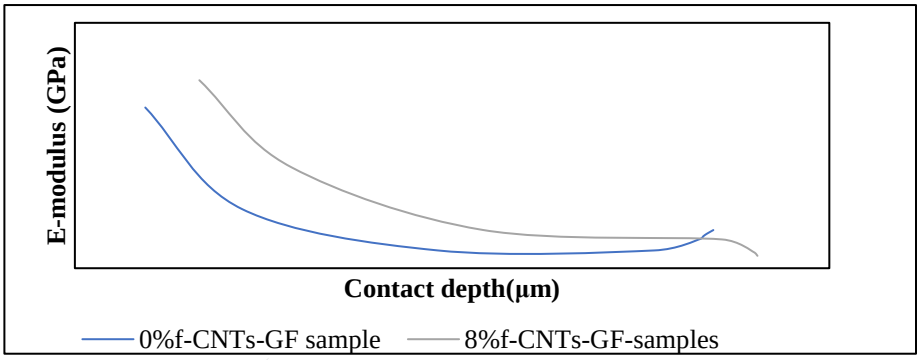

Figure3b).E-Modullus as a function of Contact Depth

3. Conclusion

This work evaluate the processing of *F-CNTs* by Solution Dip coating method for manufacturing *F-CNTs* and epoxy (Glass fiber) composite. The said method improves the factors responsible for better functioning of the composite i.e. Dispersion, alignment and interaction of *F-CNTs* with epoxy (Glass fiber). The product composite formed is tested via several characterization tests. The results manifested that increasing the concentration of *F-CNTs* on glass fiber enhances the properties-strength, E-Modulus- of the composite material. With such high strength properties the composite can be utilized in Aerospace, sports, Automotive Product, Satellite etc.

4. References

1. Bin HAO1, Peng-Cheng Ma1, *COMPARATIVE STUDY ON MONITORING STRUCTURAL DEFECTS IN FRPS USING GLASS FIBERS WITH CARBON NANOTUBES AND GRAPHENE COATING.* conference, 2015.
2. Gogotsi, Y., *Nanomaterials Handbook*2017. 2nd edition.
3. In-Yup Jeon1, D.W.C., Nanjundan Ashok Kumar1 and Jong-Beom Baek1, *Functionalization of Carbon*

Nanotubes. Carbon Nanotubes - Polymer Nanocomposites, 2011.
4. Díez-Pascual, A.M., *Chemical Functionalization of Carbon Nanotubes with Polymers.* 2021: p. 64–83.
5. Garima Mittal a, V.D.a., Kyong Yop Rhee a,*, Soo-Jin Park b,**, Wi Ro Lee c, *A review on carbon nanotubes and graphene as fillers in reinforced polymer nanocomposites.* Journal of Industrial and Engineering Chemistry, 2014: p. 18.
6. R. RAMLEE1, M.M., 2, Z. A. MOHD ISHAK1, 2, AND A. R. MOHAMED3, *Properties of Glass Fiber-Carbon Nanotube (CNT)/Epoxy Composites.* Journal of Polymer Materials 2013. **30**: p. 103-116
7. Xiaoning Tang1 , X.Y., *Dip-coating for fibrous materials: mechanism, methods and applications.* Sol-Gel Sci Technol, 2017. **81**.
8. Lijun Wang, L.T., * Shaomin Zhu, Jiaji Liang, and Haichen Zhang, *Enhancing the Mechanical Performance of Glass Fiber-Reinforced Polymer Composites using Multi-Walled Carbon Nanotubes.* Advance Engineering Material, 2020.
9. K K Mahato*, D.K.R., R K Prusty, K Dutta, B C Ray, *Tensile behavior of MWCNT enhanced glass fiber reinforced polymeric composites at various crosshead speeds.* IOP Conf. Series: Materials Science and Engineering 2017. `**178**.
10. Delong He, B.F., Hang Zhao, Xiaoxin Lu, Minhao Yang, Yu Liu, Jinbo Bai, *Design of Electrically Conductive Structural Composites by Modulating Aligned CVD-Grown Carbon Nanotube Length on Glass Fibers.* 9, 2019. **3**.
11. Ajay Vasudeo Rane, S.T., *Methods for Synthesis of Nanoparticles and Fabrication of Nanocomposites.* 2018.
12. Yuanyuan Shang, 2,‡ Baohui Shi,2,5,‡ Sagar M Doshi,2,3 Tiankuo Chu,2 Guixue Qiu,1 Aihua Du,1,* Yong Zhao,4 Fujun Xu,5 Erik T Thostenson,2,3 Kun Kelvin Fu2,3,*, *Rapid nano-welding of carbon coatings onto glass fibers by electrothermal shock.* Applied Materials and interfaces, 2020.
13. Ashish Warrier a, A.G.a., b,*, Olivier Rochez b, Luca Mezzo b, Frederic Luizi b, Larissa Gorbatikh a,Stepan V. Lomov a, Aart Willem VanVuure a, Ignaas Verpoest a, *The effect of adding carbon nanotubes to glass/epoxy composites in the fibre sizing and/or the matrix.* Composites: Part A 41 (2010) 532–538, 2010: p. 7.
14. Bahador Dastorian Jamnani, S.H., Saeed Rahmanian, Suraya Abdul Rashid, Sa'ari b. Mustapha, and Sepideh Keshan Balavandy, *Grafting Carbon Nanotubes on Glass Fiber by Dip Coating Technique to Enhance Tensile and Interfacial Shear Strength.* journal of Nanomaterials, 2015. **2015**: p. 7
15. Fang Liu , S.D., 2 and Jianing Zhang2, *Mechanical Properties of Epoxy and Its Carbon Fiber Composites Modified by Nanoparticles.* journal of nanomaterials, 2017. **2017**: p. 10.
16. Fang Liu, S.D., and Jianing Zhang, *Mechanical Properties of Epoxy and Its Carbon Fiber Composites Modified by Nanoparticles.* Journal of Nanomaterials, 2017. **2017**: p. 10
17. Mehran Tehrania, A.Y.B., Majid Manteghib, Zhixian Zhouc, Marwan Al-Haika, *Integration of carbon nanotubes into a fiberglass reinforced polymer composite and its effects on electromagnetic shielding and mechanical properties.* IMECE2013-65202, 2013: p. 7.
18. Rathinasabapathi.G, K.A., *Exploration of Nano Fillers (Multi Walled Carbon Nano Tubes and Graphene Powders) in the Reinforcement of Epoxy/Glass Fibre Polymers (GFRP).* International Journal of Innovative Technology and Exploring Engineering (IJITEE), 2019. **8**(12): p. 5.

Comparative Performance Analysis of Ferric Oxide (Fe_2O_3/H_2O, Fe_2O_3/EG) based Nanofluids in Solar Compound Parabolic Collector

Muhammad Faizan Zafar[1, *], Muzaffar Ali[1], Muhammad Kaleem[2], Javed Akhtar[3]

[1]Department of Mechanical Engineering, UET, Taxila, 47080

[2]Department of Energy Engineering, UET, Taxila, 47080

[3]Department of Mechatronics Engineering, University of Chakwal, 48800

**Corresponding author*

Email: faizanmaju17@gmail.com

Abstract

Solar energy is the most abundant and globally freely available source of clean, renewable and sustainable energy. Different solar collectors are used to extract thermal energy for many low to medium temperature applications. Conventional heat transfer fluids used in these collectors such as water and ethylene glycol bear low thermal conductivity which negatively impacts their performance. Many research studies conclude that nanoparticles dispersed into conventional heat transfer fluids improve their thermal characteristics. In this experimental study, Fe_2O_3/H_2O and Fe_2O_3/EG nanofluids are characterized and performance evaluation is carried out in compound parabolic collector. The experimentation is performed with various volumetric concentrations (0.025,0.05,0.075%) of nanoparticles at flowrates 0.02 kg/s and 0.01 kg/s under real climate conditions of Taxila, Pakistan. Preparation of the nanofluids is done with two step method with the aid of homogenization and ultrasonication. Visualization technique is used to check stability of nanofluids for 48 hours after preparation. Thermal conductivity and dynamic viscosity are measured with the help of thermal properties analyzer and viscometer respectively. The results revealed that the maximum thermal conductivity enhancement of 30.8% is achieved for Fe_2O_3/H_2O with 0.075% volumetric concentration at 25°C. In addition, maximum temperature difference and thermal efficiency of 8.59°C and 74.59%, respectively is attained for Fe_2O_3/H_2O with 0.075% volumetric concentration at 0.02 kg/s. Maximum thermal efficiency enhancement of 31.49% is recorded for Fe_2O_3/H_2O with 0.075% volumetric concentration at 0.01 kg/s.

Keywords: Thermal Characteristics, Thermal Efficiency, Visualization Technique, Volumetric Concentration.

Nomenclature/Abbreviations

A	Solar Collector Area [m^2]
Al_2O_3	Aluminum Oxide
CPC	Compound Parabolic Collector
CuO	Cupric Oxide
EG	Ethylene Glycol
Fe_2O_3	Ferric Oxide
PTC	Parabolic Trough Collector
SDBS	Sodium Dodecyl Benzene Sulphonate
T	Temperature [°C]
G_e	Radiations [$Wm^{-1}K^{-1}$]
Q_u	Useful Solar Heat Gain [W]
Q_s	Solar Heat Flux [W]
$\dot{m}$	Mass Flowrate [kg s^{-1}]
ΔT	Temperature Difference
Cp	Specific Heat Capacity [J kg^{-1} K^{-1}]

Greek Symbols

ρ	Density [$kg.m^{-3}$]
ϕ	Volumetric Concentration [%]
η	Thermal Efficiency [%]

Subscripts

a	Aperture
bf	base fluid
i	inlet
o	outlet
nf	nanofluid
np	nanoparticle

1 Introduction

Focus of the world is shifted towards the clean sources of the energy due to climate changes occurring from the past few years. Renewable energy resources can play an important role in development as they are ecofriendly resources. Solar energy is among the renewable and sustainable energy resources and it can be used in industrial/domestic fluid heating and in electricity production [1]. Pakistan and its neighboring countries including Iran, Afghanistan and India have huge potential of solar energy. The Pakistan's geographical belt lies in 24-37^o latitude North and 62-75^o East in longitude [2]. There are almost 300 sunshine days available throughout the year [3].

For low temperature applications, flat plate collectors and evacuated tube collectors are commonly utilized, concentrating collectors such as parabolic trough collector and compound parabolic collector are used for medium to high temperature applications. PTC is an industrial scale proven technology [4] but it is not being used at small scale industrial units due to its high manufacturing and land cost. CPC is cost effective because it uses less space and it is a stationary solar collector requires no tracking [5].

Utilization of the nanofluids is among the thermal enhancement methods used for the heat transfer enhancement between working fluid and absorber tube. Nanofluid has increased thermal conductivity as compared to the conventional fluids such as water and ethylene glycol but one of the limitation of the nanofluid is the higher viscosity due to addition of nanoparticles [6].

Utilization of nanofluids in different solar thermal applications is studied earlier. In a recent study, the performance analysis of CPC was carried out by using Al_2O_3/H_2O nanofluid as compared to the conventional fluid (water). Temperature difference and thermal efficiency enhancement of 10^{o}C and 19% was achieved respectively [7]. In another study, increase in thermal conductivity of 30% was achieved as compared to conventional fluid such as water by using CuO/water nanofluids in CPC [8]. In a similar study, thermal conductivity enhancement of 12.7% was achieved by utilizing CuO/water nanofluids [9]. In an experimental study, Al_2O_3/H_2O and Fe_2O_3/H_2O nanofluids were used in PTC. The maximum thermal efficiency enhancement of 13% and 11% was achieved by using Al_2O_3/H_2O and Fe_2O_3/H_2O respectively at mass flowrate of 2 L/min [10].

In a research Study, stability analysis of 0.5 vol. % Al_2O_3/H_2O nanofluid was performed by sedimentation technique up to 30 days. Stability of the nanofluids decreased with the increase in storage days. Results revealed that the longer ultrasonication reduced sedimentation and thus increase stability of the nanofluid [11]. In another study, (CuO)/deionized water nanofluid was prepared in various volumetric concentrations (0.08,0.16,0.40%) with two-step preparation method and stability analysis is carried out with visualization technique up to 96 hours. Nanofluids are found to be stable [12]. Similarly, copper oxide nanoparticles were synthesized by using wet chemical method. The nanoparticles then dispersed into ethylene glycol with various volumetric concentrations

(0.01-0.1%). Stability analysis is carried out through visualization technique and results revealed that the thermophysical properties increases with the increase in volumetric concentration of nanoparticles (0.01-0.1%) and decreases with the increase in temperature (25-65^{o}C) [13].

It can be observed from the relevant literature study, that the nanofluids are used in solar collectors for the enhancement of thermal efficiency. The performance of these collectors can be enhanced with innovative heat transfer fluids. Experimental studies related to the use of nanofluids in CPC is under researched. Performance analysis of Ferric oxides based nanofluids is not done before in solar CPC. In this experimental study, characterization and comparative performance analysis of Fe_2O_3/H_2O and Fe_2O_3/EG is done with two conventional fluids such as water and ethylene glycol in CPC under a subtropical climate, Taxila Pakistan.

2 Materials and Methods

In this section, detail about selection of nanoparticles, preparation of nanofluids along the experimental setup and key parameters used in this study are given.

2.1 Selection of Nanoparticles

Ferric oxide nanoparticles with 99.5% purity were purchased from US Research Nanomaterials, Inc. [14] with an average diameter of 20 nm. Nanoparticles has specific heat capacity and density of 670 (J kg^{-1} K^{-1}) and 5180 ($kg.m^{-3}$) respectively.

2.2 Preparation of Nanofluids

Two step method was used to prepare Fe_2O_3 based nanofluids using H_2O and EG as base fluid. Nanofluids in different volumetric concentrations (0.025,0.05,0.075%) were prepared with the help of magnetic stirring, shear homogenization and ultrasonication process. Step by step preparation of nanofluids is shown in Figure 1.

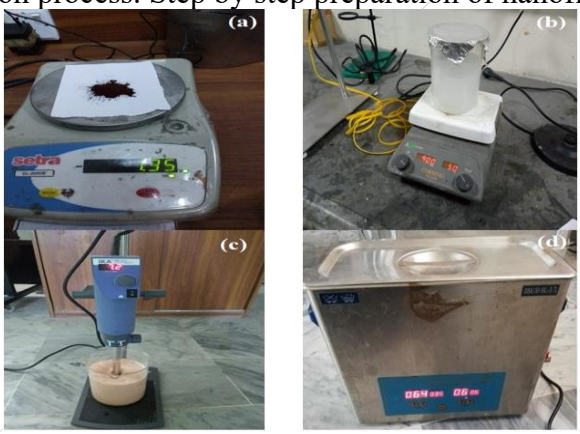

Figure 1: Nanofluid preparation (a) Weighing nanoparticles (b) Magnetic stirring (c) shear homogenization (d) Ultrasonication

First of all, weighed nanoparticles were initially mixed into base fluid with the help of glass rod. Then magnetic stirrer was operated at up to 60^{o}C and 950 rpm for dispersion of nanoparticles into base fluid. After magnetic stirring, Ultra-Turrax shear homogenizer was used at high rpm for better mixing of nanoparticles. Now, SDBS was added as surfactant into dispersion and placed in a sonication bath for 1.5 hours at 40Khz frequency to remove clustering of nanoparticles. SDBS is anionic surfactant that is compatible with H_2O and EG [15].

2.3 Thermal Conductivity Measurement

Thermal conductivity of Fe_2O_3/H_2O and Fe_2O_3/EG nanofluids was measured with the help of TEMPOS thermal analyzer at 25^{o}C with various volumetric concentrations (0.025,0.05,0.075%). The accuracy of the device is ± 10 %. Calibration of the equipment was done before the start of the experimentation with conventional fluid such as water. KS-3 sensor was used for this experimentation with measurement range of 0.2 to 2 (W/m. K).

2.4 Dynamic Viscosity Measurement

Viscosity of Fe_2O_3/H_2O and Fe_2O_3/EG nanofluids at (20,40,60^{o}C) with various volumetric concentrations (0.025,0.05,0.075%) was measured with the help of Brookfield DV-E Viscometer. Viscosity of nanofluid is also critical because pumping power requirement is directly linked with the viscosity of the fluids. First of all, spindle

was selected according to the requirement and the 30 ml samples were placed in viscometer. The required temperature and spindle speed were fixed and then the viscosity of nanofluids was measured.

2.5 Experimental Setup and Measurement Procedure

The compound parabolic collector is consisted of SS (Stainless-Steel) reflector and absorber tube(copper) connected with fluid tanks with the help of Polypropylene pipes and fittings. Collector area and concentration ratio are the key factors which play important role in determining the performance of the solar collectors. The collector area and concentration ratio for this collector is 0.8 m^2 and 4.17 respectively. Experimental setup is shown in Figure 2.

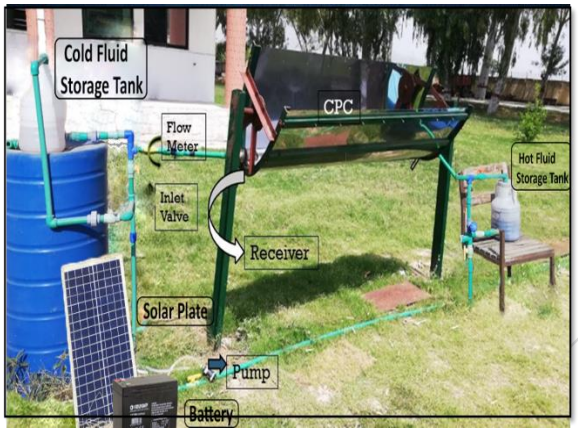

Figure 2: Experimental Setup

The compound parabolic concentrating collector was placed in East-West direction during experimentation. Tilt angle of 45°C was given to better capture the incident solar radiations by receiver. Pyranometer and K type thermocouples were used to measure radiations and temperature at inlet and outlet of absorber tube respectively. Mass flowrate of nanofluids and conventional fluids was obtained by flow sensor coupled with Arduino. The experimentation was performed in a closed loop.

Uncertainty of the equipment/ apparatus used in this experimentation is listed in the Table 1.

Table 1: Uncertainty of Apparatus

Apparatus	**Parameters**	**Uncertainty**
TEMPOS thermal analyzer	Thermal conductivity	±10%
DV-E viscometer	Viscosity	±1%
Pyranometer	Solar radiations	1-3 W/m^2
K- type thermocouple	Temperature	±0.1°C
Flow sensor	Flowrate	±2%

2.6 Key Parameters

Experimental data of thermal conductivity of ferric oxide nanofluids obtained from TEMPOS thermal analyzer is compared with the model proposed by Yu and Choi [16] given in Equation 1

$$\frac{k_{eff}}{k_f} = \frac{k_p+2k_f+2(k_p-k_f)(1+\beta)^3\phi}{k_p+2k_f-2(k_p-k_f)(1+\beta)^3\phi} \quad (1)$$

$Cp_{nf} = (1-\phi)Cp_{bf} + \phi Cp_{np}$Specific heat capacity, density and required mass of particles in solution can be find by using Equations 2, 3 and 4 respectively [17]

$$\rho_{nf} = (1-\varphi)\rho_{bf} + \varphi\rho_{np} \quad (2)$$

$$W_{np} = \left(\frac{\phi}{100-\phi}\right) * \left(\frac{\rho_{np}}{\rho_{bf}}\right) * W_{bf} \quad (3)$$

$$(4)$$

After inclusion of thermal conductivity, density and specific heat capacity equations, performance parameters such as useful solar energy gain and efficiency of the system can be find out with the help of Equations 4-6 [18].

$\eta = \frac{Q_u}{Q_s}$The thermal efficiency of CPC is calculated by using Equation 4

(5)

The useful solar thermal collector gain is calculated by Equation 5

$$Q_u = \dot{m} * C_p * (T_o - T_i) \quad (6)$$

The solar energy entering into collector is given by Equation 6

$$Q_s = A_a * G_e \quad (7)$$

3 Results and Discussion

In this section, stability analysis, thermal conductivity and dynamic viscosity measurement of the ferric oxide based nanofluids is presented. The performance analysis of nanofluids is presented in terms of temperature difference and thermal efficiency achieved of the solar CPC system.

3.1 Stability Analysis

Stability analysis of Fe_2O_3/H_2O and Fe_2O_3/EG nanofluids is done with visualization technique. Nanofluids were prepared with 0.075% volumetric concentration. Stability analysis through visualization technique is shown in Figure 3.

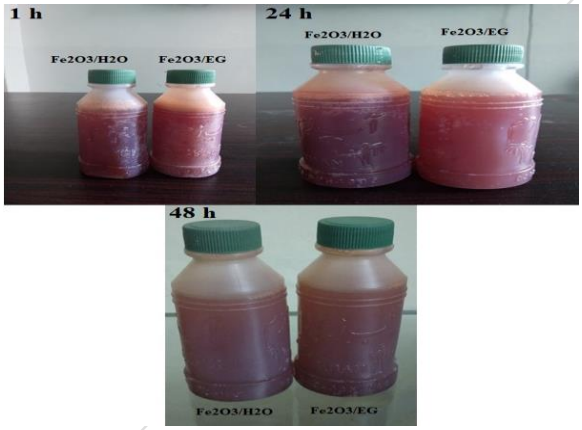

Figure 3: Stability Analysis of Fe_2O_3/H_2O and Fe_2O_3/EG with Visualization Technique

SDBS was used as surfactant with 10% by weight of the nanoparticles present in the base fluid such as water and ethylene glycol. Nanofluids were found to be stable for 48 hours after preparation. Slow sedimentation of nanoparticles occurred after 48 hours.

3.2 Characterization of Nanofluids

Ferric oxide (Fe_2O_3) nanofluids were characterized by measuring the thermal conductivity and dynamic viscosity at three different volumetric concentrations and temperature range. Thermal properties analyzer (TEMPOS) and Brookfield (DV-E) viscometer was used for the measurement of thermal conductivity and Viscosity.

3.2.1 Thermal Conductivity

Thermal conductivity of nanofluids with volumetric concentrations (0.025,0.05,0.075%) at 25°C was measured by TEMPOS thermal analyzer. Average value of thermal conductivity is recorded by taking three measurements for each nanofluid. Thermal conductivity rises when volume fraction (%) of the nanoparticles in base fluid increases. Variation in thermal conductivity of Fe_2O_3/H_2O and Fe_2O_3/EG nanofluids with volumetric concentrations at 25°C is shown in Figure 4.

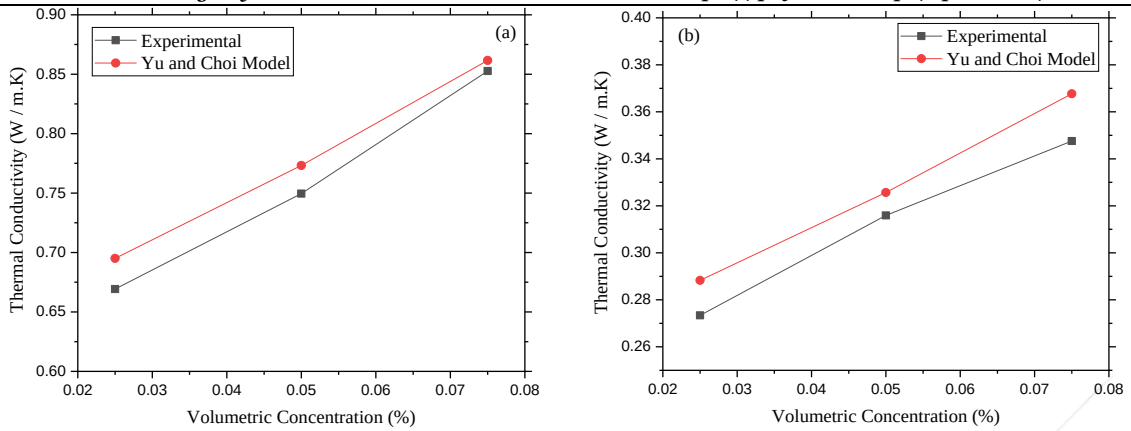

Figure 4: Variation in thermal conductivity ratio with volumetric concentration of (a) Fe_2O_3/H_2O (b) Fe_2O_3/EG

Thermal conductivity of both nanofluids compared with the Yu and choi model (theoretical). The experimental values have shown same trend as obtained through theoretical model. Highest thermal conductivity of the Fe_2O_3/H_2O and Fe_2O_3/EG is obtained by with 0.075% volumetric concentration.

3.2.2 Dynamic Viscosity

Viscosity of nanofluid is critical as it is directly related with the pumping power requirement. In this experimental study the factors affecting viscosity of the nanofluids were examined such as temperature and volumetric concentration of nanoparticles in base fluid.

Viscosity of the nanofluids decreases with the increase in temperature and increases with the increase in volumetric concentration of nanoparticles in base fluid. Variation in dynamic viscosity of Fe_2O_3/H_2O and Fe_2O_3/EG nanofluids with different volumetric concentrations and temperature (20,40,60°C) at 100 rpm is shown in Figure 5.

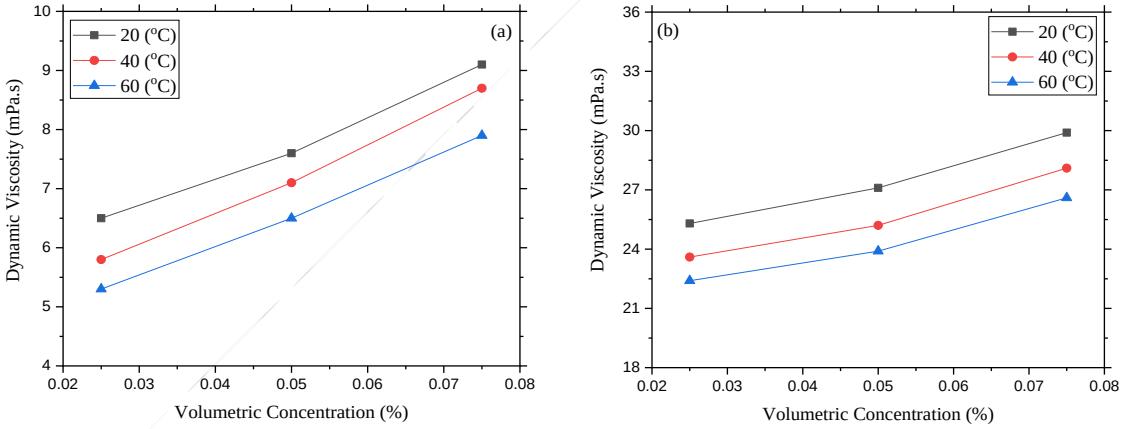

Figure 5: Variation in viscosity with temperature and volumetric concentration of (a) Fe_2O_3/H_2O (b) Fe_2O_3/ EG

Weakening of intermolecular bonding occurs at elevated temperatures because the molecules absorb more energy, move faster. This results in decrease in viscosity at elevated temperatures. RV-1 spindle was used for the experimentation with fixed spindle speed of 100 rpm. Fe_2O_3/EG nanofluids have more viscosity then the Fe_2O_3/H_2O nanofluids.

3.3 Performance of Solar CPC

Performance parameters such as temperature difference and efficiency of the system are used for the analysis of CPC solar collector obtained by using ferric oxide based nanofluids with multiple volumetric concentrations at two flowrates (0.01kg/s, 0.02kg/s). Performance of the nanofluid is also compared with the conventional fluids such as water and ethylene glycol.

3.3.1 Weather Conditions

Ambient temperature and solar radiations were measured with the help of K-type thermocouple and Pyranometer

respectively. The weather conditions of Taxila, Pakistan for March and April is shown in Figure 6.

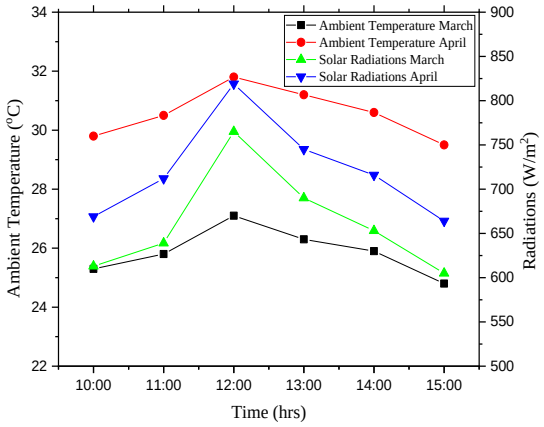

Figure 6: Weather Conditions of March and April

The overall impact of ambient temperature changes from 25°C to 32°C while radiations changes from 600 W/m^2 to 820 W/m^2. The peak value of ambient temperature and solar radiations is recorded at 12:00 hours.

3.3.2 Temperature Difference

Temperature difference is obtained by the temperatures of fluid measured with the help of K-type thermocouple inserted at inlet and outlet of the absorber tube. Comparison of the temperature difference of nanofluids with 0.025% and 0.075% volumetric concentration at 0.02 kg/s and 0.01 kg/s is shown in Figure 7 and Figure 8 respectively.

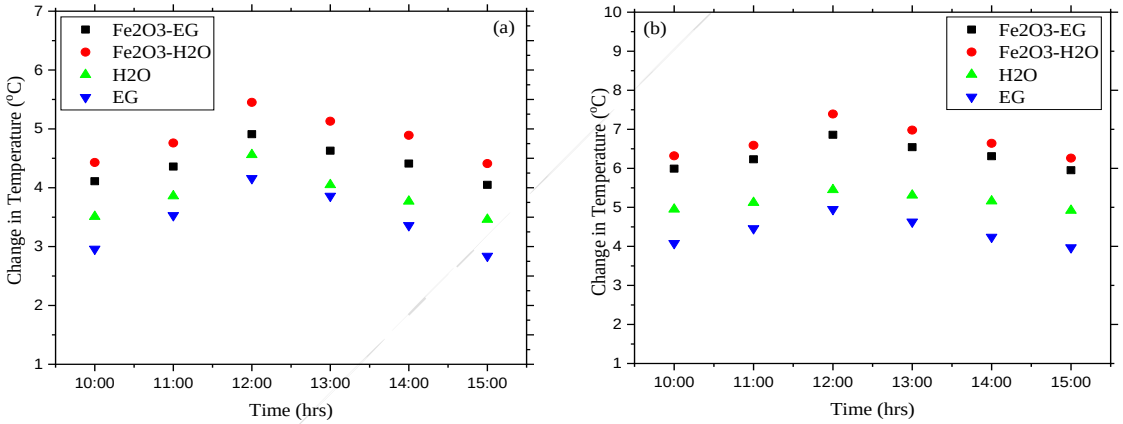

Figure 7: Temperature Difference of Nanofluids with 0.025% Volumetric Concentration at (a) 0.02kg/s (b) 0.01kg/s

The maximum temperature difference is achieved by utilizing Fe_2O_3/H_2O nanofluid. Temperature differences of 5.45°C and 7.39°C are achieved for 0.025% volumetric concentration at 0.02, 0.01kg/s respectively and temperature differences of 6.25°C and 8.59°C are achieved for 0.075% volumetric concentration at 0.02 kg/s, 0.01kg/s respectively. It is evident from the results that temperature difference is increasing with the decrease in the flowrate of the system. Nanofluids have higher temperature difference than the water and ethylene glycol.

3.3.3 Thermal Efficiency

Comparison of the thermal efficiency of the nanofluids with 0.025% and 0.075% volumetric concentration of nanoparticles at multiple flowrates is shown in Figure 9 and Figure 10 respectively.

Thermal efficiency indicates the overall performance of solar thermal collector which directly changes with intensity of solar radiations. At constant flow rate and weather conditions, the thermal performance of CPC increases due to enhanced surface area nanofluids properties. The maximum thermal efficiency of CPC is obtained by utilizing Fe_2O_3/H_2O nanofluid. Thermal efficiencies of 65.04% and 53.55% are achieved for 0.025% volumetric concentration at 0.02, 0.01kg/s respectively. Thermal efficiencies of 74.59% and 57.26% are attained for 0.075% volumetric concentration at 0.02, 0.01kg/s respectively. Thermal efficiency of CPC is decreasing with the decrease in flowrate of the system as seen from the results.

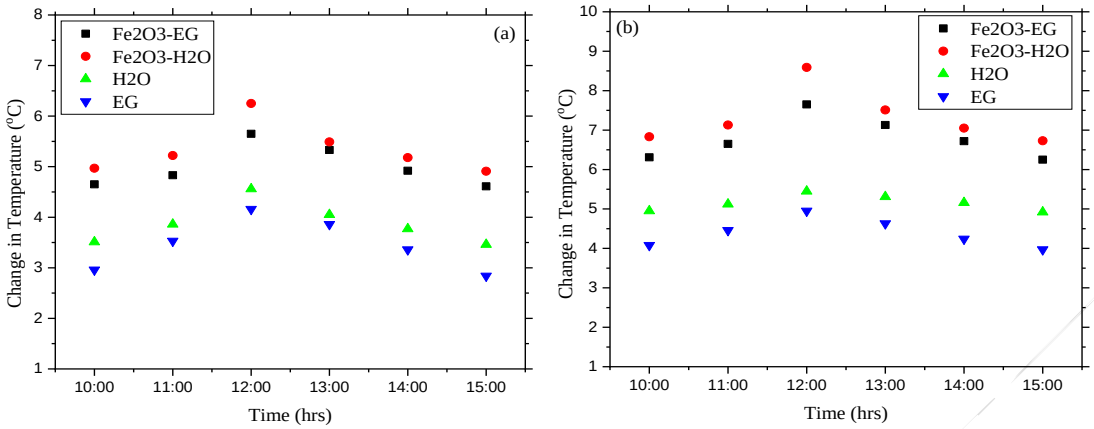

Figure 8: Temperature Difference of Nanofluids with 0.075% Volumetric Concentration at (a) 0.02kg/s (b) 0.01kg/s

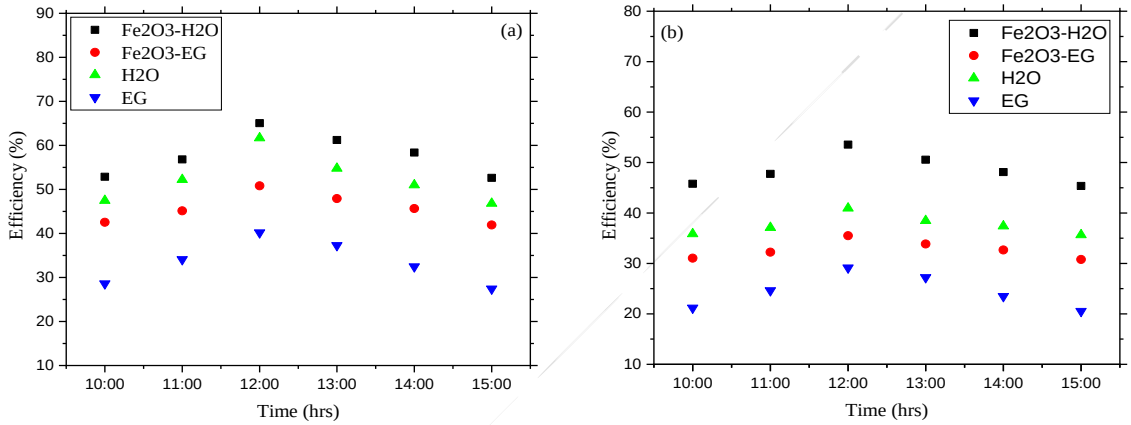

Figure 9: Thermal Efficiency of Nanofluids with 0.025% Volumetric Concentration at (a) 0.02kg/s (b) 0.01kg/s

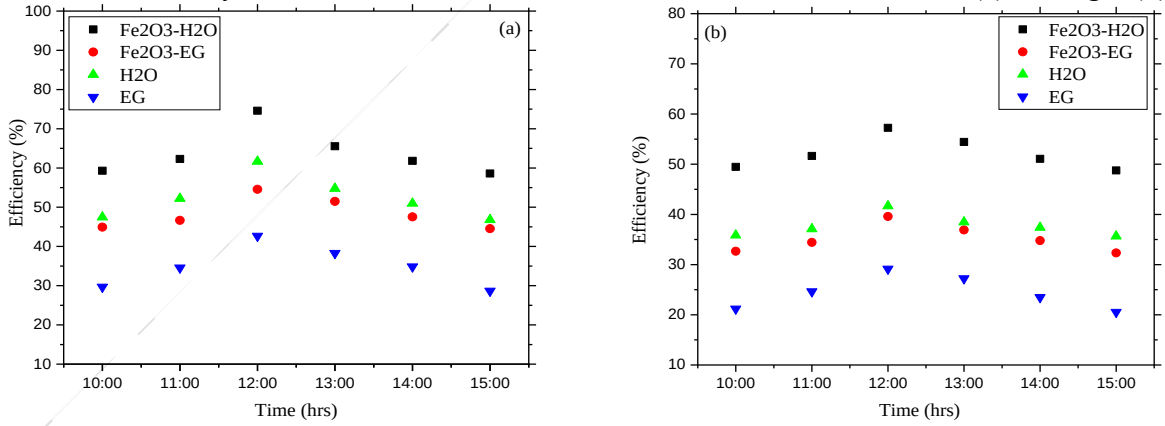

Figure 10: Thermal Efficiency of Nanofluids with 0.075% Volumetric Concentration at (a) 0.02kg/s (b) 0.01kg/s

4 Conclusion

In this experimental study, stability analysis and characterization of Fe_2O_3 based nanofluids is carried out. The performance of non-tracking, stationary solar compound parabolic collector is evaluated in typical subtropical climatic conditions of Taxila, Pakistan. Stability analysis is carried out with the help of visualization technique. Prepared samples of Fe_2O_3/H_2O and Fe_2O_3/EG with 0.075% volumetric concentration were examined for 48 hours after preparation. Nanofluids were found to be stable. Thermal conductivity is measured with the help of TEMPOS thermal analyzer and compared with the theoretical model. The results revealed that the maximum thermal conductivity enhancement of 30.8% is achieved for Fe_2O_3/H_2O with 0.075% volumetric concentration at

25ºC. The performance analysis of the solar CPC is conducted using two mass flowrates (0.02 kg/s, 0.01kg/s) under different ambient temperatures from 25°C to 32°C. The maximum outlet temperature obtained by the solar collector was 59ºC for Fe_2O_3/H_2O nanofluids at 0.01 kg/s with 0.075% volumetric concentration. In addition, maximum temperature difference and thermal efficiency of 8.59ºC and 74.59%, respectively is attained for Fe_2O_3/H_2O with 0.075% volumetric concentration at 0.02 kg/s. Maximum thermal efficiency enhancement of 31.49% is achieved for Fe_2O_3/H_2O with 0.075% volumetric concentration at 0.01 kg/s. Finally, as seen from the results, nanofluids shown better results as compared to the conventional fluids such as water and ethylene glycol utilized in the study. Low flowrate of the nanofluids yield higher temperature differences but low thermal efficiencies. Fe_2O_3/H_2O is more suitable to use in CPC as compared to Fe_2O_3/EG. Array of CPC in series and parallel combination and hybrid nanofluids can be utilized in future for better thermal performance of solar CPC.

5 References

[1] G. Mittelman, M. Epstein, "A novel power block for CSP systems," Sol. Energy, vol. 84, pp. 1761-1771,2010.

[2] U.K. Mirza, M.M. Maroto-valer, N. Ahmad, "Status and outlook of solar energy use in Pakistan," vol. 7, pp.501–514,2003.

[3] A.W. Bhutto, A.A. Bazmi, G. Zahedi, "Greener energy: issues and challenges for Pakistan-solar energy prospective," Renew. Sustain. Energy Rev., vol. 16, pp. 2762-2780,2012.

[4] Hachicha, A. A. et al., "Heat Transfer Analysis and Numerical Simulation of a Parabolic Trough Solar Collector," *Applied. Energy*, vol. 111, pp. 581–592,2013.

[5] J. Akhter, S.I.Gilani, H.H. Al-kayiem, et al. "Optical performance analysis of single flow through and concentric tube receiver coupled with a modified CPC collector under different configurations," *Energies*,Vol. 12,2019.

[6] J. Akhter, S.I.Gilani, H.H. Al-kayiem,et al. "Experimental evaluation of thermophysical properties of oil-based titania nanofluids for medium temperature solar collectors," *Materialwissenschaft und Werkstofftechnik,* Vol. 51, pp. 792-802, 2020.

[7] F. Akhtar, M. Ali, N.A. Shiekh, M. Shehryar, "Experimental Investigation of Solar Compound Parabolic Collector Using Al_2O_3/H_2O Nanofluid in a Subtropical Climate," *Thermal Science*, 2020.

[8] L. Lu, Z. H. Liu, and H. S. Xiao, "Thermal performance of an open thermosyphon using nanofluids for high-temperature evacuated tubular solar collectors. Part 1: Indoor experiment," *Sol. Energy*, vol. 85, pp. 379–387, 2011.

[9] Z. H. Liu, R. L. Hu, L. Lu, F. Zhao, and H. S. Xiao, "Thermal performance of an open thermosyphon using nanofluid for evacuated tubular high temperature air solar collector," *Energy Convers. Manag.*, vol. 73, pp. 135–143, 2013.

[10] M. A. Rehan, M. Ali *et al.*, "Experimental Performance Analysis of Low Concentration Ratio Solar Parabolic Trough Collectors with Nanofluids in Winter Conditions," *Renewable Energy*, vol. 118, pp. 742-751, 2017.

[11] I. M. Mahbubul, E. B. Elcioglu, M. A. Amalina, and R. Saidur, "Stability, thermophysical properties and performance assessment of alumina–water nanofluid with emphasis on ultrasonication and storage period," *Powder Technol.*, vol. 345, pp. 668–675, 2019.

[12] N. A. Bin-Abdun *et al.*, "Heat transfer improvement in simulated small battery compartment using metal oxide (CuO)/deionized water nanofluid," *Heat Mass Transf. und Stoffuebertragung*, vol. 56, no. 2, pp. 399–406, 2020.

[13] M. Warjri and J. Narayan, "Synthesis, characterization and physicochemical properties of cupric oxide nanoparticles and their nanofluids," *Mater. Today Proc.*, vol. 18, pp. 1176–1184, 2019.

[14] US Research Nanomaterials, Inc, Iron Oxide Nanopowder/Nanoparticles, Available at: *http://www.usnano.com/inc/sdetail/233*.

[15] A. Gallego, K. Cacua, B. Herrera, D. Cabaleiro, M. M. Piñeiro, and L. Lugo, "Experimental evaluation of the effect in the stability and thermophysical properties of water-Al2O3 based nanofluids using SDBS as dispersant agent," *Adv. Powder Technol.*, vol. 31, no. 2, pp. 560–570, 2020.

[16] W. Yu, S.U.S Choi, "The role of interfecial layers in enhanced thermal conductivityof nanofluids: a renovated maxwell model," *Journal of nanoparticle research*, vol. 5, pp.167-171, 2003.

[17] A. B. Kasaeian, "Convection Heat Transfer Modeling of Ag Nanofluid Using Different Viscosity Theories," *IIUM Eng. J.*, vol. 13, 2012.

[18] E. Bellos, D. Korres, C. Tzivanidis, and K. A. Antonopoulos, "Design, simulation and optimization of a compound parabolic collector," *Sustain. Energy Technol. Assessments*, vol. 16, pp. 53–63, 2016.

Comparison of Experimental and CFD analysis of Vortex Tube Using Different RANS Models

Mehran Meer*, Hamza Awan, Fawad Ali , Ameer Hamza, Hamza Sajid, Muhammad Ali Kamran

Mechanical Engineering Department, University of Engineering and Technology Peshawar, Peshawar 25000

**Corresponding author*

Email: mehranmeer77@gmail.com

Abstract

The Energy separation phenomena in Vortex tube is always remained a matter of interest for its turbulent nature. The current study focuses on swirl flow behavior of vortex tube considering different RANS turbulence models, namely Standard k- ε, Kω -SST, k-kl-ω and Transition SST. For this purpose Numerical study was carried out on a 3D model, using four RANS models. A Computational domain has been created in ICEM –CFD using air as a fluid medium. The simulations were carried out in fluent codes. Vortex tube with identical dimensions was manufacture and tested with same operating conditions. The validation was performed by comparing the numerical simulation results in term of cold temperature, against the experimental results. RANS models were able to project the general flow behavior in the vortex tube. The standard K- ε model predicted the thermal separation in good agreements with the experimental results. Therefore Standard K- ε turbulent model is recommended for any further investigation.

Key words: CFD Analysis, Energy separation, Swirl flow, turbulent models.

Introduction

Vortex Tube is a simple mechanical device without any moving parts, which produces two streams of different temperature simultaneously from a single injection of pressurized gas. It requires less maintenance and do not need any electrical or chemical driven mechanism. This swirl flow in the vortex tube is created by tangential introduction of the compressed air through the nozzles into the tube, which gives rise to the two circular vortices, one at the periphery with hotter air and other at the centre of the tube with the colder air. The difference between the two temperatures is term as temperature separation..

Vortex tube can be classified into two groups that are parallel and counter flow vortex tubes. The schematic of the standard counter flow vortex tube is shown in the Figure 1. It consists of a vortex generator that has tangential inlets, a long main tube where the temperature separation occurs, a cold exhaust from where the core cold stream exits the vortex tube, and a hot exhaust from where the peripheral hot stream exits the vortex tube. The hot side is also equipped with a control plug that is cone-shaped and that is directly responsible for controlling the cold mass fraction. It mainly pushes back the flow of the inner vortex in opposite direction, which come out on the cold exit on the other end of tube.

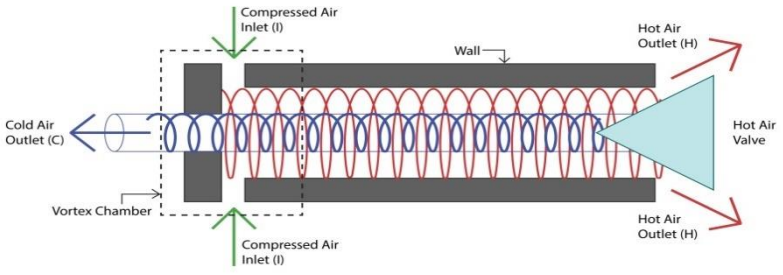

Figure 1: Schematic diagram of Vortex tube flow

In spite of the fact that this cooling device has low COP, the simplicity of the device and its low maintenance and cost makes it a desirable for many low temperature applications. Refrigeration by Vapor

Compression is undesirable in small scale cooling Which includes, Spot Cooling, Dehydration of gases, Electrical Panel Cooling and Personalize Cooling (Avdhoot N. Jejurkar, 2015). Keeping in mind the importance and advantages of the Vortex tube, Researchers have used various Experimental, analytical and Numerical approach to study the thermal separation phenomenon in the Vortex tube.

This device was discovered by Ranque in 1933 (RANQUE 1933) and later on improved by Hilsch in 1947 (Hilsch 1947). Different theories were presented to explain the phenomena of temperature separation by different Scientists. Kassner and Knoernschild introduce the free and force vortex theory(Kassner and Knoernschild 1948), Kurosaka proposed acoustic streaming theory (Kurosaka 1982), Ahlborn and Groves gave secondary circulation theory (Ahlborn and Groves 1997). Due to some limitations of the experimental work, some attempts were also made to find the concepts behind energy separation using Computational fluid dynamics (CFD).In this regards, Frohlingsdrof et al. (Fröhlingsdorf and Unger 1998) studied the energy separation in the vortex tube tube using $K-\varepsilon$ model. Aljuwayhel et al. (Aljuwayhel, Nellis, and Klein 2005) simulated a 2D axisymmetric CFD model to find the fluid flow in the vortex tube. Skye used commercially available vortex tube for comparison (Skye, Nellis, and Klein 2006). Rattanongphisat et al. (Rattanongphisat, Riffat, and Gan 2008) proposed a 3D numerical studies using the standard ke 3 model to study the physical behaviour of the flow such as temperature and pressure inside the vortex tube. Eimsa-ard et al. (Eiamsa-ard and Promvonge 2007) selected Algebraic Stress Model (ASM) and Standard k-ε turbulence model. ASM had good agreement with experimental results on comparison.

Methods

Physical Model:

A standard vortex was designed which was later on manufactured. It mainly consists of the Hot side tube , Cold side tube, Chamber, and Control Valve. The design perimeters and dimensions of the model is given table 1. Six tangential nozzles were used as an inlet. Aluminum was selected as a material for the manufacturing of the Vortex tube. To compare and validate the experimental results a similar 3D CFD model was also generated having same perimeters.

Table 1: Geometer Parameters of the Model

Total Tube Length	170mm
Hot side Length	140mm
Cold Side Length	30mm
Working Tube Diameter	14mm
Cold orifice Diameter	3mm
Nozzle Diameter	2mm
Number of Nozzles	6

Experimental Work:

For the testing of vortex tube, a testing rig was developed. The rig is capable of measuring different measurable variables that is pressure, temperature and mass flow on each side. The rig is capable of measuring three temperatures known as T1, T2, and T3 by using K-type thermocouples. T1 is the temperature of the inlet air, T2 is the temperature of the hot side stream and T3 is the temperature of the cold side stream, and all of these temperatures were displaced on temperature indicators. Additionally, two mass flow meters and a pressure gauge were also used for measuring mass flow rate on hot and cold sides and pressure of inlet air, respectively. The experimental setup is presented in Figure 2.

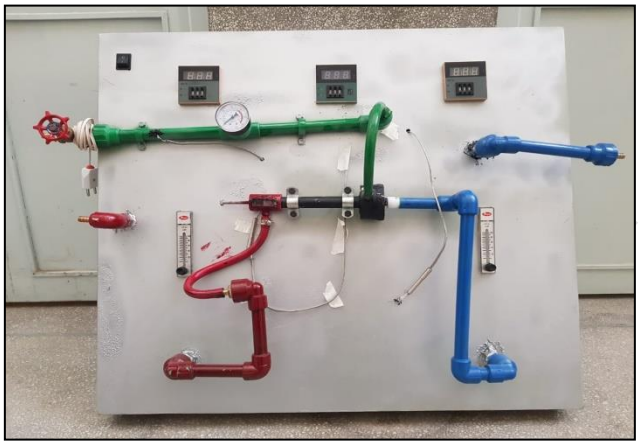

Figure 2: Experimental Setup

Numerical Approach:

Mesh:

A three dimensional geometrical model is design in CAD software used for the numerical study. The geometrical parameters of this model corresponds to the parameters of the experimental vortex tube.. For better accuracy a structured meshing domain has been created in ICEM CFD. The ICEM-CFD is an integrated tool in Ansys Workbench that is used for generating a structured mesh, an unstructured mesh, or a combination of these known as the hybrid mesh. It should be recognized that all the dimensions of the parts are kept constant with the experimental one. The structured mesh is generated using O grid technique. computational domain has been shown in Figure 3

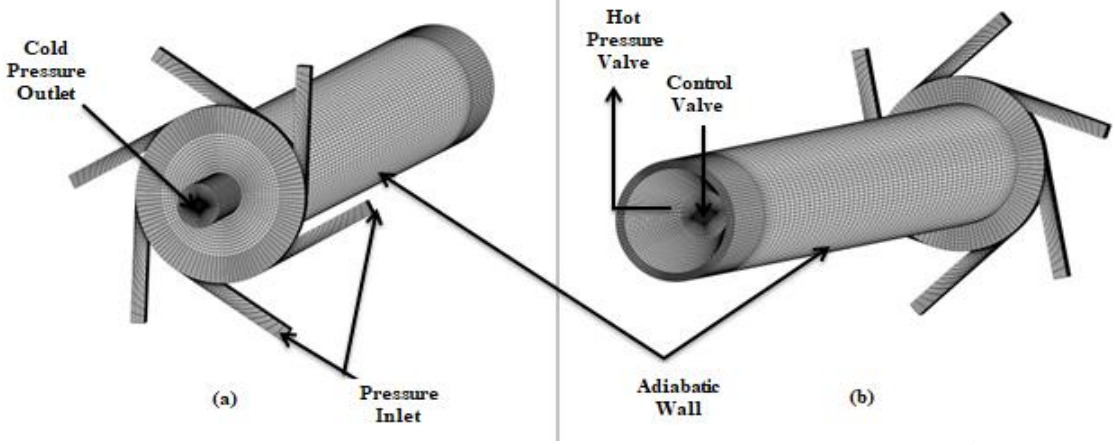

Figure 3: a) Meshing Front View b) Meshing back view

Governing Equations:

Flow is considered as the compressible. The following governing equations are numerically solved for mass, momentum, and energy conservation, respectively.

Continuity Equation:

$$\frac{\partial}{\partial x_i}(\rho u_i) = 0 \qquad (1)$$

Momentum Equation:

$$\frac{\partial}{\partial x_j}(\rho u_i u_j) = \frac{\partial p}{\partial x_i} + \frac{\partial}{\partial x_j}\left[\mu\left(\frac{\partial u_i}{\partial x_j} + \frac{\partial u_j}{\partial x_i} - \frac{2}{3}\delta_{ij}\frac{\partial u_k}{\partial x_k}\right)\right] + \frac{\partial}{\partial x_j}\left(\overline{-\rho u_i' u_j'}\right) \qquad (2)$$

Energy Equation:

$$\frac{\partial}{\partial x_i}\left[u_i \rho\left(h + \frac{1}{2}u_j u_j\right)\right] = \frac{\partial}{\partial x_j}\left[K_{eff}\frac{\partial T}{\partial x_j} + u_i(\tau_{ij})_{eff}\right] \qquad (3)$$

Where,

$$K_{eff} = K + \frac{c_p \mu_t}{Pr_t} \qquad (4)$$

u_i = rate of total energy lost due to convection

K_{eff} = Heat transfer due to conduction

$(\tau_{ij})_{eff}$ = Energy Dissipation

To consider for compressibility effect, flow behavior, the ideal gas equation is employed given below:

$$p = \rho RT \qquad (5)$$

It should be noted that all the four turbulence models are selected to see the solution accuracy effects due to turbulence modeling.

Boundary Conditions:

For analysis, It is necessary to define boundary conditions at Inlets, wall, and outlets.

At inlet the pressure inlet boundary condition is 500000-pascal pressure as gauge pressure and thermal boundary conditions as 305 K inlet temperature was defined.

For outlets, we have two outlets in this case at the hot side; pressure outlet boundary conditions were defined. The value of pressure is varied to get the different cold mass fraction. At the cold side, pressure outlet boundary conditions were defined. The pressure values are kept at ambient conditions, that is 101325 pa. Walls are defined with adiabatic wall boundary conditions with no slip. The heat flux at wall is consider as 0 W/m^2

Computations start off with the pressure based solver and steady state conditions. Simple algorithm is used for the velocity coupling. The convergence basis on residual scale is set to 10-6 for energy and 10-3 for both continuity and momentum.

Results

Computations start off with the pressure based solver and steady state conditions. Simple algorithm is used for the velocity coupling. The convergence basis on residual scale is set to 10-6 for energy and 10-3 for both continuity and momentum. The setup was run in Ansys Fluent and Tech plot and Ansys post processing is used for all the solutions.

This section mainly focuses on the validation of the numerical models and flow visualization. Results from each model were compared with obtained experimental data. Figure 4 show the temperature distribution for all the numerical models.

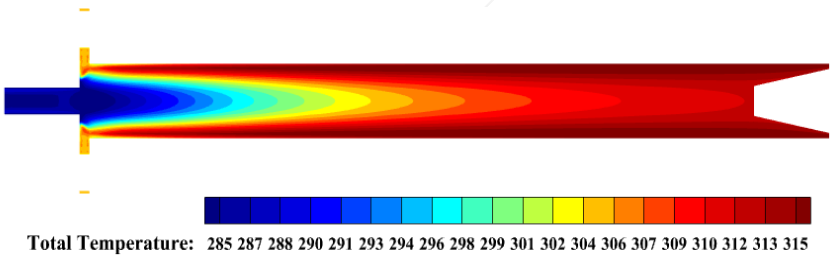

Standard K-ε

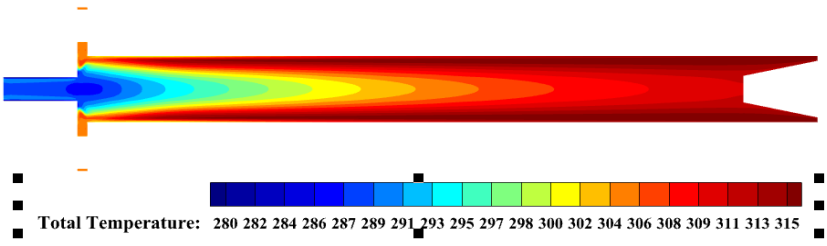

SST K-ω

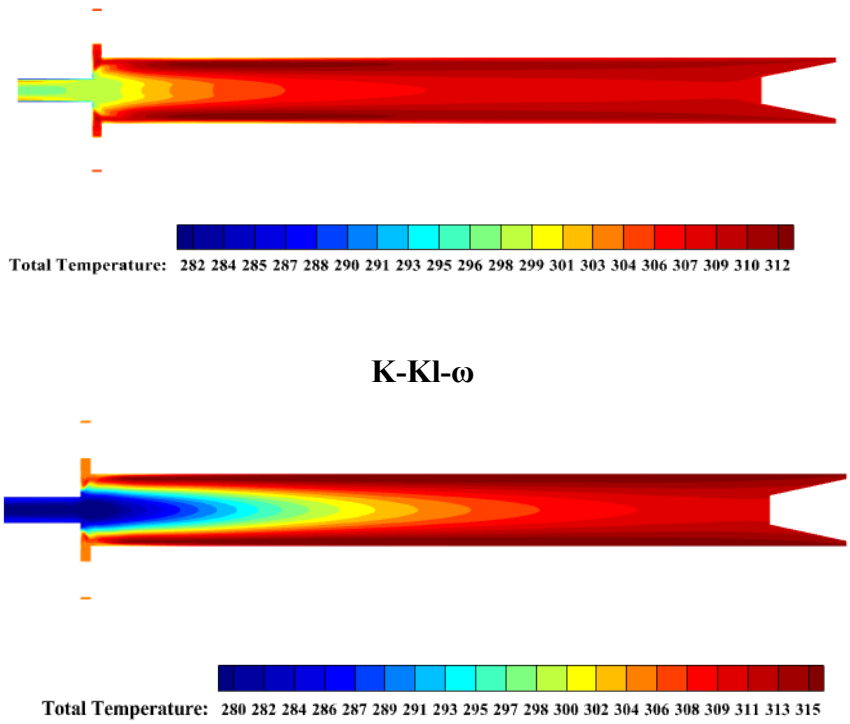

Figure 4: Temperature Contour by Different Turbulent models

From Figure 4, one can observe the difference among these models based on temperature distribution. For Standard K- ε model and Transition SST model, the cold temperature contour represents a very similar temperature distribution. However, For the SST K-ω model, the cold temperature distribution is gradually limited to 291 K temperature. This clearly shows that temperature distribution by the SST K-ω model is different from the above models. And finally, looking at K-Kl-ω model-based temperature distribution results, it has cooled the core vortex with minimum effects as compared to the other models.

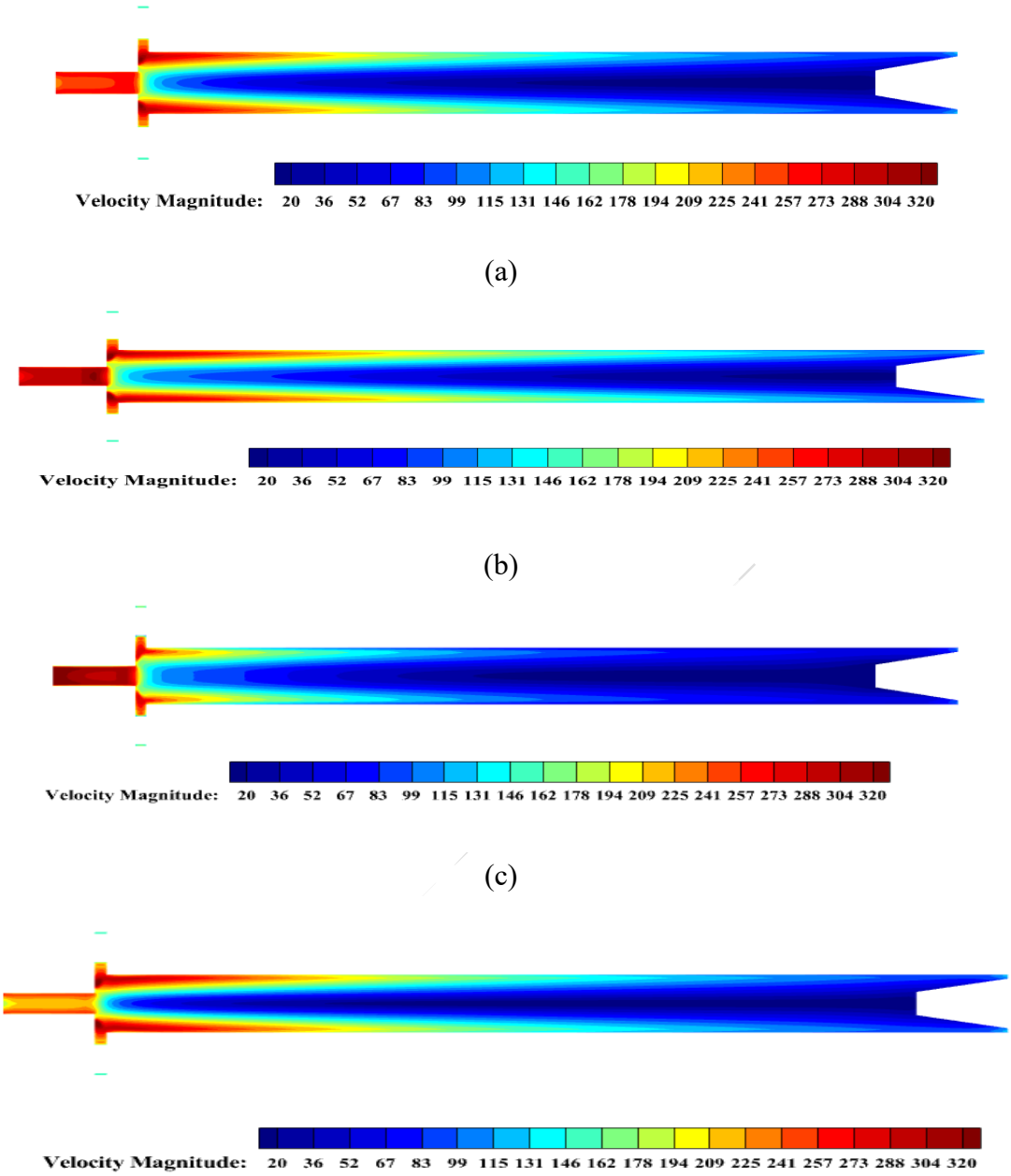

Figure 5: Velocity Magnitude Results a) K- ε model b) Transition SST model c) SST K-ω d) K-Kl-ω

From Fig 5 the k-ε model and Transition SST model show the behavior of velocity friction phenomena clearly. Because it shows that the cold vortex is flowing with a very low-velocity magnitude while the peripheral vortex flows with a very high magnitude of velocity. However, the k-kl-ω model shows a weak velocity distribution in terms of internal frictions.

Figure 6 below shows that a high turbulent viscosity can be found on the central region of the vortex tube predicted by the Transition SST model in a range of 0.14 to 0.16 kg/m-s. In the case of the standard k-ε model, the range for turbulent viscosity is between 0.09 to 0.1 kg/m-s. This shows optimum turbulences The k-kl-ω and k-ω SST model predicted a low turbulence effect and this was the reason due to which cold temperature

did not reach the experimental value. Thus, one can relate the turbulences to the thermal separation that thermal separation is high in RHVT when the turbulence is highly captured by the RANS model.

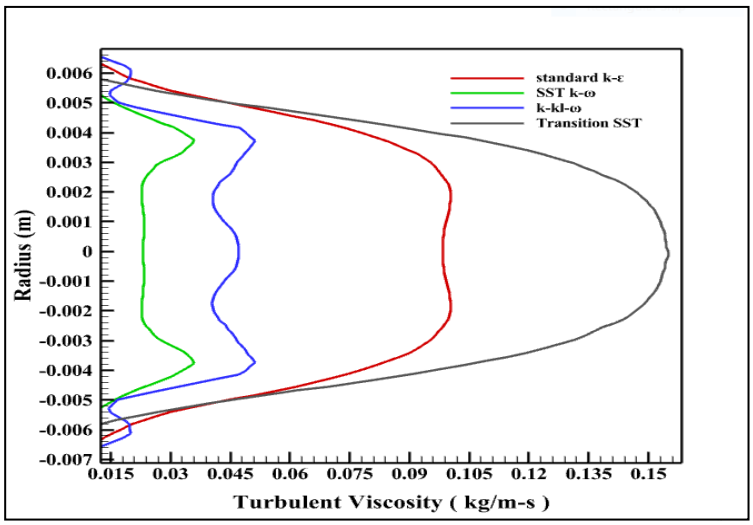

Figure 6: Turbulent Viscosity Predictions by Different Models along Radial Length

The pressure and velocity distribution along radial path using RANS models is discussed next. The pressure and vecloity distribution for all the models is shown in Figure 7.

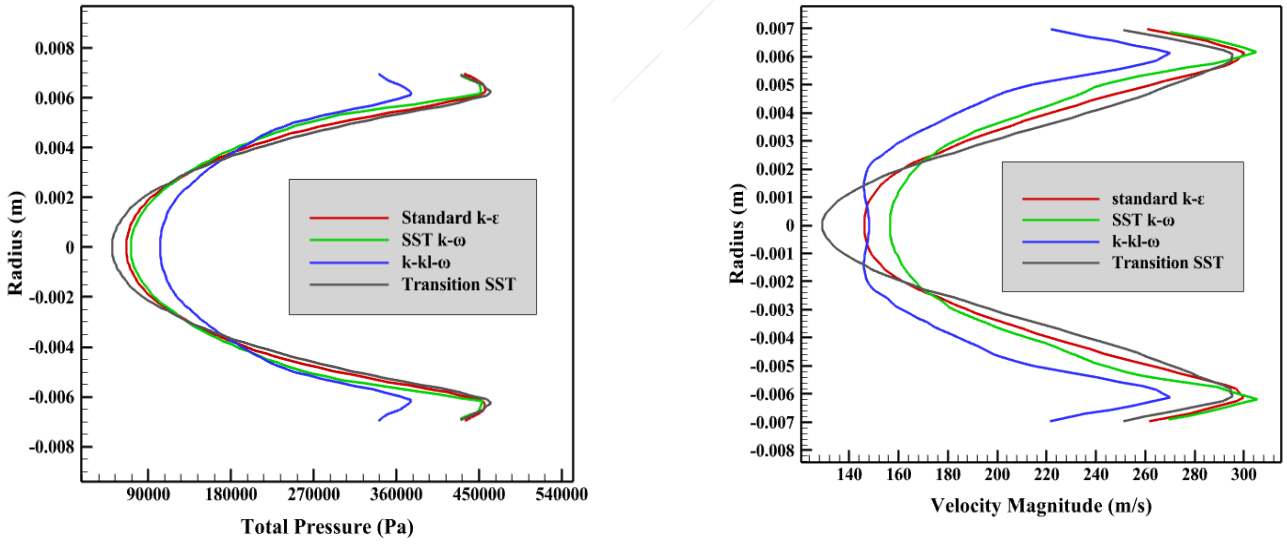

Figure 7: (a) Pressure distribution along radial direction using different models, (b) Velocity distribution along radial direction using different models.

From Figure 7, it is seen that the transition between the minimum and maximum velocity is very high by k-ε and the Transition SST model. On the other hand, this effect is very low predicted by the low Reynold turbulence models.

The same effect has been shown on total pressure plots below, where the pressure range for Standard K-ε and Transition SST is 50000 Pa to 470000 Pa. On the other hand, the pressure range for the K-Kl-ω model is between 110000 Pa to 380000 Pa.

It is necessary to validate our numerical results with the experimental result so that one can confidently

proceed with any numerical investigation further. For this purpose following two parameters were considered

I. Cold Temperature: this is the temperature observed at the cold side of the vortex tube. It is formed when the swirl flow of the vortex tube passes through the cold orifice. It has been measured in kelvin.

II. Cold Mass Fraction (α): it is the ratio of cold mass flow rate to the total inlet flow rate. It is a dimensionless number that has an inverse relationship with the drop in cold temperature.

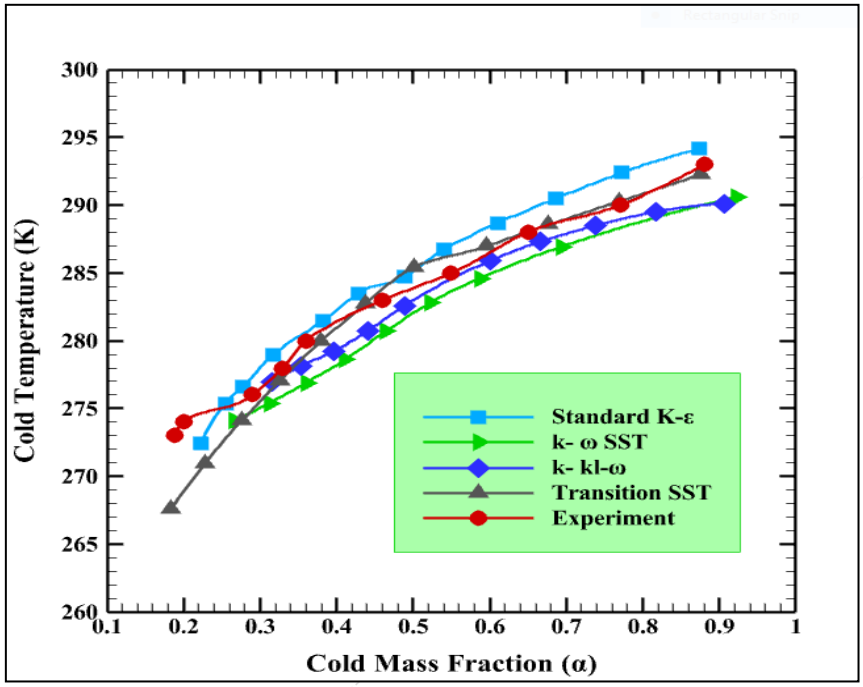

Figure 8: CFD Validation with Experimental Results using Different Turbulent Models

In the above the comparison is done between the four RANS models and Experimental result. The standard k-ε model predicted that the temperature separation is in good agreement with the experimental behavior. At low cold mass fraction, it predicts a high drop in cold temperature while as the mass fraction increases the temperature drop decreases. In a similar pattern, the Transition SST model also predicts a good thermal separation almost similar to the K-ε model. The figure shows that it predicts very well thermal separation when the cold mass fraction is low, however, it under predicts the results as the cold mass fraction is increased. Whereas the 2 equations RANS model K-ω SST under predicted the numerical results.

From these reasons standard k-ε model is prefer over other turbulent models. Therefore it is recommended to be used for any further investigation.

Conclusions

A three dimensional numerical simulations were carried out for the various turbulent models. Their results were validated with the obtained experimental results. Base on the numerical and experimental results following conclusions were made.

- It has been concluded from the temperature contours that the standard K-ε model and Transition SST cooled the core vortex with the maximum effect.

- From the Velocity magnitude results, K-ε model shows the velocity friction phenomena clearly followed by Transition SST model.
- The turbulent viscosity or eddy viscosity is an indicator that tells how much the flow is turbulent. K-ε model vortex tube predicts the optimum range of turbulent viscosity among others turbulent models.
- It is observed from pressure distribution plot that transition SST model under predict while k kl w over predict the values.
- In velocity, SST omega over predict while transition sst under predict the velocity profile.
- It was concluded that the Standard K-ε model predicts the results in good agreement with the experimental results. Therefore, it is recommended to be used for any further investigations.

References

.Ahlborn, Boye, and Stuart Groves. 1997. "Secondary Flow in a Vortex Tube." *Fluid Dynamics Research* 21(2):73–86. doi: 10.1016/S0169-5983(97)00003-8.

Aljuwayhel, N. F., G. F. Nellis, and S. A. Klein. 2005. "Parametric and Internal Study of the Vortex Tube Using a CFD Model." Pp. 442–50 in *International Journal of Refrigeration*. Vol. 28.

Eiamsa-ard, Smith, and Pongjet Promvonge. 2007. "Numerical Investigation of the Thermal Separation in a Ranque-Hilsch Vortex Tube." *International Journal of Heat and Mass Transfer* 50(5–6):821–32. doi: 10.1016/j.ijheatmasstransfer.2006.08.018.

Fröhlingsdorf, W., and H. Unger. 1998. "Numerical Investigations of the Compressible Flow and the Energy Separation in the Ranque-Hilsch Vortex Tube." *International Journal of Heat and Mass Transfer* 42(3):415–22. doi: 10.1016/S0017-9310(98)00191-4.

Hilsch, R. 1947. "The Use of the Expansion of Gases in a Centrifugal Field as Cooling Process." *Review of Scientific Instruments* 18(2):108–13. doi: 10.1063/1.1740893.

Kassner, Rudolf, and Eugen Knoernschild. 1948. "Friction Laws and Energy Transfer in Circular Flow - Technical Report No. F-TS-2198-ND."

Kurosaka, M. 1982. "Acoustic Streaming in Swirling Flow and the Ranque-Hilsch (Vortex-Tube) Effect." *Journal of Fluid Mechanics* 124:139–72. doi: 10.1017/S0022112082002444.

RANQUE. 1933. "Experiencesd Sur La Detente Giratoire Avec Productions Simultanes d'un Echappment d'air Chand et d'un Echappment d'air Froid." *J. Phys. Radium* 112–14.

Rattanongphisat, W., S. B. Riffat, and G. Gan. 2008. "Thermal Separation Flow Characteristic in a Vortex Tube: CFD Model." *International Journal of Low-Carbon Technologies* 3(4):282–95. doi: 10.1093/ijlct/3.4.282.

Skye, H. M., G. F. Nellis, and S. A. Klein. 2006. "Comparison of CFD Analysis to Empirical Data in a Commercial Vortex Tube." *International Journal of Refrigeration*. doi: 10.1016/j.ijrefrig.2005.05.004.

Batch Scale Biodiesel Production from Waste Cooking Oil

Mehmood Ali[1]*, Muhammad Shahid[1]

[1] *Department of Environmental Engineering, NED University of Engineering and Technology, Karachi-75270, Pakistan*

[1*]*Corresponding author Email: mehmood@neduet.edu.pk*

Abstract

Utilization of conventional fossil fuels in power generation and transportation sectors increased the concentration of greenhouse gases in the atmosphere promoting climate change/ global warming issues. Therefore, biofuels (biodiesel and bioethanol) are getting importance for mitigating greenhouse gas emissions. Basically the scope of this research study was to design and fabricate 10 L batch scale biodiesel production unit based on considering mass balance of the system components such as; storage container, methoxide mixing vessel and reactor vessel with mixer. The volume occupied by waste cooking oil (WCO) and methanol/ catalyst mixture in the reactor was found to be 10 L. The reactor capacity was found 14.5L, whereas the methoxide mixing chamber volume was calculated as 2.5 L, assuming 20% excess volume in the reactor as free board space. WCO was converted successfully into biodiesel by two step esterification /transesterification reactions. In pre-treatment reaction, oil to methanol ratio 5:1 and 0.2 % sulphuric acid by weight of WCO was used, while the reaction time was 2 hrs to complete with continuous stirring at 700 rpm and at a reaction temperature of 65°C. For second step reaction, the molar ratio was 5:1 (WCO/methanol) and base catalyst (KOH) was 1% by weight of WCO. The reaction temperature and time were 65 ˚C and 1hr respectively with agitating the mixture at 700 rpm. WCO Biodiesel conversion yield of 97% was obtained, while 2.6 % glycerol was recovered as a by-product. WCO biodiesel produced physico-chemical properties were found in accordance with International Biodiesel Standards (ASTM D6751 and EN 14214). Mass balance performance (%) of WCO biodiesel produced was calculated as 78.3 %. Biodiesel produced from WCO reduces the use of recycled edible oil that is unfit for human consumption, while also lowering waste management costs.

Key words: Biodiesel; Transesterification; Waste Cooking Oil; Alternate fuel; Renewable energy

1. Introduction

The earth's existing fossil fuel supplies are being depleted at an alarming rate, causing a negative impact on the ecology. To the aforementioned issues, power generation and transportation are considered key contributors in degrading environment causing climate change and global warming [1]. Over the last few years, there has been a trend among the general public toward renewable energy sources for power generation and transportation systems, as well as the development and consumption of biofuels [2]. Biodiesel is becoming popular biofuel because it serves a dual purpose: it is an environmentally beneficial fuel that emits less carbon, sulphur content and having ample supply of raw materials for its production such as waste cooking oils (WCO). Producing biodiesel from waste cooking oil (WCO) is one of the best alternative fuels for reducing emissions caused by compression ignition engines. It can reduce emissions by up

to 85% due to lower hydrocarbon, SO_2, CO and smoke emissions in the engine exhaust. However, CO_2 and NOx levels were found higher as compared to mineral diesel. WCO biodiesel is suitable for any diesel engine from a technical, economic, environmental, and tribological standpoint [3]. However, while producing biodiesel from WCO is a cost-effective method, the high free fatty acid (FFA) in WCO is a major bottleneck in the transesterification process. WCO is exposed to esterification utilising acid catalysts for catalysed reaction to lower FFA content, if the acid value of WCO is above 5.5 mg KOH/g, indicating increased FFA content. FFA level was reduced to 88.8% at 60°C with a 1:2.5 methanol to oil molar ratio in a previous study. Then, at 50 °C, transesterification was carried out in the presence of an alkali catalyst (KOH), and the yield of fatty acid methyl ester (FAME) was determined as 94% in the presence of 1% catalyst [4]. Another study conducted by Ouangi F. *et al,* observed that biodiesel was produced with refined edible vegetable oil and WCO in a 10 L apparatus at a temperature of 65 ˚C for 1 hr reaction time. Biodiesel yield of refined oil was as good as 97.5% whereas from WCO, it was 93.2%. Base catalyst KOH 1.2% by weight was used and with methyl alcohol to oil molar ratio of 1:6 for the conversion time of 60 min [5]. Mechanically agitated laboratory scale reactor vessels have been devised and manufactured in the past to produce biodiesel. It has long been recognised that batch stirred reactors are a fundamental mode of biodiesel synthesis. With improved mass turbulence distribution, effective heat transfer, and precise mixing control provided by agitator design, the laboratory scale reactor simplifies operation. The results revealed that biodiesel made from sunflower waste cooking oil met the necessary biodiesel fuel criteria. In the intended lab scale batch reactor, the transesterification reaction was found to be successful when sodium hydroxide (NaOH) was used as a catalyst. The production and conversion of produced biodiesel from waste cooking oil in a lab scale reactor at 70 °C employing a 3 % by weight NaOH catalyst resulted in biodiesel yield between 94 % and 96 % [6]. The current research project is based on the design and fabrication of a batch scale biodiesel production unit that with holding capacity of 10 L. Design calculations are based on mass flow of system components such as the WCO container vessel, potassium methoxide mixing container and reactor vessel. WCO was used as a feedstock to study its conversion into biodiesel (methyl ester) and subsequently characterization of its fuel properties to be conducted.

2. Methodology

The design and fabrication of 10 L capacity batch scale unit calculations are based on determining the capacity of the vessels necessary for biodiesel production, using mass balance of the system under consideration. The storage container, catalyst/methanol chamber, and reactor vessel dimensions were estimated. A simplified process flow diagram (PFD) was created based on the previous literature [7] for additional batch scale unit design calculations (see **Figure 1).**

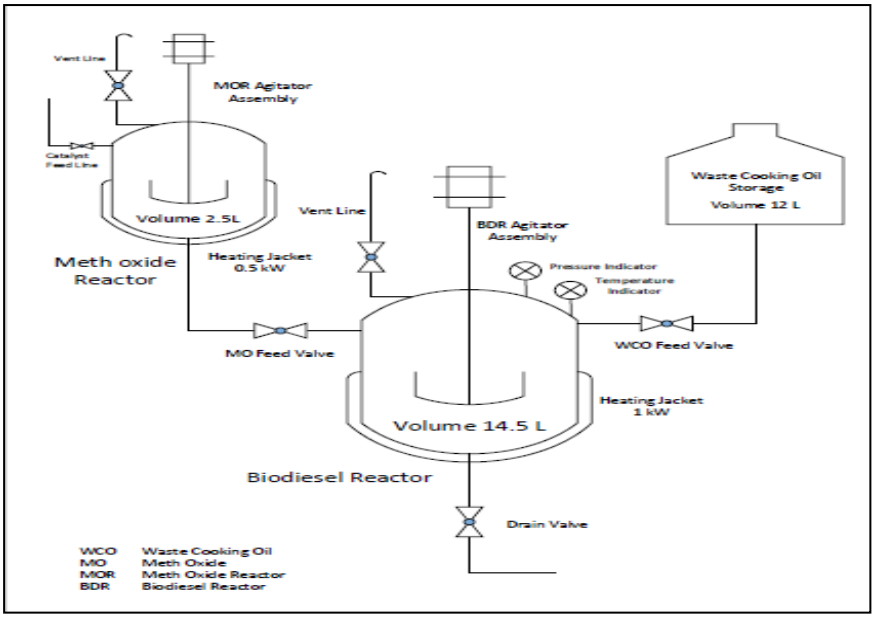

Figure 1 Simplified process flow diagram for biodiesel production batch scale setup

2.1 Volume of reactor and catalyst /methanol mixing vessel

Mass balance of the 10 L biodiesel production system, the mass of 10L WCO was calculated by (density = mass/ volume) by multiplying the density of WCO 900 kg/m^3 with 10 L. However, the volume of methanol required for transesterification reaction was 2 L (i.e. 20 % by volume of oil) and KOH catalyst used 1% by weight of WCO (0.09 kg) multiplied by its density 2044 kg/m^3, which occupies 0.044 L. The ultimate volume of the reactor was computed using a 20% extra volume assumption for the free board space in the reactor by using following expression;

$$Total\ volume\ of\ the\ reactor = (Volume\ of\ WCO + Volume\ of\ Methanol + Volume\ of\ Catalyst)\ x\ 20\% \quad (1)$$

2.2 Dimensions of reactor and catalyst /methanol mixing vessel

Depending on the diameter of standard available pipes, stainless steel pipes (grade SS 304) were selected having 8 inches diameter for reactor vessel and 4 inches diameter for catalyst /methanol mixing vessel, for making both ends welded for its conversion into vessels [8]. The reactor vessel was equipped with a temperature sensor / controller, mixer speed controller and pressure gauge to monitor the process during its operation. Based on the volume of the reactor and catalyst /methanol mixing vessel (V), height of vessels (h) were determined by substituting the vessel radius (r) using the following equation;

$$(2) V = \pi r^2 h$$

2.4 Reactor and catalyst /methanol mixing vessel agitator's electric power requirements

Considering the dimensions of reactor and catalyst /methanol mixing vessels, its driving motor electric powers were calculated. The equations used for agitator power calculations are mentioned below [9];

$$(3) R_e = \frac{D^2 N P}{\mu}$$

$$(4) N_p = \frac{P}{\rho n^3 D^5}$$

Where Np = Power Number; Re = Reynolds Number; P = Shaft Power (W); ρ = Fluid density (kg/m$_3$); μ = Fluid Dynamic Viscosity (kg/m. s); N = Agitator Speed (rpm)

In order to calculate the *Re*, it was assumed that the diameter of agitator in reactor vessel is 3.2 inches (0.081m), mixing speed required 700 rpm, density of WCO (900 kg/m^3) and dynamic viscosity of WCO (3.59 x10^{-5} kg/m.s). Considering Re value and finding D/ DT ratio (i.e. diameter of agitator / diameter of reactor vessel), the corresponding value of Np was found from the standard power correlation curve to calculate the power correlation for single three-bladed propellers [10]. The electric motor's power requirement is then calculated by substituting the values in Equation (4). Similarly, the same procedure was followed for the power requirement of electric motor for catalyst /methanol mixing vessel, where the agitator diameter 1.6 inches (0.040 m) was assumed, while the density of methanol (774 kg/m^3) and dynamic viscosity of methanol (4.49 x10^{-4} kg/m.s) at 40 ^{o}C were considered in design equations.

2.4 WCO container

12 L HDPE (high density polyethylene) plastic container was purchased from the market for storing raw WCO and was provided with a funnel at the top for filling the WCO.

2.5 WCO and acid value (AV) test:

WCO was obtained from different food outlets in Karachi. Initially, WCO acid value was measured by titrimetric method to find free fatty acid content. Then if its AV is greater than 5.5 mg KOH/g of oil by weight of catalyst then the esterification reaction is required by acid catalyst , whereas it is below than 5.5 mg KOH by weight, then transesterification reaction is employed [4].

2.6 Operating batch scale unit

WCO obtained was filtered by using a cotton cloth to remove suspended solid particles after its use at food outlets. 12 L filtered WCO was charged into the storage container

bottle and then it was transferred to the reactor vessel. WCO was heated for 1 hr in reactor with outlet vent kept opened to remove moisture content at 60 ºC using the temperature controller. The preheated and moisture free WCO (10L) was subjected to esterification process by adding sulphuric acid 0.2 % by weight of WCO, whereas methanol to WCO molar ratio was 5:1. The reaction time, temperature and mixing speed of agitator were 2 hrs, 65 ˚C and 700 rpm respectively. The system was connected with a condenser to reflux the methanol evaporated during the reaction back to the reactor vessel. After reaction the mixture was allowed to settle impurities along with decanting top layer of methanol/water mixture. In the second stage, transesterification was performed by using potassium hydroxide (KOH 1% by weight of the WCO and methanol to oil ratio 5:1 was used) [4]. Reactor temperature was set at 65 ˚C and stirrer speed was maintained at 700 rpm, while reaction time was 1 hr. After base transesterification process, the mixture of biodiesel and glycerol was allowed to drain into a transparent HDPE container to separate out both products. After separation, the biodiesel was water washed with distilled water at a temperature of 50°C to remove the glycerol content as well as other contaminants. Then biodiesel was dried in an oven at 80ºC for 30 min to remove moisture content and then its physico-chemical properties were measured. The biodiesel yield was measured by the following equation;

$$Biodiesel\ yield\ (\%) = \frac{Volume\ of\ biodiesel\ produced}{Volume\ of\ WCO} \times 100 \quad (5)$$

2.7 Mass performance of the biodiesel produced

The mass performance of the biodiesel produced was calculated using Equation (6), which is the mass of biodiesel produced, divided by the total mass of catalyst, methanol, and WCO used in the transesterification reaction [11];

$$Mass\ performance\ of\ biodiesel\ produced\ (\%) = \frac{Mass\ of\ biodiesel\ produced}{Mass\ of\ KOH + Mass\ of\ methanol + Mass\ of\ WCO} \quad (6)$$

3. Results and discussion

3.1 Biodiesel and glycerol yield

The acid value of neem oil was found 5.8 mg KOH/ g of oil; therefore two step esterification-transesterification processes were employed to avoid saponification and soap formation. Biodiesel and glycerol yields were 97% and 2.6 % by volume produced. Fatty acid profile of WCO, showed the presence of oleic acid, palmitic acid, stearic acid and linoleic acids in its composition.

3.2 Calculated design parameters:

The dimensions and power requirements were calculated based on mass balance of the storage container, catalyst / methanol vessel with electric mixer and reactor vessel with stirrer. The design parameters were calculated and presented in **Table 1**. The volume reactor was found 14.452 L keeping in view the free board surface for reactants

evaporating during the process, with electric power requirement of stirrer was 328 W. Similarly, the volume of catalyst /methanol mixing vessel was calculated as 2.452 L for batch biodiesel production of 10 L, its electric power requirement was calculated as 25 W.

Table 1 Calculated design parameters

Design parameters	Calculated values
Volume of reactor vessel	14.452 L (approx. 14.5 L)
Volume of catalyst /methanol mixing vessel (methoxide reactor)	2.452 L (approx. 2.5 L)
Volume of WCO storage container	12 L
Diameter of reactor vessel	8 inches (0.203 m)
Diameter of catalyst /methanol mixing vessel	4 inches (0.101 m)
Height of reactor vessel	0.444 m
Height of catalyst /methanol mixing vessel	0.302 m
Power requirement of electric motor (for reactor vessel)	328 W
Power requirement of electric motor (catalyst /methanol mixing vessel)	25 W

Table 2 Physical and chemical properties of biodiesel produced

Parameters	WCO	Biodiesel	ASTM D 6751
Biodiesel yield (%)	-	97	-
Acid value of oil (mg KOH/ g of oil)	5.8	-	0.80 (max)
Density (kg/m^3)	900	872	0.860 to 0.900
Kinematic Viscosity (mm^2/s)	39.9	4.5	1.9 to 6.0
Flash Point (^{o}C)	336	177.64	130 C min
HHV (MJ/kg)	-	41.55	> 35

3.3 Characterization of biodiesel produced:

The produced biodiesel physical and chemical characteristics were measured and presented in **Table 2.** The results were found in compliance with International Biodiesel Standard (ASTM D 6751).

3.4 Mass performance analysis of the biodiesel produced

The mass performance of the biodiesel produced was calculated as 78.3 %. Basically, it showed that sufficient mass of oil has been converted into biodiesel (methyl ester) as compared to input masses of WCO, methanol and catalyst (KOH) used.

4. Conclusions

Using a batch scale setup (10L) that was built and fabricated locally, WCO was successfully

converted into biodiesel. The reactor vessel, WCO storage container, and catalyst/methanol mixing chamber were all designed with freeboard space in mind, based on the system's mass balance. The properties of WCO biodiesel have been proved to meet international standards (ASTM D6751 and EN 14214). This batch scale setup should be utilized to look into WCO biodiesel optimization conditions in the future.

Acknowledgment: The authors would to thanks NED University of Engineering & Technology, Karachi for providing lab facilities and resources to conduct this research study.

References

[1] A. K. Agarwal, "Biofuels (alcohols and biodiesel) application as fuels for internal combustion engines" *Progress in Energy and Combustion Science,* vol. 33, pp. 233-271, 2007.

[2] H. Yaqoob et al., "Potential of waste cooking oil biodiesel as renewable fuel in combustion engines" *Energies,* vol. 14, pp. 1-20, 2021.

[3] L. G. D.H. Qi. H. Chen, "Experimental studies on the combustion characteristics and performance of a direct injection engine fueled with biodiesel/diesel blends" *Energy Conversion and Management*, vol. 51, pp. 2985-2992, 2010.

[4] Sana Sadaf, Javed Iqbal, Inam Ullah, Haq Nawaz Bhatti, Shazia Nouren, Habib-ur-Rehman, Jan Nisar, Munawar Iqbal. Sahar, "Biodiesel production from waste cooking oil: An efficient technique to convert waste into biodiesel" *Sustainable Cities and Society,* vol. 41, pp. 220-226, 2018.

[5] M. K. Fatiha Ouanji, "Production of biodiesel at small-scale (10 L) for local power generation" *International Journal of hydrogen energy*, vol.42, pp. 8914-8921, 2017.

[6] Patil K.D., Khedkar S.V., Inamdar N. Topare N.S., "Lab scale batch reactor design, fabrication and its application for biodiesel production''. In: Pawar P.M., Balasubramaniam R., Ronge B.P., Salunkhe S.B., Vibhute A.S., Melinamath B. (eds)," *Techno-Societal (2020)*, 2021.

[7] X. W. Dennis Y.C. Leung, "A review on biodiesel production using catalyzed transesterification" *Applied Energy,* vol. 87, pp. 1083-1095, 2010.

[8] R. F. Elisa Helena Siegel Moecke et al, "Biodiesel production from waste cooking oil for use as fuel in artisanal fishing boats: Integrating environmental, economic and social aspects" *Journal of Cleaner Production,* vol. 135, pp. 679-688, 2016.

[9] "Chemical Engineering Design. In R. K. SINNOTT, Coulson & Richardson's" *Chemical Engineering,* vol. 6, 1999.

[10] Joseph B. Gray, Vincent W. Uhl, "Mixing Theory and Practice," *Academic Press, USA,* Vol. II Hardcover, 1967.

[11] P. B. Hector I. Velasquez, "Exergy Analysis of Palm Oil Biodiesel production by Base catalyzed methanolysis" *International Congress of Mechanical Engineering (ABCM), Brasilia, Brazil*, vol. 19, 2007.

An Energy Nexus Study on Stress Analysis of Buried Fuel Pipelines under Railway Tracks to find Safe Depth

Hamza Sajid*, Saad Ahmad, Gul Haider, Mehran Meer

Mechanical Engineering, University of Engineering and Technology Peshawar, University Town, Peshawar 29000.

**Corresponding author*

Email: hamza913114@gmail.com

Abstract

Every year, the world's energy demands surge, but the finite natural resources, used to fuel industrial society deplete. These natural resources are in short supply and scarce. While they do arise naturally, their replenishment can take hundreds of thousands of years. As a result, it is critical that we make the best use of all available resources and avoid their wastage. Pipelines are one of the primary means of transporting these resources, predominantly fuels, from the point of supply to the point of consumption. They offer a less expensive, safer, and faster means to transfer energy throughout the country. Fuel transportation is critical to the country's economy and hence pipelines are often buried underground at a great depth to protect them from damage and keep them away from natural life. This research paper examines the safe depth for pipes beneath railway tracks. Static, dynamic, fatigue, and internal stresses are investigated and assessed on pipelines at various depths. Analytical calculations using techniques such as Spangler's Direct Earth Load Method (DELM), Timoshenko's, Bousinessq's, Westergaard and PCA are compared to actual experiments conducted under the railway track using an Arduino-based load cell system at varying depths. The results showed that when there is no traffic on the track, pipelines experience static loading due to soil weight as it depends on soil density, stone concentration, and compaction. When a train passes, both static and dynamic loads are applied. The buried pipeline's creep and fatigue failures are caused by static and dynamic loading, respectively. This study's main goal is to analyze the buried pipeline's load distribution due to static and dynamic loads and recommend a safe depth to avoid failure. This study concludes that for low pressure pipelines, 8 to 9 ft. is the *critical depth*, resulting in the lowest stress values and factors of safety greater than or equal to 3, while 6 ft. is the first safest depth.

Key words: Dead load, static load, live load, dynamic load, combined load, PCA method, fatigue failure, soil weight.

1 Introduction

Global energy demand is expected to skyrocket over the next few decades. This is primarily due to projected global population growth as well as the economic and industrial growth of developing countries. It has been estimated that the annual energy consumption will reach 778 Etta Joule by 2035 (OPEC, 2013). Today about 78% of our energy needs are fulfilled by non-renewable sources such as coal, gas, and oil (OurWorldinData, 2019). These fossil fuels are

not infinite, and their replenishment can take hundreds of years. It is estimated that the reserves of coal, natural gas, and oil is depleted in 114 years, 52 years, and 51 years, respectively (OurWorldinData, 2019). Therefore, it is important that we make best use of all the natural resources which are currently available. Fuel transportation plays a critical role in this regard. Most of the times, these fuels are transported through pipelines which are buried under the ground to provide them support. The burying of these pipelines helps not only to preserve the visual aesthetics of the region but also protects the pipelines against various environmental factors. These factors may result in the mechanical failure of the pipe across the bends or the connection joints, hence resulting in significant energy loss.

The resources extracted from the mines and refined in the refineries need to be transferred to every household and every industry of the country. While the physical solid goods are transferred through a complex system of vehicular transportation, these same can't be done for the resources in fluid form, as it will not only exorbitantly increase the cost of transportation but also it will result in wastage of material itself in excessive amounts. Another reason why such an approach can't be adopted is since in many cases the fluid resources which need to be transferred are much more prone to fire and are therefore hazardous. Since vehicular transportation is always at greater risk of road accidents and other such events therefore such an approach can't be taken all the time. According to the U.S. Department of Transportation's Office of Hazardous Materials Safety, there are almost 15,000 incidents related to transporting hazardous materials in 2011. Therefore, pipelines offer the safest and most cost-effective method of energy transportation. But often, these pipelines travel underneath the railway tracks and are prone to failure due to the forces exerted by the train. It has been estimated that the next 20–30 years will bring an unprecedented demand for a hike in rail transport in terms of the axial load and the numerical strength of trains in service (A. H. S. Garmabaki, 2019). Furthermore, Gould, Boulaire, Marlow, and Kodikara found that seasonality impacts could be observed in pipes failure data and presented that pipe failures occur due to the complex and intricate interaction of different factors including pipe attributes, soil properties, and weather conditions (Gould, 2009). While a significant amount of work has been done to find the stress distribution on buried pipelines using numerical methods such as Finite Element Method, little to no work has been done using experimental setups. For example, Khademi performed the finite element analysis for the polyethylene gas pipes buried underground (Khademi-Zahedi, 2019) and Jie Zhang and Zheng Liang performed similar analysis using simulation software but disregarded the external dynamic load and considered only the dead load of the soil (Jie Zhang, 2016). Similarly, a lot of work has been done to predict the behaviour of pipelines under seismic loading, but the work done with regards to external loading is severely limited. Moreover, no work has been done to find the stress analysis of buried pipelines which are crossing under the railway tracks other than the pioneering work by Marston and by Merlin G. Spangler back in 1964 (Spangler, 1964). Therefore, our research aims to fill this literature and research gap by

carrying out experimental analysis of the steel pipelines buried under the railway tracks and to provide a framework for further studies in this field. Therefore, the primary objective and success criteria of the project is to find a safe depth for the pipe which gives us a normal and fatigue factors of safety of more than 2. The secondary objectives of our study are:

- To find a percentage decrease in load with respect to depth.
- To know the effect of static loading on pipelines.
- To know the effect of dynamic loading on pipelines.
- To find the minimum safest depth based on the pipe dimensions on which the live load is virtually zero.

Our problem entails the stress analysis of the buried gas pipelines under the railway track by using experimental techniques to find the effect of depth on the pipelines based on loading conditions such as dead load and dynamic load.

2 Methods

3.1 Experimental Setup and Procedure:

The experiment is performed using an Arduino based load cell system. The load cell which is used for the experiment is an S-type load cell. S-type load cell is chosen because of its versatility, high precision and its sensitivity to in-line loading conditions. The load cell specifications are HTC-500 with maximum load capacity of 500 kg, weighing 665 grams and having dimensions of 2.95 x 1.97 inches. The load cell is mounted on top of a pipe using a casing with welded bolt on top of it, as shown figure 1. The pipe buried is API X70 having a diameter of 4 inches and thickness of 4 mm.

The experiment is conducted as shown in the figure 2. So, the whole experimental procedure is divided into the following 7 steps:

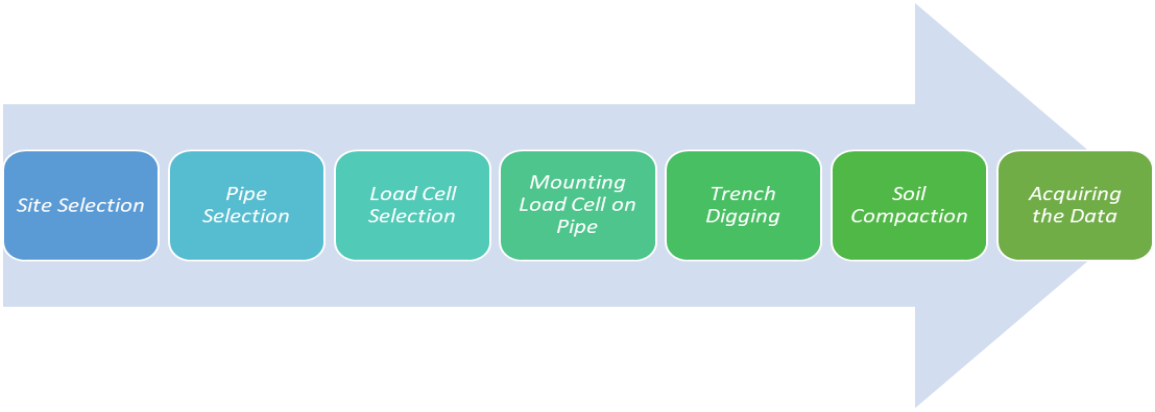

Figure 1: Methodology of the Experiment

Site Selection

1. **Site Selection:** Azakhel Junction, District Nowshera
2. **Pipe Selection:** API X70
3. **Load Cell Selection:** S-type
4. **Load Cell Mounting:** Welded Bolt Ring

5. **Trench Digging:** Automatic and Manual Excavation using Auger Boring and Shoveling
6. **Soil Compaction:** Using Proctor Compaction Test
7. **Data Acquisition:** Arduino and Excel

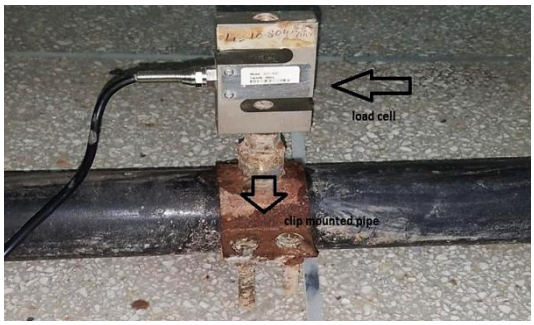

Figure 2: S-type Load Cell Mounted on a Pipe

First of all, a trench is dug where the load cell would be buried. Then we mounted the load cell on top of the pipe and buried it inside that trench, under the railway track. After achieving the proper compaction percentage, we waited for the train to arrive. In the meantime, configured the Arduino sketch to give us the reading of the dead load and save it in the form of EXCEL sheet. Later the Arduino is configured to give us the readings of only the live load on passing of train. 2 experiments are performed per day. The total number of experiments which are performed are 6 with depths ranging from 1 ft. to 6 ft. With each experiment we went 1 ft. further below the ground.

Figure 3: Working on-the site to install Load Cell

3.1 Material and Site Selection:

In order to perform the experiment, the first task is the selection of the site. The site which is selected for the experiment is Azakhel Railway Junction, Nowshera, KPK. This site is selected mainly for 2 reasons, first, the topography of the location is favorable for us. This is because the railway track is 1 meter above the ground therefore it made it easy for us to dig the trench and bury the load cell and secondly, it is a very active site meaning that daily 3 trains pass

through the track.

3.2 Measurements:

The data gathered through the Arduino is in the form of a fluctuating waveform like a sinusoidal wave. This is due to the fact that a train is composed of different boogies, as each boogie passes the load diminishes and the start acting again due to the 2nd boogie. Following readings are obtained from the on-site experiments.

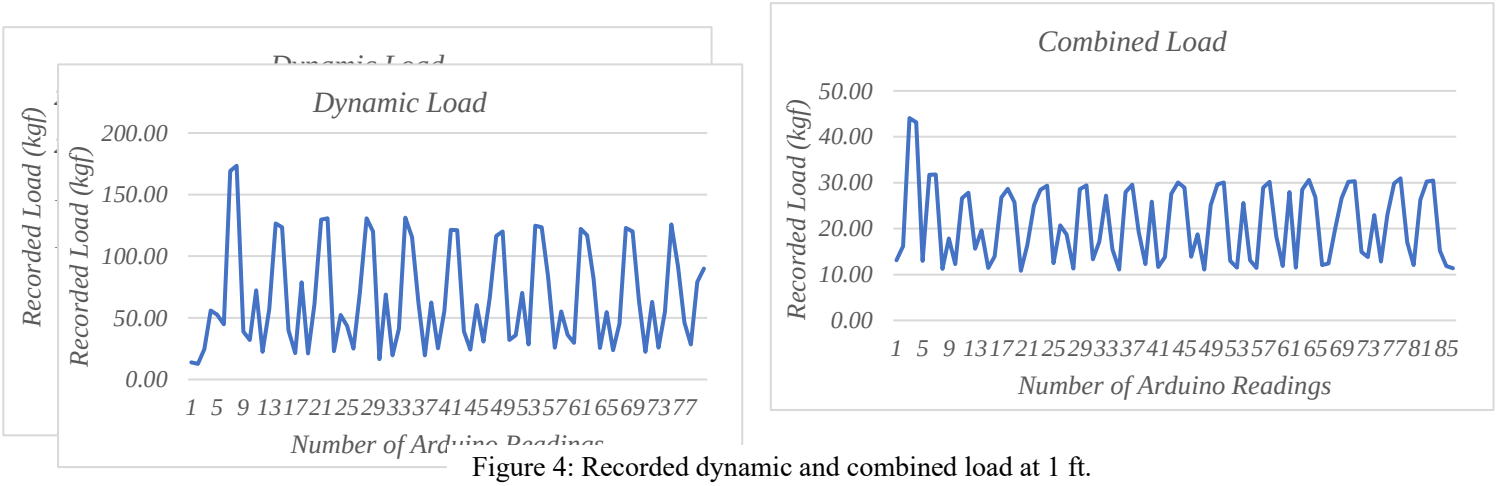

Figure 4: Recorded dynamic and combined load at 1 ft.

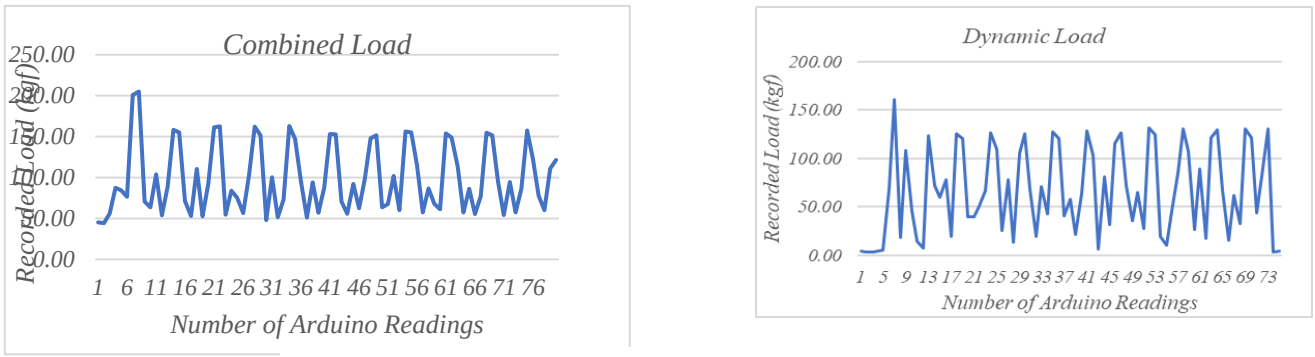

Figure 5: Recorded dynamic and combined load at 2 ft.

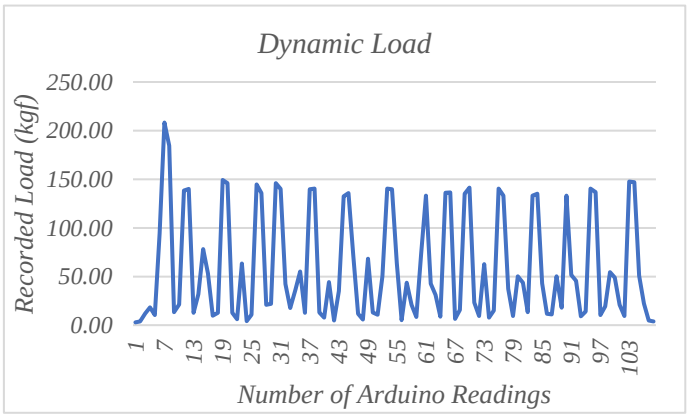

Figure 6: Recorded dynamic and combined load at 3 ft.

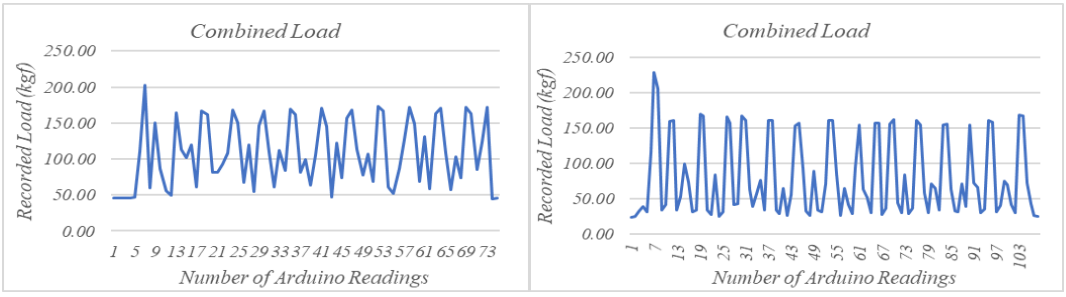

Figure 7: Recorded dynamic and combined load at 4 ft.

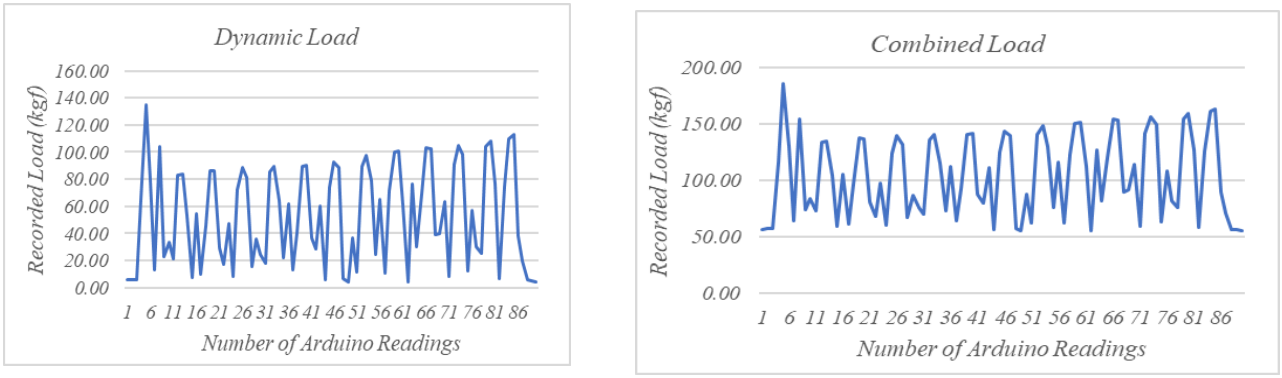

Figure 8: Recorded dynamic and combined load at 5 ft.

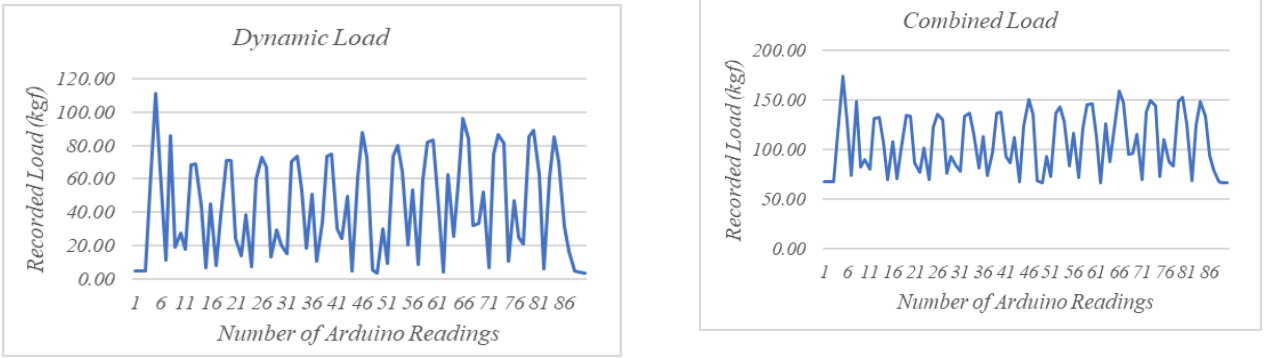

Figure 9: Recorded dynamic and combined load at 6 ft.

Calculations:

The pipelines which are buried under the ground experience two types of loads, dead load, and dynamic load. Dead load, also called static load, is due to the applied weight of the soil while the dynamic load is the time-dependent load due to external factors such as passing train, pedestrians etc. Several theories have been put forward to calculate both the types of loads. For Dead Load, there are 2 main methods to calculate soil load, first is Marston's Earth Load Method for rigid pipes (Yong Tian, 2015) and 2nd is Direct Earth Load Method for flexible pipes. Direct Earth Load method is the modification of Marston's Earth Load method but for flexible pipes (American Water Works Association, 1961). For our experiments, we are using Direct Earth Load method because for our experiments, we are using flexible pipe and the trench width is also taken as outside diameter of the pipe.

$$W_D = \gamma HD$$

Where W_D = the load on the pipe in lb per linear ft; γ = specific weight of the soil in lb per cubic ft; H = height of the soil prism above the pipe; and D = outside diameter of the pipe.

Similarly, for the calculation of live load, there are also number of methods. They are Spangler's Single Load Method (CROSSINGS, 1984), Timoshenko's Beam Methods (Ike, 2019), Boussinesq's Point Load Method (Jumikis, 1962), Portland Cement Association (PCA) Method (CROSSINGS, 1984), Uniform Load Method (CROSSINGS, 1984), and Westergaard's Method (Goswami, 2015). While each method has its own limitation, we decided to go for Portland Cement Association Method due to the following three reasons: 1). Only Uniform Load Method and PCA Method assumes protective slab over the road which coincides with our experimental conditions, 2). PCA method is the most conservative out of the 2 methods mentioned above, and 3). It is the recommended method by the literature whenever a concrete protective slab is present (CROSSINGS, 1984). The ballast which is present on the experimental site is almost rigid and hence is assumed to be a protective slab. Therefore, to find the effect of live load on our pipes, we use the PCA method which is given by:

$$\sigma = \frac{CP}{R_s^2}$$

$$where\ R_s = \sqrt[4]{\left(\frac{Eh^3}{12(1-v^2)E'}\right)}.$$

C = Load Coefficient and R_s = Radius of Stiffness , E = Modulus of Elasticity of Concrete, v = Poisson's Ratio and

E′ = Elastic Modulus of Soil.

For hoop stress (primary stresses) we use the Barlow's formula (CROSSINGS, 1984):

$$S_h = \frac{p}{2t}(D - 2t)$$

Where S_h = hoop stress, p = the internal pressure, D = Pipe outside diameter, and t = thickness of pipe wall.

Secondary stresses are stresses in the pipe caused by external forces. The combined external force is usually expressed in terms of lb per unit length of pipe, denoted by W. The combined secondary stress computed using Spangler's Stress Formula is (CROSSINGS, 1984):

$$S = \frac{3K_b WEDt}{Et^3 + 3K_z pD^3}$$

Where S = stress in psi, K_b = the bending parameter, and K_z the deflection parameter. K_b and K_z are the functions of the bedding angle, and they depend on laying conditions of the pipelines (CROSSINGS, 1984) and E = Modulus of Elasticity of Pipe Material in psi. Here,

$$W = W_D + W_L + W'_D$$

Where W_D = Dead Load, W_L = Live Load = σD, and W'_D = Slab Load = 2.371 psi.

Hence the total stress in the pipe is:

$$S_T = S_h + S$$

For quantifying the horizontal deflection (within range of use in the pipe, we use the Iowa Formula (Spanglers's) (American Water Works Association, 1961):

$$\Delta X_1 = \frac{(JK_a Wr^3)}{EI + 0.061E'r^3}$$

Where ΔX_1 = the maximum deflection in the pipe, inches; J = the deflection lag factor (1.5 suggested by Spangler); K_a = the bedding factor (equivalent to K_z); r = the mean radius of pipe in inches; E′ = the modulus of elasticity of subgrade reaction in psi (table in (CROSSINGS, 1984)); and I = the moment of inertia of pipe wall in^4/in.

Here. W is the total load on the conduit, same as W in secondary stresses, but here we can also use the following formula to calculate W:

$$W = \frac{1}{12}\left(\frac{W_D D}{B_D} + W_L\right)$$

Where W = total load on flexible pipe (lb./linear in. of pipe); W_D = dead load (lb./linear ft. of pipe); W_L = live load (lb./linear ft. of pipe); D = pipe diameter (ft); and B_D = trench width at top of pipe (ft).

4. Results

4.1 Experimental Stresses in Pipe:

To summarize the readings taken through the Arduino and to get the units consistency, we

multiply our max loads, at each depth, with 2.2 to convert kgf to pounds (lb.) and then divide by the area of the disc used during experiments i.e., 0.35 ft^2 to get the corresponding stresses in the pipe in psf.

Table 2: Experimental values of stresses at different depths in psf.

Depth (ft.)	*Dead Load (psf)*	*Dynamic Load (psf)*	*Combined Load (psf)*
1	*67.08*	*1462.52*	*1529.60*
2	*129.30*	*1309.31*	*1438.61*
3	*198.66*	*1089.10*	*1287.76*
4	*261.81*	*1008.27*	*1270.08*
5	*321.18*	*847.78*	*1168.96*
6	*393.96*	*698.70*	*1092.66*

4.1 Site Specifications:

Following values are used for all the calculations:

Table 3: Values of commonly used variables and experimental conditions

Characteristic	***Value***
Specific weight of the soil, $\boldsymbol{\gamma}$ $(\frac{lb}{ft^3})$	*89*
External diameter of pipe, D (in.)	*4*
External diameter of pipe, D (ft.)	*0.333*
Length of sleeper (mm)	*2400*
Length of sleeper (ft.)	*7.874*
Width of sleeper (mm)	*300*
Area of sleeper (ft^2)	*6.713*
Mass of sleeper (kg)	*260*
Mass of sleeper(lb.)	*573.201*
Load, P (lb.)	*57344*
Internal pressure (psi)	*175*
Diameter of disc (in.)	*4*
Thickness of the Pipe, t (in.)	*0.0774*
Modulus of elasticity, concrete (psi)	*4 x* 10^6

Modulus of elasticity, soil (psi)	*500*
Poisson's ratio, pipe	*0.2*
Height of slab, h (in.)	*8.267*
Yield strength of pipe, (ksi)	*70*
Bending parameter, K_b	*0.157*
Deflection parameter, K_Z	*0.096*

4.2 Analytical Stresses in Pipe:

By using the analytical formulas, mentioned in the Method section, we get the following values for Dead and Live loads:

Table 4: Analytical stresses in pipe calculated using formulas mentioned in Method section

Depth (ft.)	*Dead Load (psf)*	*Dynamic Load (psf)*	*Combined Load (psf)*
1	*89*	*2487.53*	*2576.53*
2	*178*	*2268.85*	*2446.85*
3	*267*	*1981.83*	*2248.83*
4	*356*	*1735.80*	*2091.80*
5	*445*	*1462.45*	*1907.45*
6	*534*	*1189.56*	*1723.56*

4. 3 Percentage Deviation:

The following percentage differences are observed between the values of experimental and analytical stresses. The reasons for such differences are explained in the conclusion section of this paper.

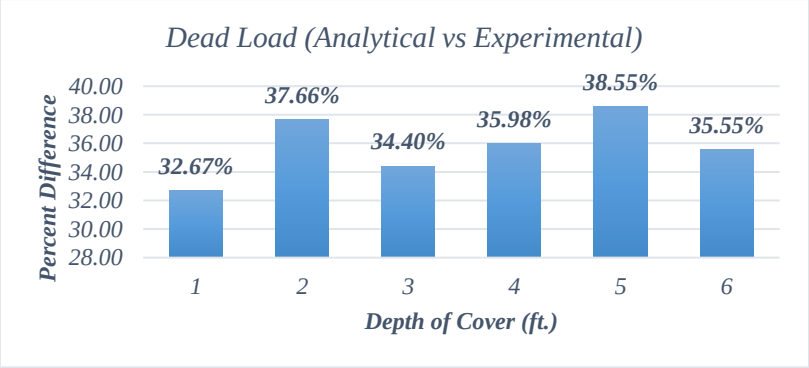

Figure 10: Percent difference between experimental and analytical values of stresses due to dead loads

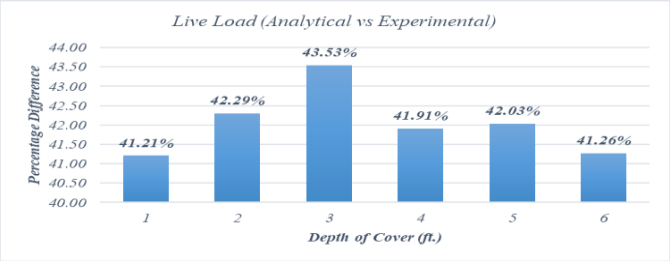

Figure 11: Percent difference between experimental and analytical values of stresses due to live loads

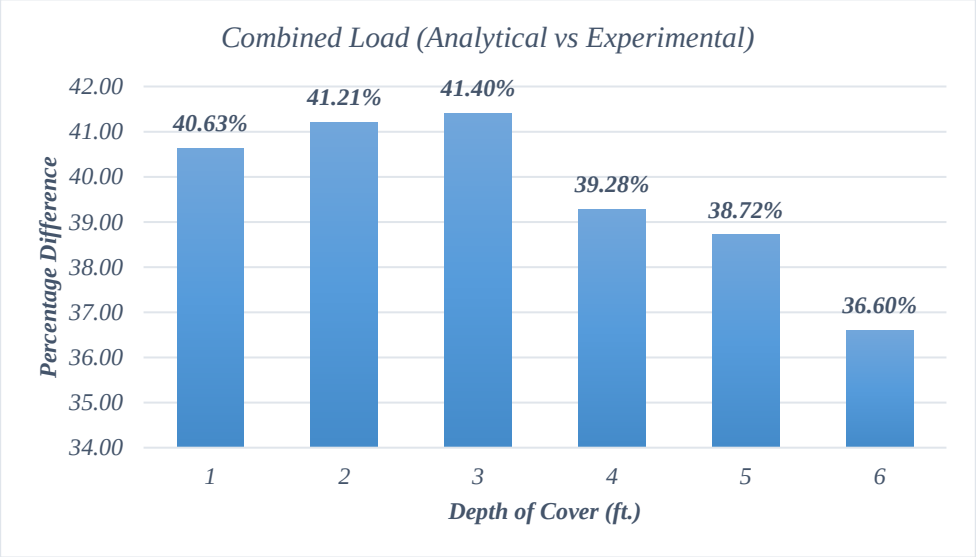

Figure 12: Percent difference between experimental and analytical values of stresses due to combined loads

The **average** percent differences between the analytical and experimental results for stress due to dead loads, live loads and combined loads are **35.80%**, **42.04%**, and **39.64%**, respectively.

4.4 Total Combined Stress:

The combined stress can be calculated using the equation:

$$S_T = S_h + S$$

The hoop stress or primary stress in our case, with an internal pressure of 175 psi, is:

$$S_h = \frac{p}{2(0.0774)}(4 - 2(0.0774) = 4270.009\, psi = \ \ 614881.3\, psf.$$

Similarly, the secondary stresses and combined stresses are calculated using:

$$S_t = \frac{3K_b WEDt}{Et^3 + 3K_z pD^3}(\approx S) + S_h$$

Table 5: Combined stresses due to all the combined loads and internal pressure.

Depth (ft.)	*W (lb./in.)*	*S (psi)*	*S_t (psi)*
1	*78.643*	*18993.83*	*23263.84*
2	*76.18*	*18380.4*	*22650.41*

3	*71.818*	*17294.24*	*21564.24*
4	*68.595*	*16491.61*	*20761.62*
5	*64.613*	*15500.01*	*19770.02*
6	*61.533*	*14733.04*	*19012.6*

4.5 Factors of Safety:

Here we calculated factor of safety for both the normal loading condition as well as fatigue loading condition. Our results will show that the buried pipes are more prone to fatigue failure rather than normal failure. Here the normal failure criterion is onset of deformation i.e., *Yield Strength* of the pipe. We get the following factors of safety for normal loading based on total combined stress and yield strength of the pipe.

Table 6: Factors of safety vs depth for normal loading

Depth (ft.)	*S_t (psi)*	*FOS*
1	*23263.84*	*3.0089615*
2	*22650.41*	*3.0904518*
3	*21564.24*	*3.2461149*
4	*20761.62*	*3.3716059*
5	*19770.02*	*3.5407147*
6	*19012.6*	*3.6817689*

For fatigue loading, we considered the pipe to be a uniform beam of circular cross-sectional area supported by two end supports, the end supports being the rail tracks. The load is applied as a point load in the center of the beam. We used Soderberg criteria on the data we acquired from the Arduino since it is the most conservative criteria and calculated the following fatigue factors of safety:

Table 7: Factors of safety vs depth for fatigue loading

Depth (ft.)	*Fatigue FOS*
1	*0.979*
2	*1.089*
3	*1.315*
4	*1.436*
5	*1.916*
6	*2.084*

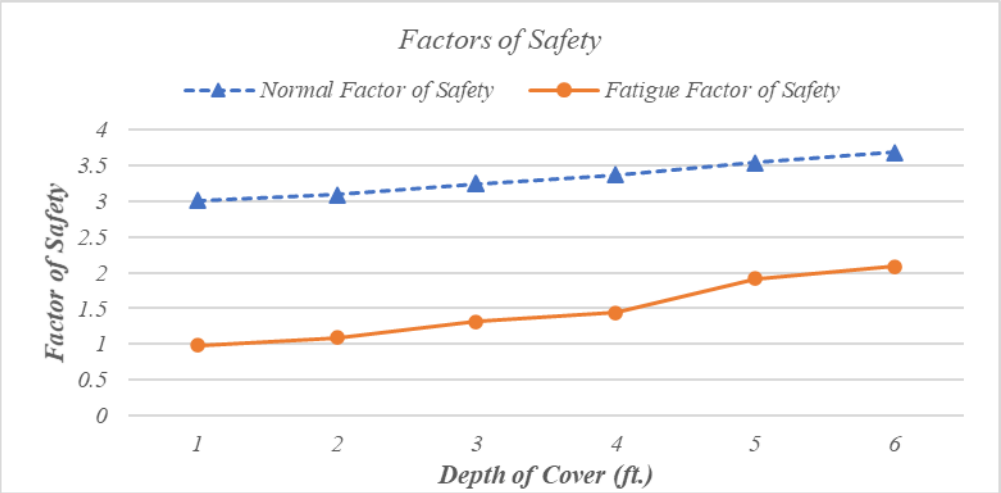

Figure 13: Normal vs Fatigue Factor of Safety

5. Conclusions

Recalling our main research objectives, the primary objective of our research is the identification of a safe depth for buried pipelines. The significance of buried pipelines can hardly be underestimated since they transport the fuels of the economy in an already energy-deprived world. From the results, we get the following conclusions and key findings:

1. As we go down the earth, the dead load increases drastically but at the same time the live load also decreases. A point will arrive where dead load will cross the live load and this is the point of *critical depth*, here the total combined load is minimum, and stresses produced will also be minimum. This is the sweet spot where the pipelines should be buried, and hence our safest depth. For our experiments, we found that our *critical depth* is around 8ft. for experimental setup and 8.5ft. for analytical setup and the corresponding normal and fatigue factors of safety at 8ft. are (based on linear trendline extrapolation) 3.99≈4 and 2.96≈3, respectively. The literature doesn't suggest any factor of safety for buried pipelines based on normal and fatigue loading conditions, so going by rule of thumb, any FOS above 2 is considered safe, so based on this for fatigue loading condition 6ft. is the first safest depth to bury the pipes, if 8ft. is not preferred due to any reasons.
2. Buried pipelines are more susceptible to failure due to fatigue loading rather than the normal loading. This is due to the fact that the dead weight of the soil results in creep failure since it is a static load which is always present and also at shallow depths it contributes little to the failure when compared with the live load. The engine of an average train weighs over 106 tons, therefore, the

passing train exerts a substantial amount of load on the pipes in the form of cyclic loading.

3. There is an average difference of 35.80%, 42.04%, and 39.64%, for dead, live, and combined load, respectively between analytical and experimental results. This could be due to the following 3 reasons, 1). The ballast of the railway track is assumed to be a rigid protective slab while in reality, it is not completely rigid and had some degree of elasticity as well, 2). The loading conditions on the track where not completely identical to the loading conditions of the methods described, the load is assumed to be point load while in reality, the load from the railway tracks travels downward in the form of diverging waves, 3). The soil composition and compaction of the site are not completely identical to the ones described in standards; therefore, some error may have occurred due to that.
4. Using the Iowa formula, we get the horizontal/vertical deflections to be $2.92\ x\ 10^6$ inches for 1 foot and $1.805\ x\ 10^6$ inches for 6 feet. Literature suggests that the amount of deflection which can cause the collapse of the flexible pipe is 20% of the nominal diameter (American Water Works Association, 1961). The 20% of our nominal diameter is 0.8 inches. Our deflections are far low as compared to the failing criteria; therefore, we are safe in this department. Furthermore, literature suggests that for steel pipes, permitting a 2% deflection is a good practice and for larger diameters it can be as high as 10% (American Water Works Association, 1961).

While this research is carried out with due diligence and care but there are certain parameters and variables which are overlooked. This research has raised many questions in need of further investigation. Therefore, further research can be carried out in this field using this research as a groundwork. First of all, the results of this research can be verified and validated through numerical solution methods such as finite element analysis using appropriate boundary conditions. Furthermore, we carried out this research only with one value of internal pressure, 175 psi, therefore we suggest extending the current investigation by applying different internal pressures. In addition to this, future studies are needed to determine the effect of changing soil conditions such as soil composition, compaction, elasticity, Poisson's ratio, and specific weight etc., on load transmittance and stress distribution can be investigated either through experimental setup or through numerical modelling. Future research can also concentrate on the effect of train speed and train frequency on transmitted load. We performed our experiment on pipe buried in a location where train passes at a speed of 60km/h, thrice a day. Another location could be selected where the train speed and train frequency vary significantly. One important aspect of this research is the selection of pipe, since this project is SNGPL-sponsored, therefore, we chose the pipe which the SNGPL mostly uses for their underground

gas transmission i.e., flexible steel pipe: API X70, OD 4 inches and thickness 0.3 inches. Literature argues that the behavior of rigid pipes (concrete) is vastly different from the behavior of flexible pipes i.e., polymer, steel etc. (American Water Works Association, 1961). Therefore, we suggest further investigation in this area where pipes of different materials and properties, such as concrete and polymer pipes, or pipes having different geometrical dimensions, such as diameter and thickness, are buried and then investigated.

References

A. H. S. Garmabaki, S. M. (2019). Underground pipelines and railway infrastructure – failure consequences and restrictions. *Structure and Infrastructure Engineering* , 412-430.

American Water Works Association. (1961). CHAPTER 8: Earth Loads on Steel Pipe . *Journal (American Water Works Association)*, 1045-1080.

CROSSINGS, B. G. (1984). H. S. Oey,1 M. ASCE, Vernon L. Greggerson, Jr.,2 A. M. ASCE and David P. Womack,3 M. ASCE. 203-222.

Goswami, I. (2015). Stress Increase Due to a Point Load. In I. Goswami, *All-in-one Civil Engineering PE Breadth and Depth 3rd Edition* (p. 569). McGraw-Hill Education.

Gould, S. B. (2009). Understanding how the Australian climate can affect pipe failure. *In OzWater' 09 Conference Proceedings.* (pp. 1-8). Australian Water Association (AWA), Australia.

Ike, C. C. (2019). Timoshenko Beam Theory for the Flexural Analysis of Moderately Thick Beams – Variational Formulation, and Closed Form Solution. *TECNICA ITALIANA-Italian Journal of Engineering Science*, 34-45.

Jie Zhang, Z. L. (2016). Mechanical behaviour analysis of a buried steel pipeline under ground overload Jie. *Engineering Failure Analysis*.

Jumikis, A. R. (1962). *Soil Mechanics.* Princeton, N.J. : Van Nostrand, 1962.

Khademi-Zahedi, R. (2019). Application of the finite element method for evaluating the stress distribution in buried damaged polyethylene gas pipes. *Underground Space 4* , 59–71.

OPEC. (2013). *World oil outlook 2013. Secretariat, Organization of the Petroleum Exporting Countries; 2013.* http://www.opec.org/.

OurWorldinData. (2019). *https://ourworldindata.org/*. Retrieved from https://ourworldindata.org/: https://ourworldindata.org/energy-mix

Shahid, R. K.-Z. ((2019)). Application of the finite element method for evaluating the stress distribution in buried damaged polyethylene gas pipes. *Underground Space 4*, 59–71.

Spangler, M. G. (1964). Pipeline Crossings Under Railroads and Highways. *Journal (American Water Works Association)*, 1029-1046.

Vertical pressure on culverts under wheel loads on concrete pavement slabs. (n.d.). Chicago, Ill. : Portland Cement Association,.

Yong Tian, H. L. (2015). Analysis of stress and deformation of a positive buried pipe using the improved Spangler model,. *Soils and Foundations*, 485-492.

Heavy metal removal from wastewater using Ionic liquids

Hilal Ahmad[1], Mansoor Ul Hassan Shah[2*], Muhammad Bilal[2], Syed Nasir Shah[3*], Mohammad Younas[2], Asim Laeeq khan[4], Waqad Ul Mulk[1], Syed Awais Ali[1]

[1]*Department of Mechanical Engineering, Faculty of Mechanical and Aeronautical Engineering, University of Engineering and Technology Taxila, 47080 Rawalpindi, Pakistan*

[2]*Department of Chemical Engineering, University of Engineering and Technology, Peshawar 25120, Pakistan.*

[3]*Department of Energy Engineering, Faculty of Mechanical and Aeronautical Engineering, University of Engineering and Technology Taxila, 47080 Rawalpindi, Pakistan*

[4]*Department of Chemical Engineering, COMSATS Institute of Information Technology, Lahore Pakistan*

**Mansoor Ul Hassan Shah*

Email: *mansoorshah@uetpeshawar.edu.pk*

Abstract

Rapid industrial development has resulted in significant wastewater contamination containing heavy metal ions in recent decades. Several separation techniques such as ion exchange, chemical precipitation, membrane separation, coagulation, and adsorption are used, but each one has its own drawbacks such as operating costs, slug generation etc. Ionic liquids (ILs) as a separation medium have attained remarkable attention for the removal of pollutants from wastewater. In the current study phosphonium-based hydrophobic ILs were used for the removal of cadmium ions from wastewater. The ionic liquids were characterized using Fourier transform infrared spectroscopy (FTIR), Scanning Electron Microscopy (SEM) and Thermo gravimetric analysis (TGA). The selected phosphonium-based ionic liquid was found to be capable of removing metal ions from wastewater. The highest removal efficiency was observed to be 84%.The results presented in current study showed the great potential of ILs as green adsorbents for the removal of cadmium metal ions from wastewater.

Key words: Ionic liquids, wastewater, heavy metal, removal

Introduction

As technology continues to advance, heavy metals in drinking water have exceeded recommended limits from regulators around the world. The main source of human exposure to heavy metals is from contaminated drinking water. The effects of drinking water contaminated with heavy metals, such as arsenic, lead, nickel, cadmium and mercury, have gradually caught the attention of the relevant departments and personnel(Fu & Xi, 2020). Heavy metal accumulation in soils is of concern in agricultural production due to the adverse effects on food safety, marketability and crop growth due to phytotoxicity, and environmental health of soil organisms (Ambika Asati1, 2016). Due to these adverse effects of heavy metals on environment it is necessary to treat the heavy metal

contaminated water before its released to environment, the different techniques used for this purpose are Coagulation/flocculation, ion exchange, flotation, membrane filtration, chemical Precipitation, electrochemical treatment, and adsorption (Carolin, Kumar, Saravanan, Joshiba, & Naushad, 2017). Among these, the adsorption method is more attractive due to its simplicity, no power consumption, low cost and easy operation. Using ionic liquids as adsorbent has certain advantages like high thermal stability, very low flammability and negligible vapor pressure ,which makes the process environment friendly(Chun, Dzyuba, & Bartsch, 2001).

In this work phosphonium based ionic liquid, Tributyl(tetradecyl)phosphoniumchloride $[P_{44414}][Cl]$, has been used for removal of Cadmium metal ions from aqueous solution. The point of zero charge and effect of other parameters like pH is being investigated for selection of optimum condition for extraction process.

Method

Materials

The ionic liquid used for Cadmium removal, namely Tributyl(tetradecyl)phosphoniumchloride $[P_{44414}][Cl]$, was supplied by Chemical Engineering department, COMSATS institute of information technology Lahore. Cadmium salt and deionized water was bought from Haq chemical Khyber bazar Peshawar.

Experimental procedure

For experiments aqueous solution of Cd was used with a concentration of 300 ppm. A specified quantity of ionic liquid was added to the solution which was then agitated for 30 minutes at 800 rpm. The two phases were then separated through centrifugation. The aqueous phase was tested through Atomic Adsorption Spectrometry (AAS) for finding out the final concentration of Cd ions. The percent removal of Cd by ionic liquid was then evaluated using the following equation.

$$\%E = \frac{Ci - Cf}{Ci} * 100$$

Where C_i is initial Cd concentration in ppm and C_f is Cd concentration in ppm after adsorption by ionic liquid.

Stock solution preparation

A stock solution of 1000 ppm (1000 mg/L) was prepared by dissolving 2.2818 g of cadmium salt in 1000 mL deionized water and stirring the solution with the help of magnetic stirrer. The rest of solution concentration required for experiments was prepared from stock solution through dilution.

Results

Evaluating point of zero charge

The point of zero charge (pH_{pzc}) is considered as the pH value at which there exists no net charge on the adsorbent surface. In this study the point of zero charge was investigated by adding ionic liquid to 0.1M solution of NaCl. The pH was adjusted to 2, 4, 6,8,10 and 12 respectively with the help of 0.1M HCl/NaOH. The solutions were then agitated for 30 minutes and then left still for 24 hours. The pH of the solutions were checked again after 24 hours and then point of zero charge was determined by plotting graph between initial pH and the change in pH. The point of zero charge was find out to be 6 for the ionic liquid. It shows the charges on the ionic liquid surfaces is positive at pH < 6 and negative at pH > 6 (Ma et al., 2019) .

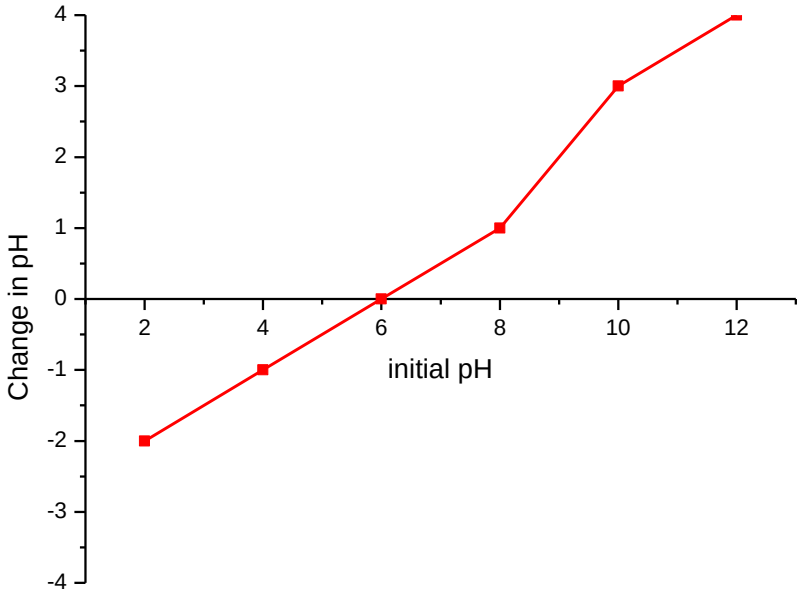

Fig.1. Points of zero charge determination by pH drift method for ionic liquid

Effect of pH on adsorption

The extraction experiments were performed at different pH ranging from 2 to 12. The maximum efficiency was noted to be at a pH of 8. Below this pH value the extraction was lower because at lower pH there is a positive charge on the surface of adsorbent as determined by point of zero charge, in which the attraction forces are weaker. The heavy metal removal process accelerates at a pH greater than 6 and its value is maximum at value of 8. Precipitation of Cadmium ions occurs at a pH higher than 8 due to which the removal of heavy metal from

aqueous solution by ionic liquid is affected.

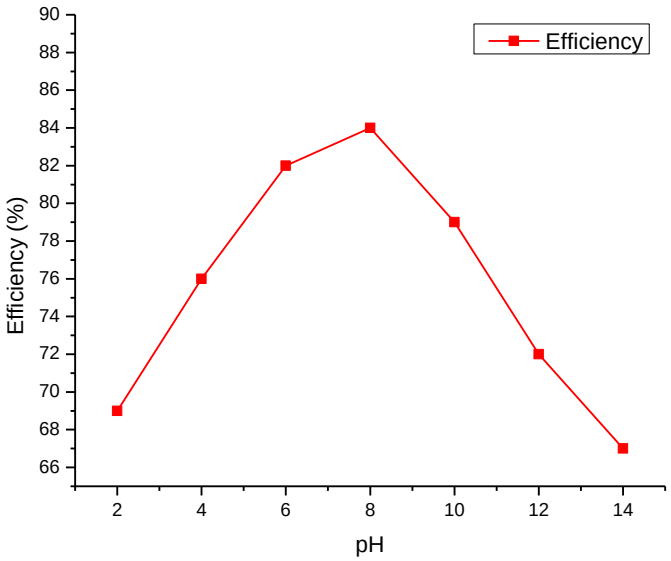

Fig.2. Effect of solution pH on removal efficiency of Cadmium ions

Conclusion

From this study it was concluded that the ionic liquid, Tributyl(tetradecyl) phosphoniumchloride [P_{44414}][Cl], showed a good extraction capacity up to 84% at a n optimum pH 0f 8.Hence this ionic liquid can be used as an adsorbent for Cadmium metal ions

References

Ambika Asati1, M. P. a. K. N. (2016). Effect of Heavy Metals on Plants: An Overview. *International Journal of Application or Innovation in Engineering & Management (IJAIEM)*.

Carolin, C. F., Kumar, P. S., Saravanan, A., Joshiba, G. J., & Naushad, M. (2017). Efficient techniques for the removal of toxic heavy metals from aquatic environment: A review. *Journal of Environmental Chemical Engineering, 5*(3), 2782-2799. doi:10.1016/j.jece.2017.05.029

Chun, S., Dzyuba, S. V., & Bartsch, R. A. J. A. C. (2001). Influence of structural variation in room-temperature ionic liquids on the selectivity and efficiency of competitive alkali metal salt extraction by a crown ether. *73*(15), 3737-3741.

Fu, Z., & Xi, S. (2020). The effects of heavy metals on human metabolism. *Toxicology mechanisms and methods, 30*(3), 167–176.

Ma, J., Li, T., Liu, Y., Cai, T., Wei, Y., Dong, W., & Chen, H. (2019). Rice husk derived double network hydrogel as efficient adsorbent for Pb(II), Cu(II) and Cd(II) removal in individual and multicomponent systems. *Bioresour Technol, 290*, 121793. doi:10.1016/j.biortech.2019.121793

On numerical solution of First-order non-linear ODEs with high frequency forcing term

Latif Ullah Khan[1*], Sakhi Zaman [1]

[1]Faculty of Achitecture, Allied Sciences and Humanities, University of Engineering and Technology Peshawar, Pakistan

[1]Corresponding author*

Email: latifmiu@gmail.com

Abstract

In this paper, we formulate a new technique for numerical solution of first-order linear and nonlinear ordinary differential equations with high frequency forcing term. Non-linear ODEs with high frequency forcing term have two main challenges: the non-linearity and the presence of high frequency. To handle both the challenges, we have implemented meshfree collocation method with Levin approach. Accordingly, the oscillatory ODE is transformed to a highly oscillatory integral with Fourier kernel. Global radial basis functions with a free shape parameter are used as basis function. The method is accurate as well as efficient in scenario of oscillatory ODEs. Numerical results are compared with some stat of the art methods in the literature [8].

Key words: Highly oscillatory ODEs, Meshless collocation method, Radial basis functions, Levin method.

Introduction

Our underlying task of the numerical solation of highly oscillatory linear and nonlinear ODEs. We considering some cases of the problem, which can be generally expressed as

$$\boldsymbol{x}' = \boldsymbol{A}\boldsymbol{x} + \boldsymbol{F}(t)h_\omega(t), \quad t \geq 0, \ \boldsymbol{x}(\boldsymbol{0}) = \boldsymbol{x_0} \in \boldsymbol{R^n}, \qquad (1)$$

where $\boldsymbol{A}$ is a coefficient matrix of a_{ij} of unknown function of $\boldsymbol{x}$, $h_\omega(t)$ is oscillating function of a frequency parameter $\boldsymbol{\omega}$ >>1, while $\boldsymbol{F}(t)$ is an analytic function. These type of ODEs appear in different field of modeling, engineering, and electronics circuit notably in the resonance frequency [5, 6]. The generalized solution of ODE (1) can be written as

$$x(t) = e^{At}x_0 + e^{At}\int_0^t e^{-A\nu}\,\boldsymbol{F}(\nu)\ h_\omega(\nu)\ \ d\nu \qquad (2)$$

In highly oscillatory ODEs the oscillatory factor ω^{-1} having main rule in the problem. Due to the presence of oscillatory factor ω^{-1} the classical numerical methods have high computational cost and some time inaccurate. Particularly, there are significant

difference between the two relevant time scales $\omega^{-1} \ll h$, where ω^{-1} used for frequency time scale and h used for step size mesh distances. For this the reason, the authors [7, 10], derived few numerical techniques for evaluation of rapidly oscillatory ordinary differential equations. Recently, state of the art numerical methods i.e. asymptotic method and Filon-types of method have been applied to approximate highly oscillatory ODEs [8].

Many prominent researchers and scientists have been contributed the numerical solution of IVPs in field of science, engineering and modeling. Researchers have been used the numerical quadrature techniques of single step methods (like as Euler methods, Runge-kutta methods), Multistep Methods (Adam-Bashforth methods and Adam-Molton methods) and some more [3, 11, 17], for the solution of IVPs. Some latest and advance numerical methods have also been developed for approximation of ODEs, like Newton-Cotes quadrature, approximation techniques based on Taylor's series expansion [15], in which multi-step methods is reduced to single step methods.

The Existing numerical methods were required additional memory if an error estimated was required. In [1], the authors have proposed a numerical method of a hybrid numerical scheme with two off-grid points for solution of general second order ODEs. The method used collocation and interpolation techniques. Recently, the author [16] presented a new Runge-kutta-type collocation methods for computation of ordinary differential equations using integral solution. It enhances the accuracy for the demonstration of Gauss-Legendre and Lobatto-III A methods. The method is similar to Butcher tableaues.

The problems in [13] have an impulsive dynamical behavior due to abrupt change at certain instant of an impulsive differential equations controlling by the solution of exact controllability with impulses. The author [9] have extended the classical method and used multi-value collocation method for numerical solution of IVPs. The problem in [5] numerically solved highly oscillatory ordinary differential equations with forcing term by asymptotic expansion method. In electronics circuits the authors [2] optimized transmission line circuit problems of coupled system of ODEs and PDEs by the waveform relaxation (WR) method. The authors [4] have solved stochastic differential equations by generalized Filon quadrature and this numerical quadrature is also applicable to a wide variety of ordinary differential equations with rapidly oscillating factors.

The multi-scale interactions of stochastic equations are frequently applicable in numerical models of weather and climate. In [14], authors have used classical Gaussian white noise process to solve the basic properties of stochastic differential equations and compared with systems described by stable L´evy processes. The authors [8] have considered an integral form solution of the highly oscillatory linear and nonlinear IVPs

and then oscillatory integrals are numerically evaluated by the asymptotic method and Filon type methods. In the current work, we have extended the algorithms [8] and applied mesh free liven type of collocation method to approximate the targeted integral.

Numerical procedure

The method is an efficient to solve the numerical ODEs and PDEs with highly oscillatory forcing term ω. Accordingly initial value problem can be written as

$$\boldsymbol{x}' = \boldsymbol{A}\boldsymbol{x} + \chi_{\omega}(t), \qquad t \geq 0, \ \boldsymbol{x}(\boldsymbol{0}) = \boldsymbol{x_0} \tag{3}$$

The generalized solution of linear ODEs (3) is given as [12]

$$\boldsymbol{x(t)} = \boldsymbol{e^{At}x(t_0)} + \boldsymbol{e^{At}} \int_{\boldsymbol{0}}^{\boldsymbol{t}} \boldsymbol{e^{-A\tau}\chi_{\omega}(\tau)d\tau} \tag{4}$$

Where A is a constant parameter and $\chi_{\omega}(t)$ is an oscillatory function containing highly oscillatory forcing term ω^{-1}. In the current work, we assume $\chi_{\omega}(t)$ as a Fourier oscillator i.e. and $\chi_{\omega}(t) = e^{i\omega g(t)}$, where $g'(t) \neq 0$ for $t \in [a, b]$. $\omega \gg 1$ is the oscillatory forcing term.

Numerical form of (4) can be written as

$$x(t_{i+1}) = e^{At_i}x(t_i) + e^{At_i} \int_{t_i}^{t_{i+1}} e^{-A\tau}\chi_{\omega}(\tau)d\tau \tag{5}$$

Meshfree collocation method with Liven approach:

Global RBFs produces the function $\varphi(r, \wp)$ by using the linear combinations for approximation of integrands of integral (5) is a univariate smooth and continues functions $\mathcal{R}(\ell)$. The intervals of (5) are sub discretizing as $[t_i = \ell_0 < \ell_1 < \cdots, < \ell_m = t_{i+1}]$ and m-centers of $\ell_0, \ell_1, \ldots, \ell_m \in \mathbb{R}$, interpolates the function

$$\mathcal{R}(\ell) = \sum_{j=0}^{m} \zeta_j \ \varphi(r, \wp), \qquad r = ||\ell - \ell_j||_2, \qquad j = 0,1, \ldots, m \tag{6}$$

where $\wp$ is the free shape parameter of RBF interpolation and also depends upon the optimal value of $\wp$. ζ_j is the unknown coefficients which satisfying the interpolation conditions and can be determined by linear equation (6)

$$\mathcal{R}'(\ell) + \iota\omega g'(\ell)\mathcal{R}(\ell) = \boldsymbol{F}(\ell)$$
$$\boldsymbol{\zeta}[\varphi'(r,\wp) + \iota\omega g'(\ell)\varphi(r,\wp)] = \boldsymbol{F}(\ell)$$

and

$$\zeta = \mathrm{B}^{-1}\mathrm{F}.$$

Where ζ is the unknown coefficient, F are m-vectors and B_{m*m} is a square of matrix can be define as

$$\mathrm{B} = \varphi'(\mathrm{r},\wp) + \iota\omega g'(\ell)\varphi(\mathrm{r},\wp) \qquad (7)$$

In matrix $\boldsymbol{B}$, $\varphi(\mathrm{r},\wp) = \sqrt{r^2+\wp^2}$ and $\varphi'(\mathrm{r},\wp) = \frac{r}{\sqrt{r^2+\wp^2}}$ are collocation points.

Right side of the integral form of (5), can be written as

$$\int_{t_i}^{t_{i+1}} e^{-A\tau}\chi_\omega(\tau)\,d\tau = \int_{t_i}^{t_{i+1}} [\mathcal{R}'(\tau) + \iota\omega g'(\tau)\mathcal{R}(\tau)]\chi_\omega(\tau)\,d\tau$$
$$= \int_{t_i}^{t_{i+1}} \frac{d}{d\tau}\,[\mathcal{R}(\tau)\chi_\omega(\tau)\,]\,d\tau$$
$$= \mathcal{R}(t_{i+1})\chi_\omega(t_{i+1}) - \mathcal{R}(t_i)\chi_\omega(t_i)$$

Thus the desired approximate solution of IVP is

$$x(t_{i+1}) = e^{At_i}x(t_i) + e^{At_i}[\mathcal{R}(t_{i+1})\chi_\omega(t_{i+1}) - \mathcal{R}(t_i)\chi_\omega(t_i)]$$

Now to find the approximate function $\mathcal{R}(t)$, we substitute the value of $\mathcal{R}(t)$ in the discretized form of the ODE (7) and find the values of the unknowns ζ_j by solving the system of linear equations. The system of equations is solved by the LU-Factorization instead of Gauss-elimination method.

Numerical assessment

For numerical justification of the proposed methods, we have considered some benchmark problem of highly oscillatory first order linear and non-linear ODEs and compared the results of the proposed methods with asymptotic method [10]. Accuracies of the proposed methods are measured in terms of infinity norm $||L||_\infty$ and absolute errors E_{abs} CPU time (in seconds) is also computed for efficiency of the new methods. Results are also compared with some methods like asymptotic method and multivalue collocation method [9] in case of highly oscillatory ODEs.

Test problem 1: Consider the following highly oscillatory ODE [9]

$$x'(t) = -x(t) - \sin(wt) + w\cos(wt), \quad t \geq 0, \quad x(0) = 0. \tag{8}$$

The highly oscillatory ODE (8) has been considered from [9]. Exact solution of oscillatory ODE is given as

$$x(t) = \sin(wt).$$

The ODE (8) is highly oscillatory and is approximated by the proposed method LCM. The results of the proposed method are more accurate than the multivalue collocation method reported in [9]. The maximum absolute errors of the new method are analyzed in **table** 1, which demonstrates that the proposed method gives the desired accuracy on increasing m. It is also shown in the **table** 1 that as we increase the value of m, the method performs better.

Table 1: $||L_{abs}||$ produced by LCM $\omega = 10^2$ and the method reported in [9].

Methods	$h = \frac{1}{40}$	$h = \frac{1}{80}$	$h = \frac{1}{160}$	$h = \frac{1}{320}$	$h = \frac{1}{640}$
LCM	2.1245e - 08	8.7465e – 09	1.8867e – 08	8.9834e - 09	2.0778e - 09
[9]	2.7642e - 01	3.2665e – 02	2.4876e – 09	1.5543e - 04	9.8568e - 06

Test problem 2: Let us consider the following non-linear highly oscillatory IVP [4]

$$x'(t) = x(t) + x^2(t)e^{i\omega t}, \quad t \geq 0, \quad x(0) = 1, \tag{9}$$

With analytic solution

$$x(t) = -e^{i\omega t} + e^{-t}(1 + e^{i\omega t}).$$

To linearize the highly oscillatory ODE (9) by substituting $u(t) = x^{1-\alpha}$

$$u(t) = x^{-1}$$

Differentiating with respect to "t", we get

$$u'(t) = x^{-2}x'$$

Equation (9) reduce to linear form

$$u'(t) = -u(t) - e^{i\omega t}, \quad t \geq 0, \quad x(0) = 1. \tag{10}$$

The transformed linear ODE (10) is approximated by the proposed LCM. Results and CPU time (in seconds) are analyzed in **table** 2 and **Fig.** 1. **Table** 2 demonstrates that the new method improves accuracy on increasing m and ω.

The computational time relative to m is calculated and displayed in **Fig.** 1 (left). We see that the new method is efficient as well. Exact solution of the oscillatory ODE is displayed in **Fig.** 1 (right). From the whole discussion, it is obvious that the LCM is an accurate tool for approximating the oscillatory type linear ODEs.

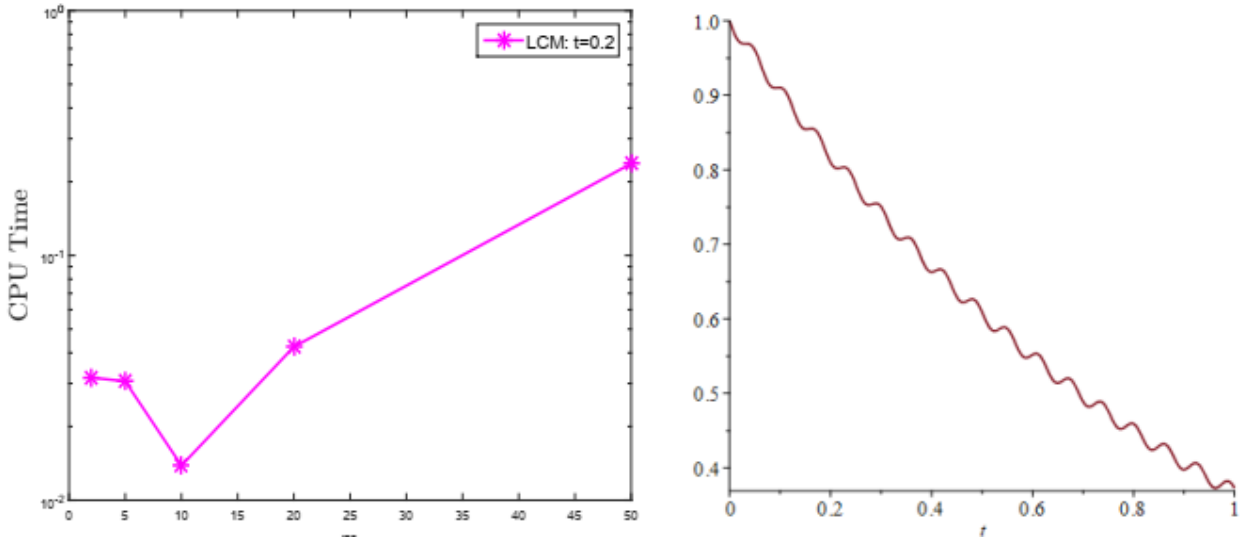

Figure 1: (Left) CPU time (in seconds) for fixed shape $\wp = 0.5$ and varying m, (Right) Analytical solution by MAPLE-16 of ODE (10).

Table 2: $||L_{abs}||$ produced by LCM $t = 0.2$ and the method reported in [4].

ω/m	2	5	10
1	$8.1454e$ - 07	$1.1735e$ - 08	$3.1253e$ – 09
10	$9.8465e$ - 06	$1.6143e$ - 10	$8.4062e$ – 11
100	$9.5645e$ - 07	$8.0054e$ - 11	$1.7334e$ – 11
500	$2.6282e$ - 09	$3.1856e$ - 11	$3.5039e$ – 11
1000	$5.1168e$ - 09	$4.3857e$ - 11	$4.4931e$ – 11

Conclusions

In this paper a new approach of Levin meshless method is proposed for approximating the numerical ODEs with oscillatory kernele$^{i\omega g(t)}$. In this work we have used the modified Levin theory with interpolation to solve the integrated form of highly oscillatory ODEs. Since highly oscillatory ODEs contains Fourier kernel with initial conditions which is difficult to solve, so we have implemented the meshless method to resolve this problem. It has been observed that this technique is numerically stable and give the accurate results. In this method the asymptotic order of convergence has also been established and verified numerically.

References

[1] AO Adeniran and BS Ogundare. An efficient hybrid numerical scheme for solving general second order initial value problems (IVPs). *International Journal of Applied Mathematics Research, 4(2): 411, 2015.*

[2] Mohammad D Al-Khaleel, Martin J Gander, and Albert E Ruehli. Optimized waveformrelaxation solution of rlcg transmission line type circuits. *In 2013 9th*

International Conference on Innovations in Information Technology (IIT), pages 136{140. IEEE, 2013.

[3] Vish Subramaniam Amos Gilat. Numerical methods for engineers and scientists. *Don Fowley, 2014*.

[4] JE Bunder and Anthony J Roberts. Numerical integration of ordinary differential equations with rapidly oscillatory factors. *Journal of computational and applied mathematics*, 282:54-70, 2015.

[5] Marissa Condon, Alfredo Deano, and Arieh Iserles. On asymptotic numerical solvers for differential equations with highly oscillatory forcing terms. *Technical report, Citeseer, 2009.*

[6] Marissa Condon, Alfredo Dea~no, and Arieh Iserles. On highly oscillatory problems arising in electronic engineering. *ESAIM: Mathematical Modelling and Numerical Analysis*, 43(4):785-804, 2009.

[7] Marissa Condon, Alfredo Dea~no, and Arieh Iserles. On systems of differential equations with extrinsic oscillation. *Discrete & Continuous Dynamical Systems-A*, 28(4):1345, 2010.

[8] Marissa Condon, Arieh Iserles, and SP Nørsett. Differential equations with general highly oscillatory forcing terms. *Proceedings of the Royal Society A: Mathematical, Physical and Engineering Sciences*, 470(2161):2013-0490, 2014.

[9] M. P. DArienzo B. Paternoster D. Conte, R. DAmbrosio. Multivalue mixed collocation methods. *Applied Mathematics and Computation*, 409:126-346, 2021.

[10] Arieh Iserles. On the numerical analysis of rapid oscillation. In *Group Theory and Numerical Analysis, CRM Proc. Lecture Notes*, volume 39, pages 149-163, 2005.

[11] David I Ketcheson. Runge-kutta methods with minimum storage implementations. *Journal of Computational Physics*, 229(5):1763-1773, 2010.

[12] Marianna Khanamiryan. Quadrature methods for highly oscillatory linear and nonlinear systems of ordinary differential equations: part I. *BIT Numerical Mathematics*, 48(4):743, 2008.

[13] JuanJ Nieto and ChristopherC Tisdell. On exact controllability of first-order impulsive differential equations. *Advances in Difference Equations*, 2010:19, 2010.

[14] C´ecile Penland and Brian D Ewald. On modelling physical systems with stochastic models: diffusion versus l´evy processes. *Philosophical Transactions of the Royal Society A: Mathematical, Physical and Engineering Sciences*, 366(1875):2455-2474, 2008.

[15] Maitree Podisuk, Ungsana Chundang, and Wannaporn Sanprasert. Single step formulas and multi-step formulas of the integration method for solving the initial value problem of ordinary differential equation. *Applied mathematics and computation*,190(2):1438-1444, 2007.

[16] Janez Urevc and Miroslav Halilovi˘c. Enhancing accuracy of runge-kutta-type collocation methods for solving odes. *Mathematics*, *9(2):174, 2021*

[17] Dennis G Zill. A first course in differential equations with modeling applications. *Cengage Learning, 2012*.

Heavy Metal Remediation from Wastewater Using Local Plant Biomass

Muhammad Bilal[1*], Mansoor Ul Hassan Shah[1*], Mohammad Younas[1]

[1]Chemical Engineering Department, UET Peshawar, 27120

[1]Mansoor Ul Hassan Shah*

Email: mansoorshah@uetpeshawar.edu.pk

Abstract

Humanity across the globe is facing serious threat in the shape of water pollution. Agro wastes have been the focus of interest as a reliable source of sustainable adsorbents for water pollution particularly heavy metal removal from wastewater. In this study, locally available plant biomass was utilized for the elimination of potentially toxic metal ions from polluted water. The synthesized bio-adsorbent was tested for its water purifications and the results were compared with the standard values. The effect of various operating parameters like contact time for adsorption, preliminary concentrations of pollutants, and temperature were carefully analyzed. The corresponding sorbent showed higher uptake capacity towards trace elements and more than 90% removal efficiency was achieved. The employed bio-sorbent showed quite better regeneration potential up till six adsorption/desorption cycles through the application of normal distilled water as an eluent. Therefore the result presented in the current study revealed the sustainable and economical use of locally available plants biomass derived bio-sorbents for the remediation of heavy metal ions.

Key words: Water pollution, heavy metal adsorption, bio-sorbent, sustainable.

Introduction

The affinity of bio-sorbents towards uptake of toxic metal pollutants from aqueous environment was explored as early as 18th and 19th centuries [1]; however, extensive bio-materials have been utilized as sorbents for the elimination and recovery of trace elements and other pollutants from water environment in last some decades. The most primitive high-tech applications of bio-adsorption techniques involved the treatment of sewage and other wastes [2]. The exploration and development of bio-sorption processes laid the foundations for a whole new and innovative technology intended at the elimination of diverse noxious pollutants. At present, bio-sorption is one of the key technique of environmental and bio-resource technology. With the passage of time, when the applications of sorbents improved, the leading challenge confronted by researchers was to pick up the best possible and encouraging biomass from particularly available diverse bio-materials [3]. For commercial applications, the leading concerning cause in selecting a biomass is its availability and cost effectiveness [4], [5]. Therefore, considering such factors, local biomass could be collected from either

agricultural or industrial wastes, or organisms that are easily attainable in hefty sums in nature; or that can also be developed rapidly for bio-adsorption purposes [6]. A variety of bio-materials have been tried for their affinities towards binding pollutants, under different circumstances, but there are no limitations to further explore novel low-cost and high efficient bio-adsorbents.

The potentially toxic metals in various industrial effluents poses serious health concerns in the communities and the environment. These trace elements could cause potential health concerns because these can move up along the aquatic food chain via bio-magnification process, after its discharge in diverse industrial and local wastewaters [7]. Trace elements are generally toxic in nature and therefore cannot be degraded by simple ordinary treatment methods, rather it could be stored and bio-accumulate in the bodies of living organisms [8]. Therefore it is necessary to eliminate the trace elements from water environment in order to achieve toxicity free water.

Different conventional treatment methods are used for the remediation of heavy metals ions from wastewater. These are ranges from, but are not limited to, electrolysis [9], chemical precipitation [10], adsorption [11], graphene based membrane separation [12] , liquid-liquid extraction [13] etc. However, such mentioned techniques have disadvantages like high energy utilization, and generation of secondary pollution [14]. Therefore, switching to an alternative, low-cost and innovative remediation method like bio-sorption is the need of time so to treat the toxic effluents of various industries, before discharging to water bodies.

Bio-adsorption, due to its environmental friendly nature, have gained widespread attention in removing trace elements from wastewater and diverse plant biomasses could be used for synthesizing bio-sorbents [15]. Different researches provided extensive applications of different adsorbent in heavy metal (cadmium, copper, ferrous, manganese, lead and zinc) remediation, ranges from, but are not limited to, obligate halophilic fungi comprising *Aspergillus flavus*, *Aspergillus gracilis*, *Aspergillus penicillioides*, *Aspergillus restrictus*, and *Sterigmatomyces halophilus* [7]. This research work is focused on assessing water purification, specifically the elimination of heavy metal from polluted water, by the locally synthesized adsorbent from the available raw biomasses. An insight to bio-sorption mechanism has also enlightened and the regeneration properties of the loaded sorbent are evaluated.

Methodology

The waste biomasses were collected locally in the form of leaves shaded from the plants and trees. Then they were duly washed with double distilled water in order to remove dust particles if there is any. The collected biomasses were oven dried at 80 ºC for some 5 hours and then size analysis was performed in Analytical Sieve Shaker. The

size ranges of about 125- 500 Microns were selected for further processing and the samples were then again washed in order to remove the colors. The powdered sample were dried again at 80 °C for 3 hours and the physically synthesized sorbent is ready to use for the respective treatment of heavy metal polluted water. **Fig. 1** illustrated the synthesis technique of the physically developed bio-sorbent.

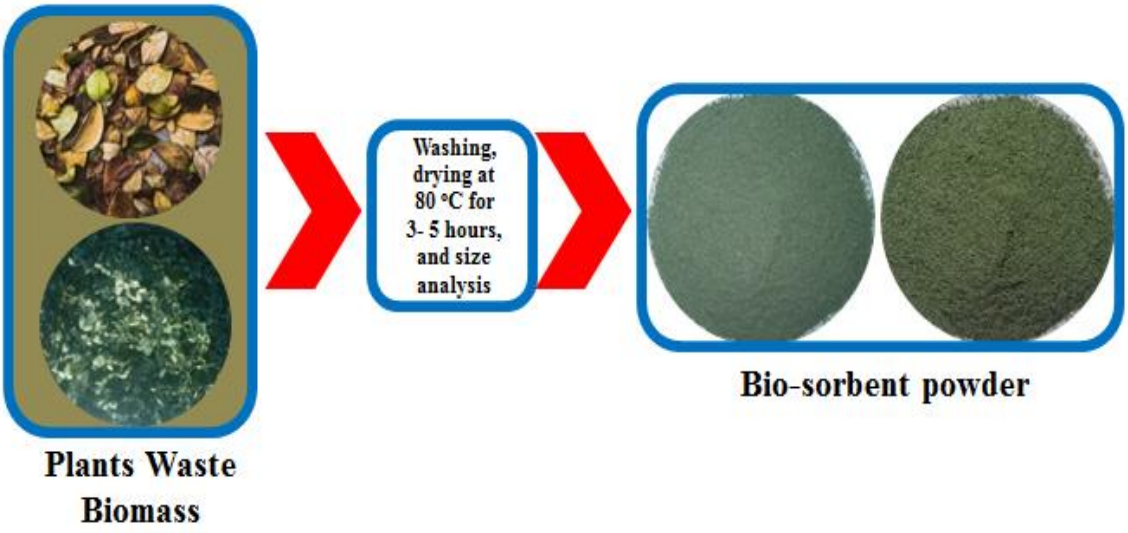

Fig. 1: Synthesis method of the locally synthesized bio-adsorbent from waste biomass.

Results and discussion

The elimination of toxic metal pollutants from wastewater is a major concern in wastewater treatment technologies. They are known to be bio-accumulative and noxious for living organisms, even in minute concentrations and are producing as a byproduct in various industries; where, they are exposing to the environment and after reaching water bodies resulting in wastewater pollution, severely affecting the aquatic and human lives. Therefore the removal of such lethal pollutants from aqueous environment is much needed in adopting a greener route. This research thesis is mainly focus on the applications of bio-sorbents for heavy metal adsorption from aqueous environment. The adsorption capacity and adsorption efficiency of the employed bio-adsorbent can be calculated by the application of the following two equations;

$$Adsorption\ capacity\ (\frac{mg}{g}) = \frac{C_i - C_o}{C_i} * 100 \qquad (1)$$

$$Adsorption\ efficiency\ (\%) = (C_i - C_o) * \frac{V}{M} \qquad (2)$$

Where C_i and C_o are the initial and final concentration of pollutant, V is the volume of solution (polluted water) used and M is the mass of utilized bio-sorbent.

Table 1: Adsorption experiments of the employed bio-sorbent

Initial concentration of pollutant (mg/L)	Final concentration of pollutant (mg/L)	Adsorption efficiency of pollutant (%)
1000	0.660	99.93
500	1.312	99.7376
100	0.245	99.755
10	0.544	94.56

Characterizations

Different characterization techniques were employed for assessing the physicochemical characteristics of the employed adsorbent. These may include FTIR- Fourier Transform Infrared spectroscopy for acknowledging the possible functional groups present on the surface of bio-sorbent, SEM- scanning electron microscopy for observing the structural behavior of the employed surfaces, BET- Brunauer-Emmette-Teller analysis for determining the surface area and pore size distribution of various bio-sorbents, and AAS- atomic absorption spectroscopy for analyzing the concentration of pollutants in wastewater before and after the adsorption. The FTIR spectroscopic results yielded versatile and diverse functional groups like amino, carbonyl, carboxyl and hydroxyl which are imperative in providing as a binding source for the accommodation of positively charged metal ions. Similarly SEM results pointed out the presence of minute pores and surface defects on the bio-sorbent's surface which acts as a diffusing portion for heavy metal pollutants through which the trace elements diffuse and seeps into the surface of adsorbent. The SEM results were acknowledged before and after the process of adsorption so to carefully exhibit and study the change in the surface of the bio-sorbent after sticking of the pollutant ions to the bio-sorbent surface. **Fig. 2** illustrates the SEM micrographs of locally synthesized adsorbent from waste biomasses. BET analysis is reflected as a foremost method to analyze surface imperfections and defects of various sorbents. The distribution of pore size and surface area of physically developed sorbents were observed using a series Surface Area and Porosity Analyzer.

Factors affecting adsorption

Adsorption is a surface phenomenon and therefore it depends upon certain key factors. The contact time for adsorption of heavy metal pollutants, preliminary concentrations of trace elements, and temperature of the polluted water are some important constraints whose effects needs to be assessed. The process of adsorption will be exothermic if the adsorption capacities of an adsorbent decreases with increase in temperature. Similarly, if the adsorption capacities increases with increase in temperature then it will results in endothermic nature of adsorption. The adsorption removal of the employed adsorbent increases with increase in the initial concentrations of the potentially toxic metal ions. This is because initially, large amount of

opening spaces were available on the surface of adsorbent which with time, the spaces occupied

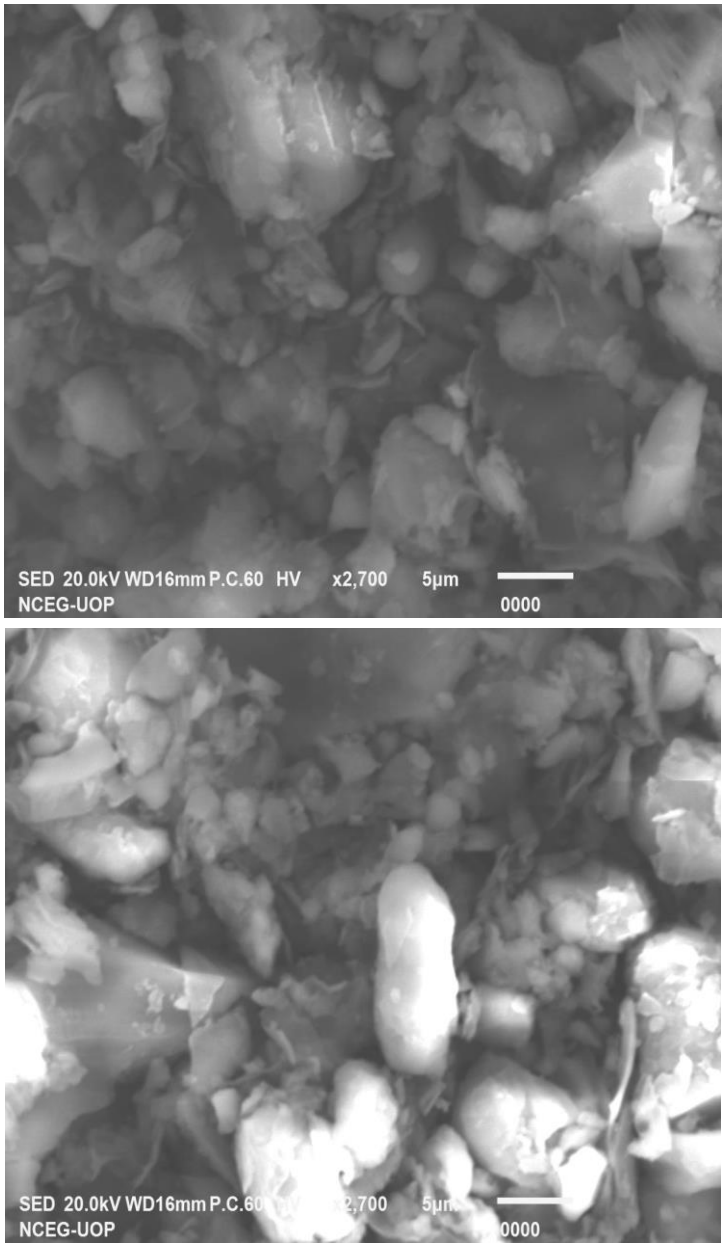

Fig. 2: SEM micrographs of locally synthesized bio-adsorbent from waste biomass.

with the heavy metal ions. There are also some other factors like pH of the polluted water, stirring speed of the magnetic stirrer, and the co-existence of simultaneous potentially toxic metal ions which needs to be explored in future recommendations.

Regeneration of loaded bio-adsorbent

The primary objective of any relevant adsorbent depicted from its applications in industries for treatment of polluted water. Therefore, for commercial processes, the bio-sorbent should possess high sorption capacities alongside the long term stability and reusability for their redevelopment [16], [17]. Therefore, it is essential to desorb trace elements from loaded bio-sorbent that have been utilized in toxic metal polluted water treatment.

Ordinary distilled water with natural pH value was used as eluent for desorbing cadmium ions from the loaded bio-adsorbents. The loaded adsorbents were made dried first then added the eluent in specific amount (1g/100mL generally) and after that, the mixture were treated with the help of magnetic stirrer a 50rpm speed at higher temperature, for about 2 hours. The treated samples are then centrifuged for 30 minutes, separating powder adsorbents from liquid eluent. At the end, the bio-adsorbents were heated again in an electric oven at 105°C for 2 hours to make them dry. The redeveloped adsorbents are now ready to use it again. The same procedures repeated for every regeneration cycle. **Table 2** represents the percentage removal of the locally synthesized adsorbent from waste biomass after each successive adsorption/desorption cycle. **Fig. 3** represents the percentage removal of pollutants in each successive adsorption/desorption cycles. The desorption capacity (mg/g) and efficiency (%) can be calculated by the use of eq (3) and (4) respectively.

$$Desorption\ efficiency\ (\%) = \frac{q_d}{q_{eq}} \times 100 \qquad (3)$$

$$Desorption\ capacity\ (q_d)\ \left(\frac{mg}{g}\right) = \frac{V \times C_o}{M} \qquad (4)$$

Where q_d is the desorption capacity in mg/g and q_{eq} is the capacity of bio-sorbent at equilibrium in mg/g, and M is the mass of the used adsorbent.

Table 2: Regeneration potential of bio-sorbent after each successive cycle.

Locally synthesized bio-sorbent	
Regeneration cycle	**Percentage removal (%)**
1st cycle	99.74
2nd cycle	99.66
3rd cycle	97.03
4th cycle	97.34
5th cycle	95.81
6th cycle	83.48

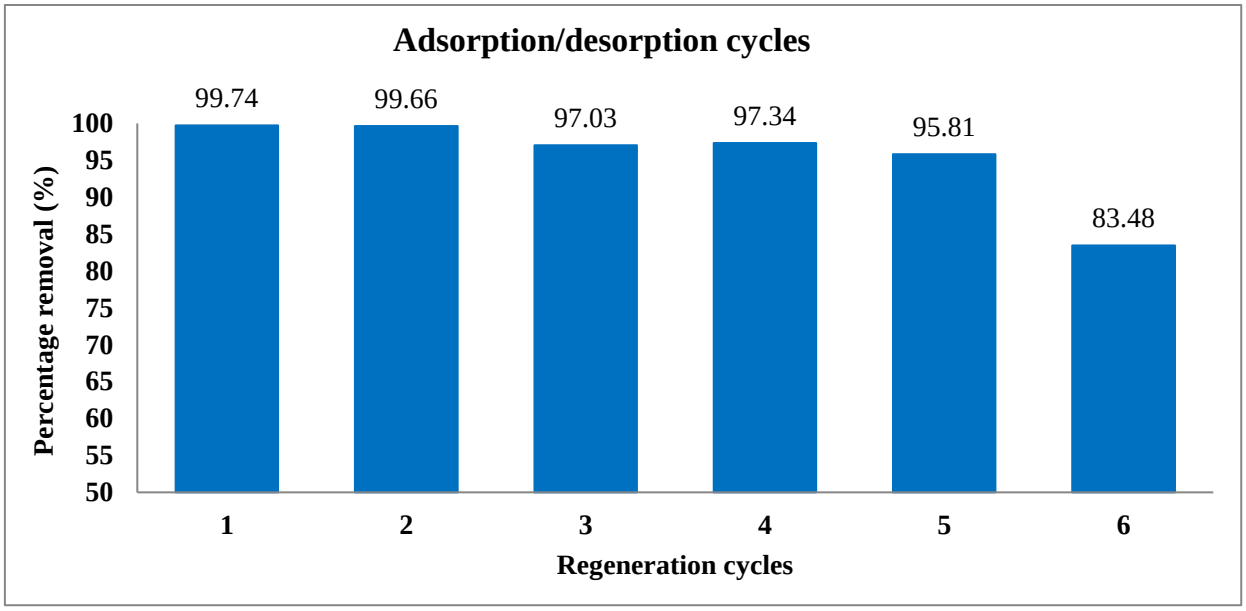

Fig. 3: Regeneration potential of locally synthesized bio-adsorbent from waste biomass.

Table 3: Comparison of different bio-sorbent applied against single/multiple pollutants.

Adsorbent	**Pollutants (Adsorbate)**	**pH**	**Temp**	**Adsorption capacity (mg/g)/ efficiency (%)**	**Reference**
Rice husk biochar	Single pollutant	----	28	93.5 mg/g	[18]
Litchi peel	Single	5	25	----	[19]
Egg shell	Single	6	Room	73	[20]
Modified orange peel	Single	7	45	82	[21]
Locally synthesized bio-sorbent	Single pollutant	6	25	99.76	This study

Conclusions

The presence of even trace amount of trace elements in wastewater often results in end of life, due to their lethal and non-degradable nature, as they tends to bio-accumulate and therefore, cannot be degraded by simple biological methods. It is much challenging to describe a widespread method that might be applied for the removal of heavy metal pollutants from wastewater. Bio-adsorption, now-a-days is holding much attention due to low-cost, efficient and innovative alternative technique for the remediation of potentially toxic heavy metal ions from aqueous environment. The current study also explored a novel bio-sorbent from the locally available plants biomasses for the successful elimination of trace element from polluted water and therefore further exploration needs to be done so to enhance its applicability in multiple or

co-existence ions in wastewater. The locally synthesized adsorbent was successfully tested for water purification in remediating potentially toxic metal ions from wastewater and the physicochemical characteristics of the powdered adsorbent was acknowledged and assessed by the application of different characterization tools. The loaded bio-adsorbent was successfully regenerated and better adsorption removal was shown till six successive adsorption/desorption cycles. This whole research showed that the employed adsorbent have the potential to be using in future research recommendations for the successful elimination of potentially toxic metal ions from polluted water.

References

[1] J. M. Modak and K. A. Natarajan, "Biosorption of metals using nonliving biomass—a review," *Mining, Metall. Explor.*, vol. 12, no. 4, pp. 189–196, 1995.

[2] A. H. Ullrich and M. W. Smith, "The biosorption process of sewage and waste treatment," *Sewage Ind. Waste.*, pp. 1248–1253, 1951.

[3] D. Kratochvil and B. Volesky, "Advances in the biosorption of heavy metals," *Trends Biotechnol.*, vol. 16, no. 7, pp. 291–300, 1998.

[4] R. H. Vieira and B. Volesky, "Biosorption: a solution to pollution?," *Int. Microbiol.*, vol. 3, no. 1, pp. 17–24, 2000.

[5] B. Volesky, "Advances in biosorption of metals: selection of biomass types," *FEMS Microbiol. Rev.*, vol. 14, no. 4, pp. 291–302, 1994.

[6] B. Volesky and Z. R. Holan, "Biosorption of heavy metals," *Biotechnol. Prog.*, vol. 11, no. 3, pp. 235–250, 1995.

[7] A. Bano *et al.*, "Biosorption of heavy metals by obligate halophilic fungi," *Chemosphere*, vol. 199, pp. 218–222, May 2018, doi: 10.1016/J.CHEMOSPHERE.2018.02.043.

[8] V. K. Gupta, M. Gupta, and S. Sharma, "Process development for the removal of lead and chromium from aqueous solutions using red mud - An aluminium industry waste," *Water Res.*, vol. 35, no. 5, pp. 1125–1134, 2001, doi: 10.1016/S0043-1354(00)00389-4.

[9] H. Luo, G. Liu, R. Zhang, Y. Bai, S. Fu, and Y. Hou, "Heavy metal recovery combined with H2 production from artificial acid mine drainage using the microbial electrolysis cell," *J. Hazard. Mater.*, vol. 270, pp. 153–159, Apr. 2014, doi: 10.1016/J.JHAZMAT.2014.01.050.

[10] Q. Chen, Y. Yao, X. Li, J. Lu, J. Zhou, and Z. Huang, "Comparison of heavy metal removals from aqueous solutions by chemical precipitation and characteristics of precipitates," *J. Water Process Eng.*, vol. 26, pp. 289–300, Dec. 2018, doi: 10.1016/j.jwpe.2018.11.003.

[11] M. Bilal, I. Ihsanullah, M. Younas, and M. Ul Hassan Shah, "Recent advances in applications of low-cost adsorbents for the removal of heavy metals from water: A critical review," *Sep. Purif. Technol.*, vol. 278, p. 119510, Jan. 2022, doi: 10.1016/J.SEPPUR.2021.119510.

[12] Y. Vasseghian, E.-N. Dragoi, F. Almomani, V. T. Le, and M. Berkani, "Graphene-based membrane techniques for heavy metal removal: A critical review," *Environ. Technol. Innov.*, vol. 24, p. 101863, Nov. 2021, doi: 10.1016/J.ETI.2021.101863.

[13] A. Łukomska, A. Wiśniewska, Z. Dąbrowski, and U. Domańska, "Liquid-liquid extraction of cobalt(II) and zinc(II) from aqueous solutions using novel ionic liquids as an extractants," *J. Mol. Liq.*, vol. 307, p. 112955, Jun. 2020, doi: 10.1016/J.MOLLIQ.2020.112955.

[14] D. Kumari, R. Goswami, M. Kumar, P. mazumder, R. Kataki, and J. Shim, "Removal of Cr(VI) ions from the aqueous solution through nanoscale zero-valent iron (nZVI) Magnetite Corn Cob Silica (MCCS): A bio-waste based water purification perspective," *Groundw. Sustain. Dev.*, vol. 7, no. November 2017, pp. 470–476, 2018, doi: 10.1016/j.gsd.2017.12.007.

[15] N. Vanhoudt, H. Vandenhove, N. Leys, and P. Janssen, "Potential of higher plants, algae, and cyanobacteria for remediation of radioactively contaminated waters," *Chemosphere*, vol. 207, pp. 239–254, Sep. 2018, doi: 10.1016/J.CHEMOSPHERE.2018.05.034.

[16] S. S. Li *et al.*, "Upon designing carboxyl methylcellulose and chitosan-derived nanostructured sorbents for efficient removal of Cd(II) and Cr(VI) from water," *Int. J. Biol. Macromol.*, vol. 143, pp. 640–650, Jan. 2020, doi: 10.1016/j.ijbiomac.2019.12.053.

[17] L. Chen *et al.*, "Preparation and characterization of the eco-friendly chitosan/vermiculite biocomposite with excellent removal capacity for cadmium and lead," *Appl. Clay Sci.*, vol. 159, pp. 74–82, Jun. 2018, doi: 10.1016/j.clay.2017.12.050.

[18] F. Huang, L.-Y. Gao, R.-R. Wu, H. Wang, and R.-B. Xiao, "Qualitative and quantitative characterization of adsorption mechanisms for Cd2+ by silicon-rich biochar," *Sci. Total Environ.*, vol. 731, p. 139163, 2020.

[19] Youning Chen, Huan Wang, Wei Zhao, and S. Huang, "Four different kinds of peels as adsorbents for the removal of Cd(II) from aqueous solution: Kinetic, isotherm and mechanism," *J. Taiwan Inst. Chem. Eng.*, vol. 88, pp. 146–151, 2018, doi: 10.1016/j.jtice.2018.03.046.

[20] Maribel S. Tizo *et al.*, "Efficiency of calcium carbonate from eggshells as an adsorbent for cadmium removal in aqueous solution.," *Sustain. Environ. Res.*, vol. 28, pp. 326–332, 2018, doi: 10.1016/j.serj.2018.09.002.

[21] V. K. Gupta and A. Nayak, "Cadmium removal and recovery from aqueous solutions by novel adsorbents prepared from orange peel and Fe 2O 3 nanoparticles," *Chem. Eng. J.*, vol. 180, pp. 81–90, Jan. 2012, doi: 10.1016/j.cej.2011.11.006.

Development of bi-metallic MOFs based mixed matrix membranes for CO2 capture optimization

Syed Awais Ali[1], Mohammad Younas[2*], Asmat Ullah [2*], Mansoor ul Hassan shah[2], Syed Nasir Shah[3], Asim Laeeq Khan[4], Waqad ul Mulk[1], Hilal Ahmad[1]

[1]*Department of Mechanical Engineering, Faculty of Mechanical and Aeronautical Engineering, University of Engineering and Technology, Taxila 47080, Rawalpindi, Pakistan.*

[2]*Department of Chemical Engineering, University of Engineering and Technology, Peshawar 25120, Pakistan.*

[3]*Department of Energy Engineering, Faculty of Mechanical and Aeronautical Engineering, University of Engineering and Technology Taxila, 47080 Rawalpindi, Pakistan.*

[4]*Department of Chemical Engineering, COMSATS Institute of Information Technology, Lahore Pakistan.*

**Mohammad Younus*

Email: m.younus@uetpeshawar.edu.pk

Abstract

The increased emission of carbon dioxide (CO2) into the environment produces serious concerns about global warming. Consequently, CO_2 is separated and captured by several techniques including; absorption, adsorption, cryogenic distillation, chemical precipitation and coagulation. However, most of these methods are energy intensive and costly. The use of polymeric membranes is limited due to tradeoff in permeability and selectivity and inorganic membranes have disadvantages of high cost and brittleness. Therefore, in this study "bi-metallic MOFs" having high surface area, porosity and adhesion is synthesized as an organic-inorganic hybrid material and developed its respective mixed matrix membrane for CO_2 capture. Gas permeation results showed that high CO_2 permeability and CO_2/N_2 selectivity of about 116 and 40 barer respectively were achieved. The results revealed that the employment of such highly porous bi-metallic MOFs provide better thermal and mechanical strength to membrane and also enhance its CO2 capturing capacity.

***Keywords*:** Metal organic frameworks, mixed matrix membranes, carbon dioxide, CO_2 permeability, energy intensive, CO2/N2 selectivity

Introduction

Rising anthropogenic emissions of greenhouse gases from rapid growing industries are causes of increase in average global temperature on earth[1]. Carbon dioxide (CO_2) is major anthropogenic greenhouse gas[2]. Chemical industries are considered as a primary source of CO_2 emission into atmosphere in which fossil fuels and natural gas are burned for numerous purposes[3]. It has been widely reported that excess emission of CO2 is recognized as major source of global warming and its accounting for about 80% of all greenhouse gases

emission[4]. Several techniques are used in past for CO2 capturing such as adsorption [5], absorption[6], cryogenic distillation [7] and amine based solvents but most of these methods are highly intensive and costly [8].

MOFs are considered as an ideal candidate for the CO_2 capture process due to their high porosity, surface area, higher thermal and chemical stability and better adhesion with polymer matrix [9, 10]. Therefore, the fabrication of MOFs based mixed matrix membranes is an attractive choice in order to obtain enhancement in CO2 permeability and selectivity[11]. Anjum et al. fabricated MMM by dispersion of modified Zr-terephthalate UiO-66 MOFs on Martmid polymer matrix and resulted that the addition of 30 wt.% filler loading showed excellent gas separation performance that resulted in enhanced CO2 permeability of about 19.4 and CO2/CH4 selectivity of about 47.7[12]. Khosravi, et al fabricated MMM by integration of CuBTC and amine functionalized CuBTC MOFs with Pebax-1657 to investigate the effect of -NH2 with CUBTC in membrane gas separation application and resulted the increase in CO2/CH4 selectivity by addition of CuBTC and -NH2-CuBTC. Gas permeation results showed the 60% enhancement in selectivity by addition of filler loadings of 20wt.% [13].

The main objective of this work is to investigate the CO2 permeability and CO2/N2 selectivity of modified mixed matrix membrane. For this purpose, bi-metallic MOFs of organic-inorganic hybrid material were synthesized and its respective mixed matrix membrane was fabricated by incorporation of MOFs with Pebax-2533. Gas permeation results were performed by varying pressure from (0.2-0.5 bar) and at temperature of 25^0C. The fabricated MMMs showed the CO2 permeability and CO2/N2 selectivity of about 116 and 38 barer at 0.5 bar pressure.

Method

Materials

Dimethyl formamide, ethanol, cupper and magnesium salts were purchased from Musa ji sons. Benzimidazole was purchased from sigma Aldrich chemical company. Methanol and synthesis facility of MOFs and membrane was provided by chemical engineering department UET Peshawar. Gas cylinders of 99.9% pure carbon dioxide and nitrogen were used. Block copolymer of Pebax 2533 comprising 80% polyethylene and 20% polyamide was purchased from Arkema.

Synthesis of MOFs

Synthesis of MOFs was done by modified method at room temperature by mixing 0.90g Cu and Mg salts with 2.3g of benzimidazole to make a solid mixture then mixture was dissolved in 300ml of dimethyl formamide (DMF) under continuous stirring for 24hrs. DMF was removed from the product by centrifuge then washing with methanol three times. Traces of DMF is hard to remove then the product was dispersed in methanol and stirred 24 hours. After DMF removal these particles are dispersed in mixture containing ethanol water mixture (70/30 by weight ratio).

Membrane synthesis

Pebax-2533 membrane was synthesized by solvent evaporation method. 3wt.% of Pebax-2533

homogenous solution was prepared in certified technical grade of ethanol. Pebax was dissolved at reflux condition of 85ºC by continuous stirring of 5hrs till the solution completely dissolved to form bubble free solution. Then the solution was cooled at room temperature to ambient temperature. 3wt.% solution then casted in Teflon petri dish to obtain pristine Pebax membrane. MOFs solution with ethanol water then added in polymer solution to synthesize MMM solution. MMM solution then stirred for 30minutes and casted in Teflon petri dish. The solvent of Petri dish was evaporated at room temperature for 24 hrs. Then placed in oven for 12 hrs. and finally increase the temperature gradually to 80^0C. These samples were kept at 80^0C over night to remove rest of solvent and gradually cool down to room temperature. The resulting membrane were of thickness from 30µm-50µm.

Results

This section describes the results of synthesized MOFs and performance of MOFs with membrane. The purpose of experimental work is to investigate the MOFs behavior as well as CO2 permeability and CO2/N2 selectivity of fabricated MMMs. The CO2 permeability and CO2/N2 selectivity are mentioned in table 1. Permeability and selectivity were tested at various pressure ranges from (0.2-0.5 bar) and the highest CO2 permeability 116 was achieved at 0.5 bar and highest selectivity 40 barer of was achieved at 0.3 bar which with increase the feed pressure permeability increase and selectivity decrease.

Table.1

MMM/Polymer	Pressure	CO2 permeability	CO2/N2 selectivity
Cu/Mg-BTC-Pebax-2533	0.3	110	40
Cu/Mg-BTC-Pebax-2533	0.4	113	39
Cu/Mg-BTC-Pebax-2533	0.5	116	38

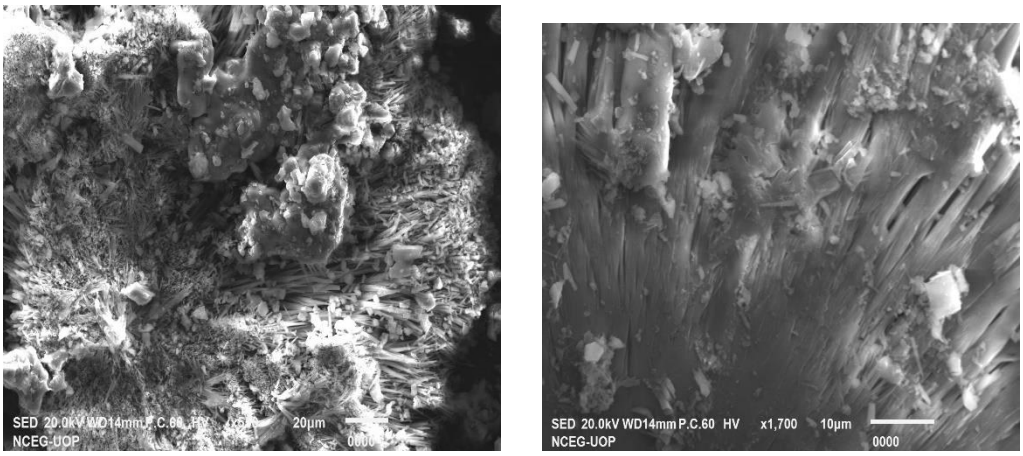

SEM images of MOFs

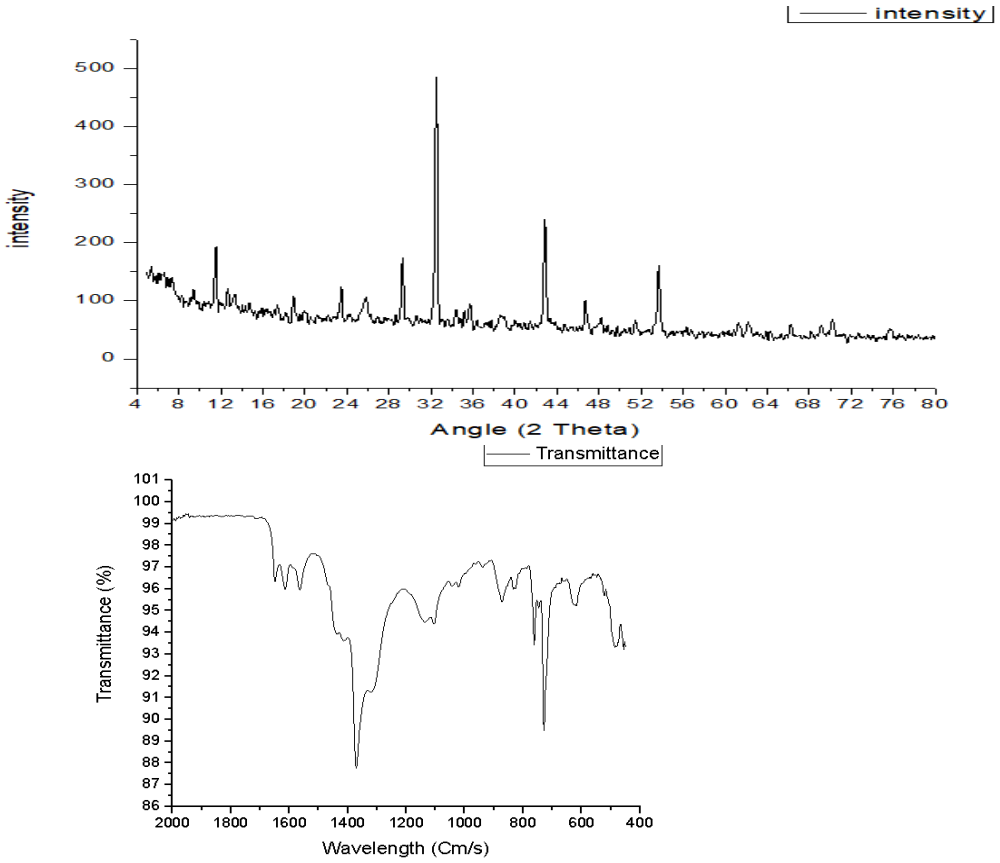

FTIR images of MOFs

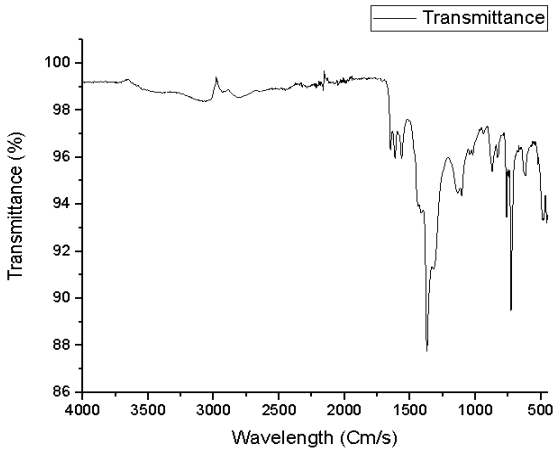

XRD images of MOFs

Conclusion

The current study showed synthesis of highly porous bi-metallic MOFs and its respective MMMs. Gas permeation results showed the highest CO2 permeability of 116 at 0.3 bar and selectivity of about 40 at 0.5 bar. The result of study showed that permeability increases with increase the gas pressure and selectivity decrease by increase in pressure. Further

improvements in MMMs synthesis are recommended to enhance the performance at high pressure.

References

[1] Y. Xu and G. Cui, "Influence of spectral characteristics of the Earth's surface radiation on the greenhouse effect: Principles and mechanisms," *Atmospheric Environment,* vol. 244, 2021, doi: 10.1016/j.atmosenv.2020.117908.

[2] N. Hajilary, A. Shahi, and M. Rezakazemi, "Evaluation of socio-economic factors on CO 2 emissions in Iran: Factorial design and multivariable methods," *Journal of Cleaner Production,* vol. 189, pp. 108-115, 2018, doi: 10.1016/j.jclepro.2018.04.067.

[3] R. Thiruvenkatachari, S. Su, H. An, and X. X. Yu, "Post combustion CO2 capture by carbon fibre monolithic adsorbents," *Progress in Energy and Combustion Science,* vol. 35, no. 5, pp. 438-455, 2009, doi: 10.1016/j.pecs.2009.05.003.

[4] F. O. Ochedi, J. Yu, H. Yu, Y. Liu, and A. Hussain, "Carbon dioxide capture using liquid absorption methods: a review," *Environmental Chemistry Letters,* vol. 19, no. 1, pp. 77-109, 2020, doi: 10.1007/s10311-020-01093-8.

[5] G. W. A. Minh T. Ho, and Dianne E. Wiley, "Reducing the Cost of CO2 Capture from Flue Gases Using Pressure Swing Adsorption," *ACS Publications,* 2008.

[6] M. Wang, A. Lawal, P. Stephenson, J. Sidders, and C. Ramshaw, "Post-combustion CO2 capture with chemical absorption: A state-of-the-art review," *Chemical Engineering Research and Design,* vol. 89, no. 9, pp. 1609-1624, 2011, doi: 10.1016/j.cherd.2010.11.005.

[7] M. J. Tuinier, M. van Sint Annaland, G. J. Kramer, and J. A. M. Kuipers, "Cryogenic CO2 capture using dynamically operated packed beds," *Chemical Engineering Science,* vol. 65, no. 1, pp. 114-119, 2010, doi: 10.1016/j.ces.2009.01.055.

[8] Z. Zhang *et al.*, "Modeling of a CO2-piperazine-membrane absorption system," *Chemical Engineering Research and Design,* vol. 131, pp. 375-384, 2018, doi: 10.1016/j.cherd.2017.11.024.

[9] S. E. M. Elhenawy, M. Khraisheh, F. AlMomani, and G. Walker, "Metal-Organic Frameworks as a Platform for CO2 Capture and Chemical Processes: Adsorption, Membrane Separation, Catalytic-Conversion, and Electrochemical Reduction of CO2," *Catalysts,* vol. 10, no. 11, 2020, doi: 10.3390/catal10111293.

[10] M. R. Mohammad Younas , Muhammad Dauda,Muhammad B. Wazir ,Shakil Ahmada,Nehar Ullaha, Inamuddinc,Seeram Ramakrishna d, "Recent progress and remaining challenges in post-combustion CO2 capture using metal-organic frameworks (MOFs)," *Progress in Energy and Combustion Science,* 2019, doi: 10.1016/j.pecs.2020.100849.

[11] M. Wang, Z. Wang, S. Zhao, J. Wang, and S. Wang, "Recent advances on mixed matrix membranes for CO 2 separation," *Chinese Journal of Chemical Engineering,* vol. 25,

no. 11, pp. 1581-1597, 2017, doi: 10.1016/j.cjche.2017.07.006.

[12] M. W. Anjum, F. Vermoortele, A. L. Khan, B. Bueken, D. E. De Vos, and I. F. Vankelecom, "Modulated UiO-66-Based Mixed-Matrix Membranes for CO2 Separation," *ACS Appl Mater Interfaces,* vol. 7, no. 45, pp. 25193-201, Nov 18 2015, doi: 10.1021/acsami.5b08964.

[13] T. Khosravi, M. Omidkhah, S. Kaliaguine, and D. Rodrigue, "Amine-functionalized CuBTC/poly(ether-b amide-6) (Pebax® MH 1657) mixed matrix membranes for CO2/CH4 separation.," *The Canadian Journal of Chemical Engineering,* vol. 95, no. 10, pp. 2024-2033, 2017, doi: 10.1002/cjce.22857.

CO_2/N_2 Separation using Supported Ionic Liquid Membrane

Waqad Ul Mulk[1], Mansoor Ul Hassan Shah[2*], Syed Nasir Shah[3*], Mohammad Younas[2], Asim Laeeq khan[4], Asmat Ullah[2], Hilal Ahmad[1], Syed Awais Ali[1]

[1]*Department of Mechanical Engineering, Faculty of Mechanical and Aeronautical Engineering, University of Engineering and Technology, taxila 47080, Rawalpindi, Pakistan.*

[2]*Department of Chemical Engineering, University of Engineering and Technology,Peshawar 25120, Pakistan.*

[3]*Department of Mechanical Engineering, Faculty of Mechanical and Aeronautical Engineering, University of Engineering and Technology, taxila 47080, Rawalpindi, Pakistan.*

[4]*Department of Chemical Engineering, COMSATS Institute of Information Technology, Lahore Pakistan.*

**Mansoor Ul Hassan Shah*

Email: *mansoorshah@uetpeshawar.edu.pk*

Abstract

Increase CO_2 emissions in the environment causes serious environmental problems. Several methods including; absorption, adsorption, cryogenic and membrane separation were used for CO_2 capture. However, most of these techniques were highly energy intensive and produce adverse effect on the environment. In this regard many studies have reported CO_2 separation from other gases like nitrogen and methane through supported ionic liquid membranes but there is always a tradeoff between permeability and selectivity. Therefore, in this study, phosphonium-based hydrophobic ionic liquid (IL) was incorporated with Polyvinylidene Fluoride (PVDF) support to achieve selective separation of CO_2 from nitrogen (N_2). The results of the present study revealed that phosphonium-based IL with PVDF showed the best separation performance for CO_2 and N_2. Hence, the results presented in the current study depicted the sustainable and economical CO_2 separation.

Keywords**:** CO_2, CO_2/N_2 separation, Energy intensive, Ionic liquids,

Introduction

Human-caused Carbon dioxide (CO_2) emissions have serious consequences [1]. CO_2, with a hazardously high proportion of 407 ppm in the environment, is mainly accountable for 60% of anthropogenic climate change. This has been identified as a major contributor to global warming, resulting in drastic climate change. [2]. Several techniques for separating CO_2 from gaseous combinations of various components and thermodynamic states have been developed and utilized in the past [3]. Using amine-based solvents for chemical and physical absorption [4]. Adsorption using solid absorbents [5] membrane separations [6] and cryogenic separation [7] are some common techniques for CO_2 removal. Because of the high temperature and pressure requirements, traditional absorption and cryogenic separation techniques consume a lot of energy and are very expensive [8].

SLMs (supported liquid membranes) are basically porous membranes with liquid solvents trapped within its pores [9]. It is an attractive approach for achieving high permeability. SLMs combine membrane extraction and stripping with their inherent separation properties [10].

Because of their high efficiency and low solvent consumption, SLMs have proven to be effective. However, its vast range of applications is limited due to solvent loss, high thickness, and a limited temperature range of operation [11].

SILMs are non-dispersive membranes in which IL serves as a selective material and is immobilized within the membrane pores by capillary forces. SILMs have a number of advantages over traditional liquid membrane methods, including a large interface area/mass transfer area per unit volume, low solvent holding, and a relatively efficient application [12]. Furthermore, the use of ILs as a separating phase in SILMs improves stability due to their exceptional characteristics such as low vapor pressure and considerably high viscosity [13]. The performance of the SILM is thought to be primarily determined by the IL immobilized within the pores of the membrane support, rather than the membrane support itself. Other research has discovered that binary contacts between ILs and support affect the condition of IL within the pores as well as the separation [14].

The primary aim of this research is to examine the CO_2/N_2 permeability and selectivity of supported ionic liquid membrane. For this purpose, SILM was synthesized by incorporating phosphonium based ionic liquid $[P_{44414}][Cl]$ Tributyl (tetradecyl) phosphoniumchloride inside PVDF support. The performance of the synthesized SILM in separating pure CO_2 and N_2 was investigated in a custom built gas permeation unit (figure 1) at room temperature and various pressures (0.2-0.5 bar). At 0.5 bar, the highest CO_2 permeability of 89 barrer and CO_2/N_2 selectivity of 25.2 were achieved.

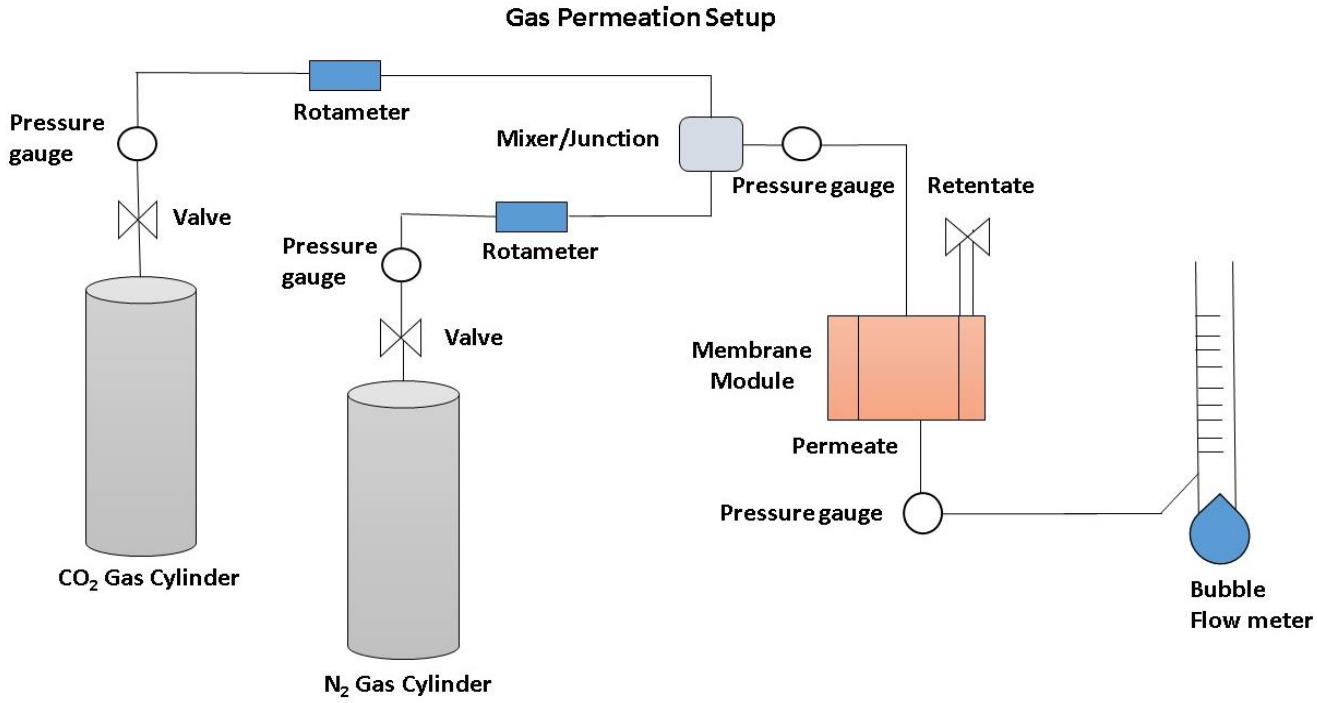

Fig.1. **Gas permeation setup**

Method

Materials

The ionic liquid used for the synthesis of supported ionic liquid membrane, namely Tributyl(tetradecyl)phosphoniumchloride $[P_{44414}][Cl]$, was kindly supplied by Chemical Engineering department, Comsats institute of information technology Lahore. Polyvinylidene

Fluoride (PVDF) membrane was kindly provided by Chemical Engineering Department, University of engineering and technology Peshawar. Without additional purification, all components were used in their original condition.

Synthesis of SILM

For the fabrication of SILM, the membrane is immobilized by placing it in a dead-end membrane filtration unit, ionic liquid was loaded on the top surface of the support with the help of a micropipette, and exerting pressure through an inert gas nitrogen at 1 bar for 20 minutes until the IL has completely filled the pores of the membrane support due to capillary action. The excess IL was wiped away with soft paper after preparing the SILM.

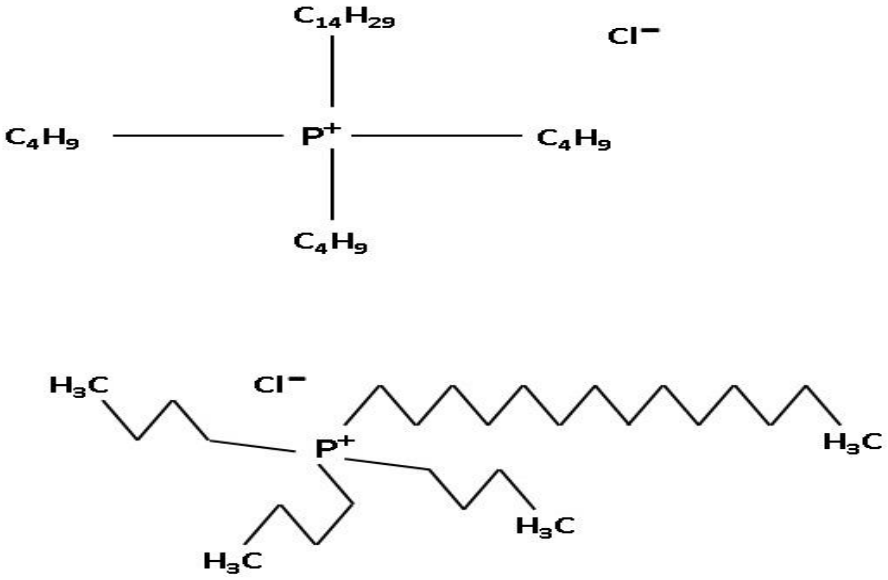

Fig.2. Structure of [P44414][Cl] ionic liquid

Results

The performance of supported ILs on a flat sheet PVDF membrane is described in this section. The goal of the research was to look into the permeability of CO_2 and N_2 and selectivity of CO_2/N_2. Figures 3 and 4 show the permeability of pure CO_2 and N_2, as well as the selectivity of CO_2 over N_2, at room temperature and various pressures. The SILM was tested at different pressures (0.2-0.5 bar), and the highest CO_2 permeability of 89 barrer was observed at pressure 0.5 bar. The highest CO_2/N_2 selectivity (30.24) was investigated at pressure 0.2 bar. The permeability of CO_2 increases as the pressure rises and the CO_2/N_2 selectivity decreases with the increase in feed pressure.

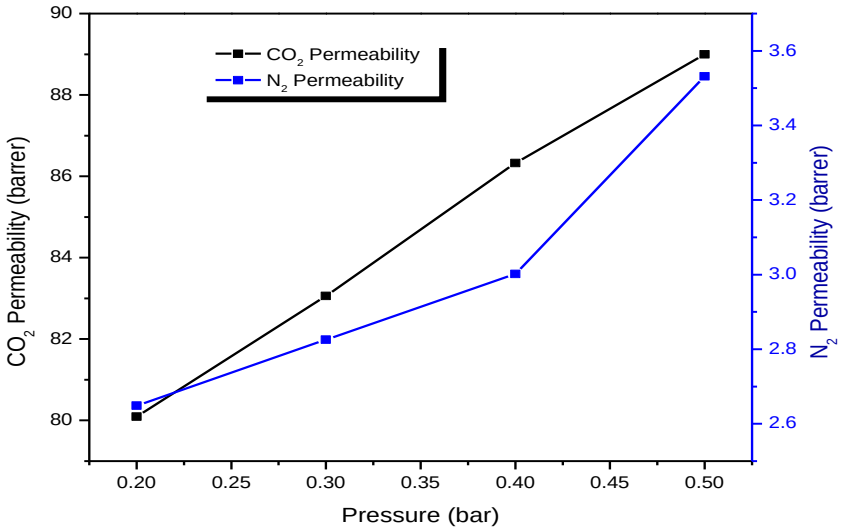

Fig.3. Permeability of CO_2 and N_2 at various pressures

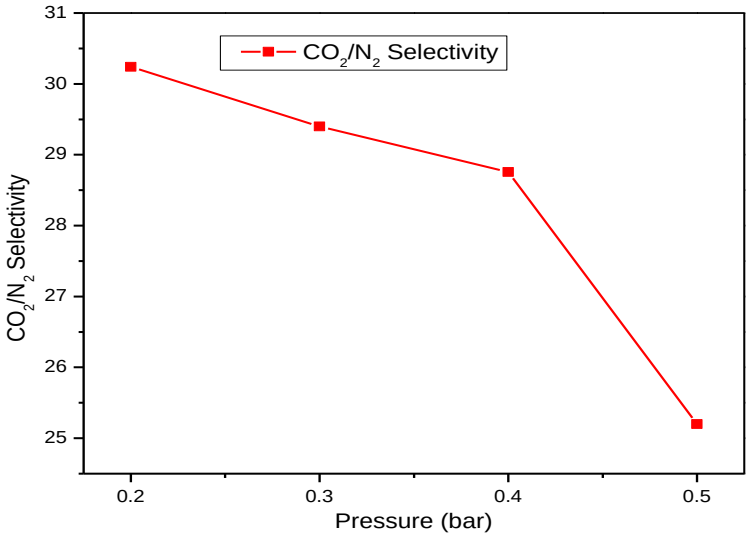

Fig.4. Selectivity of CO_2/N_2 at different pressures

As shown in figure 3 and 4, the SILM shows higher permeability of 89 barrer at pressure 0.5 bar and high selectivity at pressure 0.2 bar. As the pressure increases the permeability of gases gradually increases and the selectivity decreases accordingly.

Conclusions

The current study showed the viable fabrication and testing of SILM on a Polyvinylidene Fluoride (PVDF) support using $[P_{44414}][Cl]$ IL. The IL was completely immobilized within the pores of the membrane by applying pressure through an inert gas nitrogen. The highest permeability 89 barrer was achieved at pressure 0.5 bar and selectivity of 30 at pressure 0.2 bar. With the increase in permeate pressure, the permeability of the gases gradually increases and selectivity decreases. Further improvements in membrane are recommended to enhance the stability of SILM at high pressure.

References

[1] M. Younas et al., "Recent progress and remaining challenges in post-combustion CO2 capture using metal-organic frameworks (MOFs)," Progress in Energy and Combustion Science, vol. 80, 2020.

[2] Z. Shamair, N. Habib, M. A. Gilani, and A. L. Khan, "Theoretical and experimental investigation of CO2 separation from CH4 and N2 through supported ionic liquid membranes," Applied Energy, vol. 268, 2020.

[3] I. K. Swati et al., "Protic/aprotic ionic liquids for effective CO2 separation using supported ionic liquid membrane," Chemosphere, vol. 267, p. 128894, Mar 2021.

[4] M. Wang, A. Lawal, P. Stephenson, J. Sidders, and C. Ramshaw, "Post-combustion CO2 capture with chemical absorption: A state-of-the-art review," Chemical Engineering Research and Design, vol. 89, no. 9, pp. 1609-1624, 2011.

[5] G. W. A. Minh T. Ho, and Dianne E. Wiley, "Reducing the Cost of CO2 Capture from Flue Gases Using Pressure Swing Adsorption," ACS Publications, 2008.

[6] M. Rezakazemi, M. Sadrzadeh, and T. Matsuura, "Thermally stable polymers for advanced high-performance gas separation membranes," Progress in Energy and Combustion Science, vol. 66, pp. 1-41, 2018.

[7] M. J. Tuinier, M. van Sint Annaland, G. J. Kramer, and J. A. M. Kuipers, "Cryogenic CO2 capture using dynamically operated packed beds," Chemical Engineering Science, vol. 65, no. 1, pp. 114-119, 2010.

[8] Z. Zhang et al., "Modeling of a CO2-piperazine-membrane absorption system," Chemical Engineering Research and Design, vol. 131, pp. 375-384, 2018.

[9] M. Wang, D. Yang, Z. Wang, J. Wang, and S. Wang, "Effects of pressure and temperature on fixed-site carrier membrane for CO2 separation from natural gas," Frontiers of Chemical Engineering in China, vol. 4, no. 2, pp. 127-132, 2009.

[10] M. F. San RomÃ¡n, E. Bringas, R. IbaÃ±ez, and I. Ortiz, "Liquid membrane technology: fundamentals and review of its applications," Journal of Chemical Technology & Biotechnology, vol. 85, no. 1, pp. 2-10, 2010.

[11] Q. Y. N.M. Kocherginsky, Lalitha Seelam, "Recent advances in supported liquid membrane technology," Separation and Purification Technology, 2007.

[12] Z. Dai, R. D. Noble, D. L. Gin, X. Zhang, and L. Deng, "Combination of ionic liquids with membrane technology: A new approach for CO2 separation," Journal of Membrane Science, vol. 497, pp. 1-20, 2016.

[13] H. Gao, L. Bai, J. Han, B. Yang, S. Zhang, and X. Zhang, "Functionalized ionic liquid membranes for CO2 separation," Chem Commun (Camb), vol. 54, no. 90, pp. 12671-12685, Nov 8 2018.

[14] L. A. Neves, J. G. Crespo, and I. M. Coelhoso, "Gas permeation studies in supported ionic liquid membranes," Journal of Membrane Science, vol. 357, no. 1-2, pp. 160-170, 2010.

Dye Removal from Wastewater using Novel Bio-Adsorbents

Yasir Anwar, * Mansoor Ul Hassan Shah, Muhammad Hassan
Department of Chemical Engineering, University of Engineering and Technology, Peshawar 25120, Pakistan.
**Mansoor Ul Hassan Shah*
Email: *mansoorshah@uetpeshawar.edu.pk*

Abstract

Wastewater containing dyes is a serious environmental concern globally. Several synthetic adsorbents were employed for the remediation of dyes from wastewater, however the cost associated with these adsorbents restrict their usage on large scale. Moreover, synthetic chemical adsorbents may have the chance to leach into the water environment which will further enhance the water pollution. Therefore, in this study a low cost and environmentally benign bio-adsorbent, *Capparis decidua,* obtained from plant waste was utilized to remove tartrazine dye from wastewater. The results revealed that the developed bio-adsorbent has the capability to remove tartrazine dye from wastewater. The maximum removal efficiency of tartrazine dye was found to be 70%. The results presented in this study showed that the employment of such low cost bio-adsorbent will effectively reduce the water pollution and enhance the reusability of plant wastes.

***Keywords*:** Bio-adsorbent, wastewater, dye removal, synthetic adsorbents

1 Introduction

Dyes are compounds that have been categorized according to their composition and type. Industrially used dyes are divided into three types : anionic, cationic, and nonionic, due to the charge which they acquire once they dissolve in water [1-3].The perpetual increasing utilization of various dyes in numerous industrial sectors like textile, rubber, paper, leather and treatment etc. have caused discharging of these toxic pollutants to water. As a large number of these dyes cannot degrade easily due to their intricate structure, therefore their removal is a needed step [4]. Dyes are carcinogenic and toxic and have many negative effects on living organisms like irritation on stomach and skin [6].Dyes also decrease the oxygen demand of water and have adverse effect on marine habitats [9]. Thus it has become necessary to remove these pollutants from water before releasing them into environment [10].

The methods which were most commonly used for the removal of dyes are chemical and biological precipitation. But, these processes are used only when solute concentrations are high [11]. Several techniques reported for the remediation of dyes from wastewater includes; reverse osmosis, membrane filtration, flocculation, electro-dialysis, ion exchange, ozonation, electrochemical techniques, coagulation, bacterial action, chemical oxidation, and activated sludge and precipitation [12, 13]. All these processes are [14]. Certain disadvantages of the conventional methods include consumption of chemicals, cost and time of adsorbent

regeneration, generation of toxic sludge, and high cost of treatment of sludge [15].

Adsorption may be a bodily or a chemical method in which a material is gathered at the boundary of two phases. The two phases can be solid/gas or solid liquid. The substance which is accumulated is termed as adsorbate while the solid through which the substance is accumulated is called adsorbent [16]. Adsorption is used as an important tool for the elimination of colors pollutants from polluted water because of elevated efficiency and easy operation [17]. Adsorption systems have excellent performance but they are expensive due to which adsorption is not a viable option to be used for water treatment [18]. Bio adsorption is an efficient technique for eliminating of pollutants from wastewater and it also offers attractive alternative treatment, as it is readily available and inexpensive process [19]. Bio-adsorption offer many advantages because of low initial costs, high removal capacity, high efficiency, easy handling, nontoxic intermediates, and good separation [20, 21]. Currently, cheaper and more effective low cost adsorbents (bio-adsorbents) have been developed built on by-products from agricultural waste, poultry waste, and additional ordinary wastes as an alternative to conventional processes for wastewater treatment [22].

.

2.1 Materials

Capparis decidua plant was obtained from Lund Khwar district Mardan. The plant was dried for 10 days, and then dried in oven at 80 ºC for 8 hours. This dried sample was then crushed and passed through mesh sieve to obtain the desired bioadsorbent size i-e 50 to 300 µm.The entire chemicals used in our study were analytical grade which were obtained from a chemical shop in Peshawar, Pakistan. These chemicals were used without any purification.

2.2 Experimental Procedure

A standard solution containing 1000 ppm tartrazine dye was prepared by mixing a proper amount of tartrazine with 1000 ml of water. This standard solution was then used to prepare solutions of lower concentrations by using dilution. Adsorption of the dye from the wastewater was done using batch adsorption. Adsorbent weighing 0.5g was added to 50 ml solution at room temperature. The influence of different parameters such as pH, initial dye concentration, adsorbent dosage, contact time, and temperature were calculated. In order to study the effect of one parameter, all other parameter were kept constant. The optimum conditions were of pH 2.0, contact time 30 minutes, stirring speed 800 rpm, temperature 300k, and initial concentration of 100 mg/l. The maximum wavelength of tartrazine dye is 426nm. The equilibrium dye concentration Ce (mg/L) was determined using UV-Visible spectrophotometer operated at 426 nm. To find the percentage adsorption and capacity of the adsorbent for tartrazine, the following equations were used.

$$\%\,\boldsymbol{Sorption} = \frac{Ci - Ce}{Ce} \times \mathbf{100}$$

$$qe = \frac{v(Ci-Ce)}{m}$$

Where Ci (mg/L) is the initial concentration of the solution, q_e (mg/g) is the uptake capacity of the adsorbent for tartrazine, v is the volume of used solution and m (g) is the mass of the adsorbent used.

2.3 KINETIC MODELING

Pseudo-first order and Pseudo- second order models were used to evaluate the kinetic mechanism of adsorption.

According to pseudo-first order kinetic model, one sorption site has the ability to adsorb one dye molecule and the equation is given as [23],

$$log(qe - qt) = log\ qe - \frac{Kit}{2.303}$$

Where q_t is the adsorption capacity in mg/g at a given time and K is the pseudo first order rate constant.

According to pseudo second order kinetic model, the rate at which sorption sites are occupied is directly proportional to the number of sites which are not occupied and is expressed as [24],

$$\frac{t}{q_t} = \frac{1}{K_2 {q_e}^2} + \frac{t}{q_e}$$

Where K_2 is the rate constant of pseudo second order model and $h=K_2 {q_e}^2$ is the initial adsorption rate.

3. EFFECT OF SOME VARIABLES ON ADSORPTION

3.1 EFFECT OF PH

The pH of the solution has a great effect on the adsorption of dye from wastewater. Fig 1 shows the influence of the pH on adsorption. As the pH is increased from 2 to 10, the adsorption is decreased. Adsorption is high at lower pH i.e. in acidic medium. In basic medium the adsorption rate is low.

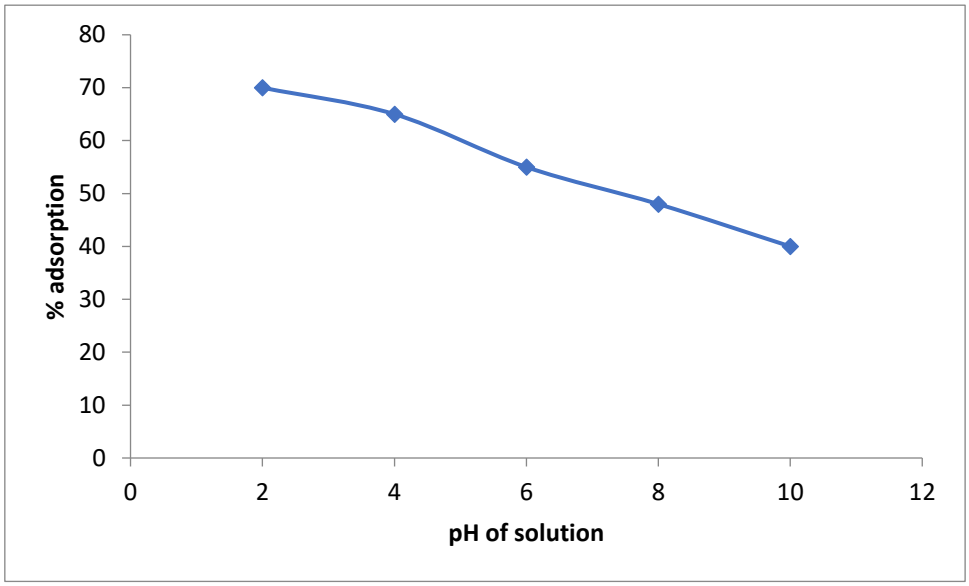

Figure 9 percent adsorption of tartrazine as a function of pH

3.2 EFFECT OF TEMPERATURE

Adsorption of tartrazine onto adsorbent is highly influenced by temperature. The effect of temperature on adsorption is shown in fig 2. Increase in temperature increases the percentage adsorption which shows that this process is favored by high temperature due to pore size enlargement.

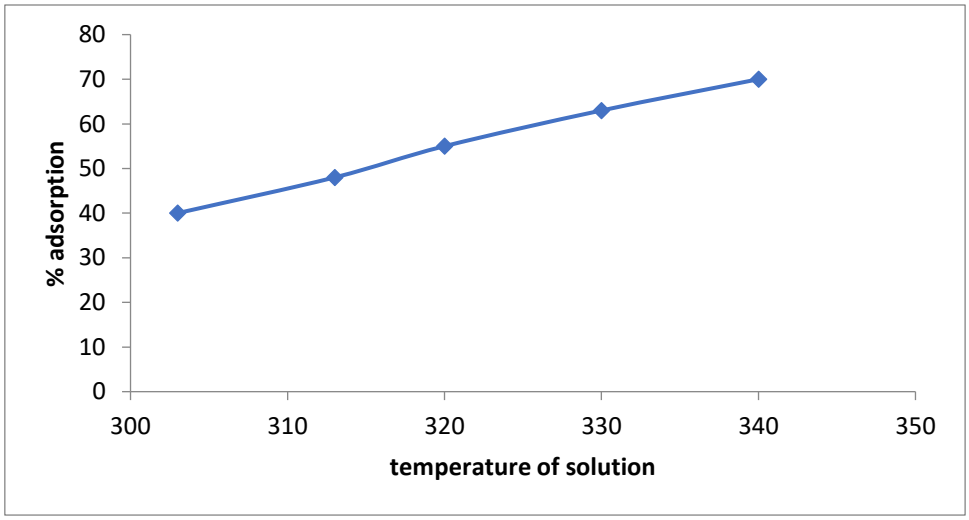

Figure 10 Percent adsorption as a function of temperature

3.3 EFFECT OF ADSORBENT DOSAGE

The effect of adsorbent dosage on the percent adsorption has been shown in figure 3 below. This figure shows that as the adsorbent dosage is increased, the percent adsorption also increases. This is because, as the adsorbent dosage increases, the number of active sites for tartrazine increases. Hence with the increase in adsorbent dose, adsorption also increases.

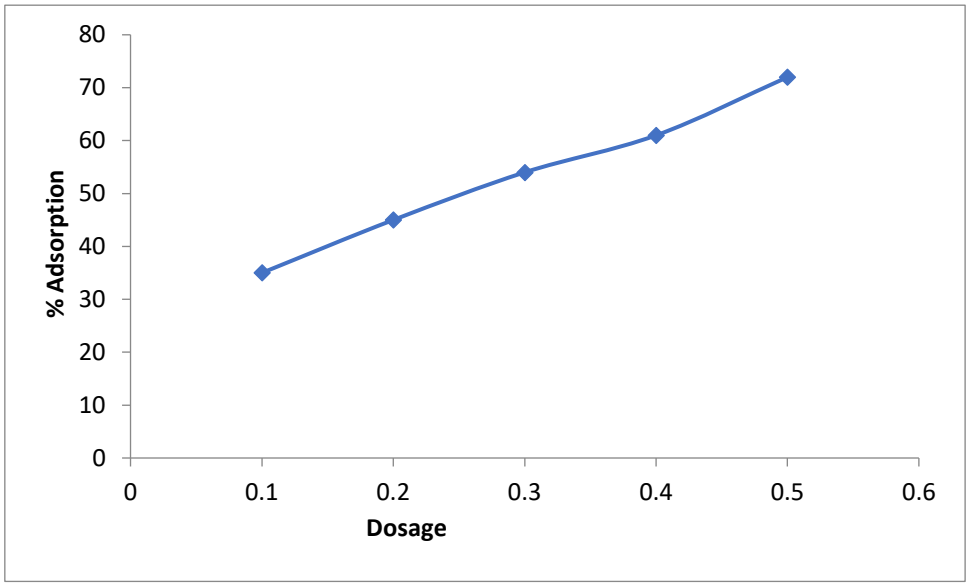

Figure 11 Percent adsorption of tartrazine as a function of dosage

Conclusions

Capparis decidua has been found to have high adsorption for tartrazine than other adsorbents which have been used earlier. Thus it can be concluded that Capparis decidua is one of the best low cost alternatives for removal of dyes from waste water.

REFERENCES

[1] Homaeigohar, S. (2020). The nanosized dye adsorbents for water treatment.Nanomaterials, 10(2), 295.

[2] Homaeigohar, S., Botcha, N. K., Zarie, E., &Elbahri, M. (2019). Ups and downs of water photodecolorization by nanocomposite polymer nanofibers.Nanomaterials, 9(2), 250.

[3] Homaeigohar, S., Zillohu, A. U., Abdelaziz, R., Hedayati, M. K., &Elbahri, M. (2016). A novel nanohybridnanofibrous adsorbent for water purification from dye pollutants.Materials, 9(10), 848.

[4] Sumanjit, T. P. S. W., &Kansal, I. (2008). Removal of Rhodamine B by adsorption on walnut shell charcoal. Surface Sci. Technol, 24, 179-193.

[5] Soni, M., Sharma, A. K., Srivastava, J. K., &Yadav, J. S. (2012). Adsorptive removal of methylene blue dye from an aqueous solution using water hyacinth root powder as a low cost adsorbent. International Journal of Chemical Sciences and Applications, 3(3), 338-345.

[6] Shakoor, S., &Nasar, A. (2016). Removal of methylene blue dye from artificially contaminated water using citrus limetta peel waste as a very low cost adsorbent. Journal of the Taiwan Institute of Chemical Engineers, 66, 154-163.

[7] Shen, K., &Gondal, M. A. (2017). Removal of hazardous Rhodamine dye from water by adsorption onto exhausted coffee ground. Journal of Saudi Chemical Society, 21, S120-S127.[8] Kushwaha, A. K., Gupta, N., &Chattopadhyaya, M. C. (2014). Removal of cationic

methylene blue and malachite green dyes from aqueous solution by waste materials of Daucuscarota. Journal of Saudi Chemical Society, 18(3), 200-207.
[9] Mahmoud, H. R., Ibrahim, S. M., & El-Molla, S. A. (2016). Textile dye removal from aqueous solutions using cheap MgOnanomaterials: adsorption kinetics, isotherm studies and thermodynamics. Advanced Powder Technology, 27(1), 223-231.
[10]Arami, M., Limaee, N. Y., &Mahmoodi, N. M. (2006). Investigation on the adsorption capability of egg shell membrane towards model textile dyes. Chemosphere, 65(11), 1999-2008.
[11]Vadivelan, V., & Kumar, K. V. (2005). Equilibrium, kinetics, mechanism, and process design for the sorption of methylene blue onto rice husk. Journal of colloid and interface science, 286(1), 90-100.
[12] Ngah, W. W., Teong, L. C., &Hanafiah, M. M. (2011). Adsorption of dyes and heavy metal ions by chitosan composites: A review. Carbohydrate polymers, 83(4), 1446-1456.
[13] Carvalho, J., Araújo, J., & Castro, F. (2011). Alternative low-cost adsorbent for water and wastewater decontamination derived from eggshell waste: an overview. Waste and Biomass Valorization, 2(2), 157-167.
[14] Rouquerol, J., Rouquerol, F., Llewellyn, P., Maurin, G., & Sing, K. S. (2013). Adsorption by powders and porous solids: principles, methodology and applications. Academic press.
[15] Bhattacharjee, C., Dutta, S., &Saxena, V. K. (2020). A review on biosorptive removal of dyes and heavy metals from wastewater using watermelon rind as biosorbent.Environmental Advances, 2, 100007.
[16] Yagub, M. T., Sen, T. K., Afroze, S., &Ang, H. M. (2014). Dye and its removal from aqueous solution by adsorption: a review. Advances in colloid and interface science, 209, 172-184.
[17] Bonilla-Petriciolet, A., Mendoza-Castillo, D. I., &Reynel-Ávila, H. E. (Eds.). (2017). Adsorption processes for water treatment and purification. Cham (Switzerland): Springer.
[18] Crini, G., Lichtfouse, E., Wilson, L. D., & Morin-Crini, N. (2019). Conventional and non-conventional adsorbents for wastewater treatment. Environmental Chemistry Letters, 17(1), 195-213.
[19] Robinson, T., Chandran, B., & Nigam, P. (2002). Removal of dyes from a synthetic textile dye effluent by biosorption on apple pomace and wheat straw. Water research, 36(11), 2824-2830.
[20] Nakkeeran, E., Varjani, S. J., Dixit, V., &Kalaiselvi, A. (2018). Synthesis, characterization and application of zinc oxide nanocomposite for dye removal from textile industrial wastewater.
[21] Yagub, M. T., Sen, T. K., &Ang, M. (2014). Removal of cationic dye methylene blue (MB) from aqueous solution by ground raw and base modified pine cone powder. Environmental Earth Sciences, 71(4), 1507-1519.
[22] Burakov, A. E., Galunin, E. V., Burakova, I. V., Kucherova, A. E., Agarwal, S., Tkachev,

A. G., & Gupta, V. K. (2018). Adsorption of heavy metals on conventional and nanostructured materials for wastewater treatment purposes: A review. Ecotoxicology and environmental safety, 148, 702-712.

[23] Akpomie, K. G., & Dawodu, F. A. (2014). Efficient abstraction of nickel (II) and manganese (II) ions from solution onto an alkaline-modified montmorillonite. *Journal of Taibah University for Science*, *8*(4), 343-356.

Recovery of Sodium Sulphate through Osmotic Membrane Distillation Crystallization in Hollow Fibre Membrane Contactor; A Computational Fluid Dynamics Approach

Syed Zia Ullah[1*], Mohammad Younas[2]
[1]Department of chemical engineering, UET Peshawar, Pakistan

[1]Corresponding author*
Email: zia.syed1992@gmail.com

Abstract

The industrial waste water containing sodium sulphate (Na_2So_4) pose a great risk to aquatic life. To save aquatic life and utilize Na_2So_4 , it needs to be recovered from industrial waste water. Due to its easy scale up and low energy consumption, membrane distillation crystallization is one of the best method for recovery of Na_2So_4 from industrial waste water. In the contemporary research, a membrane contactor with hollow fibres will be used to simulate membrane distillation crystallization process. Numerical model will be applied to recovery of Na_2So_4 from aqueous solution with Sodium chloride as osmotic agent in (HFMC). To address the transfer of solute from fiber 's one side (aqueous phase) to fiber 's other side (osmotic phase), convection-diffusion based mass transfer Navier Stokes equations will be implemented. The equations will be solved numerically in the COMSOL Multiphysics$_{TM}$ software. The transmembrane flux increased with increase of osmotic concentration while increase or decrease of feed concentration has no appreciable effect. The result were in good agreement with literature.

Key words: Computational fluid dynamics; sodium sulphate recovery; hollow fibre membrane contactor, membrane crystallization, numerical simulation

1 Introduction

The number of industries in the world are rapidly increasing due to which there is an increase in the number of the industrial waste products(Elimelech & Phillip, 2011). Waste water containing inorganic salts like sodium sulphate (Na_2So_4) is also one of them. There are many methods for recovery of Na_2So_4 from water. These include Micro filtration, Ultra filtration, Nano filtration, Reverse osmosis as shown in table 1.

Now-a-days many researchers have attraction for removal of inorganic salts from industrial waste water through clean technologies(Ahmad et al., 2020). These technologies use porous membrane contactors that achieve salts recovery through membrane distillation crystallization (Qin et al., 2017). Membrane distillation crystallization in comparison to conventional crystallization processes use low energy have theoretical 100% rejection, low operating pressure and temperature. For the determination of position of interface between feed and solvent, the membrane feature of water attraction will be used. (Shannon et al., 2008). Furthermore both phases can be selected without foaming and entrainment problems. (Nemerow, 2007).

Table 1 Characteristics of pressure driven filtration processes (Alkaisi et al., 2017)

Membrane process	Applied pressure Psi (kPa)	Minimum particle size removed	Application (type, average removal efficiency %)
Micro filtration	4-70(30-500)	0.1-3 µm	Particle/turbidity removal (>99%) Bacteria/protozoa removal(>99.9%
Ultra filtration	4-70(30-500)	0.01-0.1 µm	Particle/turbidity removal (>99%) Bacteria/protozoa removal (>99%) Virus removal/(partial credit only)
Nano filtration	70-140(500-1000)	200-400 Daltons	Turbidity removal (>99%) Color removal (>98%) Sulfate removal (>97%) Virus removal (95%)
Reverse osmosis	140-700(1000-5000)	50-200 Daltons	Salinity removal (desalination) (>99%)

There are many membrane contactors available but most recognition is given to hollow fibre membrane contactors .On both sides of the HFMC i.e. Shell and lumen sides, two phases flow consistently which form an interface through pores of fiber wall (Marjani & Shirazian, 2011). High efficiency along with recovery of inorganic salts and removal of equilibrium limitations are achieved using membrane contactors (Younas et al., 2010).Osmotic membrane distillation is based on hollow fiber membrane contactor process which feed and osmotic streams runs counter currently in tube and shell sides respectively and Na_2So_4 are obtained by the suction of water from feed side by osmotic stream through hydrophobic membrane as shown in Figure 1.

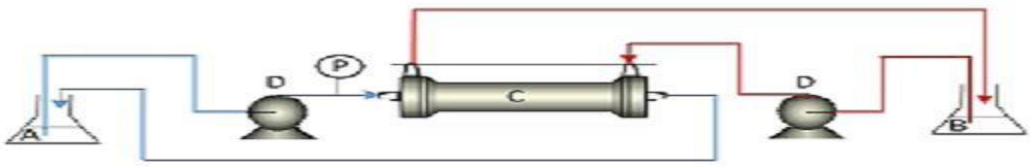

1

Figure 1. Osmotic membrane distillation-crystallization setup inorganic salts laden industrial waste water; B, Nacl solution; C, HFMC; D, pumps; P, System for controlling of pressure; E, pool for crystal widening (Salmón et al., 2018)

On recovery of Na_2So_4 from wastewater based on membrane contactors (HFMC) with hollow fibers, a great investigation has been done. However on the procedure of transport of mass and characterization of membrane contactors with hollow fibres, research is limited. Some researchers developed different mass transfer models across HFMC (Rezakazemi et al., 2013).

Diffusion through a small hole and steady axisymmetric passage represented by numerical model was presented by Sushant et al (Upadhyaya et al., 2015)and verified it with Literature. The experimental data and simulation results were in good agreement. The outcome implied that the flux increased by increasing average temperature and rate of flow of feed while with increasing permeate pressure it decreased. When the concentration of salt of feed was in parts per million of forty thousands of sodium chloride, a removal of ninety 99% was observed.

To probe in to the consequences of properties of membrane and variables of operation for sea-water desalination in modules by distillation through membrane by head-on exposure, Anas M. et al (Alwatban et al., 2019) applied computational fluid dynamics (CFD). For depiction of field of concentration, temperature and velocity, the laminar model was used while SST (shear stress turbulence) mathematical model was used for the modules containing spacers. The flow of volume through the membrane and concentration gradient at membrane interface was increased with a decrease in thickness and by increasing the rate of flow, it increased. The flux was increased more than 50% and polarization was reduced up to 50%.

1 Model Development

A 2-D axial-radial mass transfer model will be developed for flow-cell shown in Figure 2 assuming diffusion in membrane and convection-diffusion transfer of solute in tube and shell.

3.1 SIMULATION PARAMETERS

The simulation parameters that are put in to COMSOL for running of the model are given in table 2

3.2 MODEL EQUATIONS

3.2.1 TUBE SIDE

Transfer of solute in tube side is due to conduction-convection and is given by: (Muhammad et al., 2017)

$$D_{tube}\left[\frac{\partial^2 C_{tube}}{\partial r^2} + \frac{1}{r}\frac{\partial C_{tube}}{\partial r} + \frac{\partial^2 C_{tube}}{\partial z^2}\right] = u_{z-tube}\frac{\partial C_{tube}}{\partial z} \quad (1)$$

Whereas D_{tube} (m^2 s^{-1}), C_{tube} (mol m^3) and $u_{z\text{-}tube}$ (m s^{-1}) represents diffusion coefficient, concentration of water solute and axial flow velocity of tube side, respectively

The diffusion coefficient in tube side is found by pajonk correlation (Pajonk et al., 2003)

$$D = (5.6978 \times C^{-0.5239} + 5.5248) \times T \times 10^{-12} \quad (2)$$

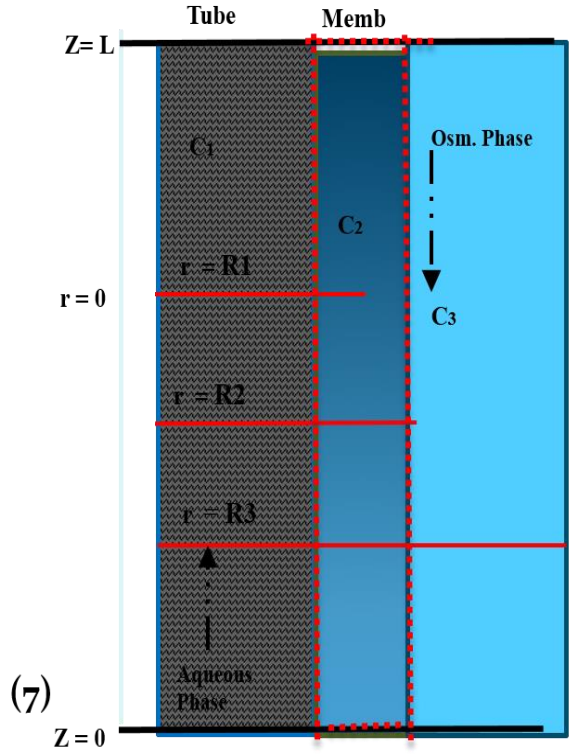

(7)

Figure 2. Speculative HFMC module flow cell

Table 2 Model simulation parameters

Tube side diffusion co-efficient , m^2/s	6.29×10^{-10}
membrane side diffusion co-efficient, m^2/s	2.51×10^{-5}
shell side diffusion co-efficient, m^2/s	4.87×10^{-10}
Activity coefficient of tube side	.871
Activity coefficient of shell side	.960
Scale factor	200

D=effective diffusion coefficient expressed in $m^2.s^{-1}$, C=NaCl concentration in aqueous phase T=temperature in K

As laminar and fully developed flow is assumed in the tube side therefore the equation used for velocity distribution in this section is given as:(Muhammad et al., 2018)

$$u_{z-tube} = 2u\left[1 - \left(\frac{r}{R1}\right)^2\right] \qquad (3)$$

Whereas, u ($m\ s^{-1}$) represents tube's inside average velocity

3.2.2 MEMBRANE

Solute transfer through membrane is done by diffusion and is given by the following equation (Razavi et al., 2016):

$$D_{mem}\left[\frac{\partial^2 C_{mem}}{\partial r^2} + \frac{1}{r}\frac{\partial C_{mem}}{\partial r} + \frac{\partial^2 C_{mem}}{\partial z^2}\right] = 0 \qquad (4)$$

Whereas D_{mem} ($m^2\ s^{-1}$) and C_{mem} ($mol\ m^{-3}$) and $u_{z\text{-}tube}$ ($m\ S^{-1}$) represents diffusion coefficient and concentration of water's solute through membrane's pores, respectively.

For diffusion coefficient of water in membrane's pores, the following correlation by Edward *et al* (Fuller et al., 1966)is used:

$$D_{AB} = 1.00 \times 10^{-8} \times T^{1.75\left(\frac{1}{MA}+\frac{1}{MB}\right)^{.5}} / \rho[(\varepsilon vf)^{\frac{1}{8}} + (\varepsilon vf)^{\frac{1}{8}}]\text{^}2 \quad (5)$$

3.2.3 SHELL SIDE

Transfer of water in the shell side is done through diffusion and convection and is given by the following equation:

$$D_{shell}\left[\frac{\partial^2 C_{shell}}{\partial r^2} + \frac{1}{r}\frac{\partial C_{shell}}{\partial r} + \frac{\partial^2 C_{shell}}{\partial z^2}\right] = u_{z-shell}\frac{\partial C_{shell}}{\partial z} \quad (6)$$

Whereas D_{shell} (m^2 s^{-1}) and C_{shell} (mol m^3) represents diffusion coefficient and concentration of water in shell side, respectively. While $u_{z\text{-}shell}$ (m s^{-1}) represents velocity of osmotic solution. The diffusion coefficient in shell side is found by equation (2).

In the shell side for velocity distribution Navier-stoke equation is used as given below:

$$\rho u_{z-shell} . \nabla u_{z-shell} - \nabla . \mu (\nabla u_{z-shell} + (\nabla u_{z-shell})^T + \nabla p = 0 \quad (7)$$

$$\nabla u_{z-shell} = 0$$

Whereas ρ (kg m^{-3}) represents density, u (m s^{-1}) the velocity vector, μ (Pa s) the viscosity, and p (Pa) the pressure:

The mass and momentum balance equations were coupled for concentration profile.

3.3 Numerical simulation

The governing equations were solved using CFD technique in COMSOL Multiphysics version 5.5 software. COMSOL software uses finite element method (FEM) for solving the model equations in this research. The membrane structural parameters are shown in Table 3.

Table 3. Membrane contactor structural parameters

Parameters	Values
No of fibres(N)	10200
Membrane module	Hollow fibre X-50
Membrane material	Polypropylene
Fiber inside radius (R_1), m	1.2×10^{-4}
Fiber outside radius (R_2), m	1.5×10^{-4}
Flowcell (Shell side) radius (R_3), m	2.47×10^{-4}
Length of the module (L), m	0.16
Porosity (ε)	0.4
Tortuosity (τ)	1/ ε

4. Results

4.1 MODEL VALIDATION

The validation of the presented axisymmetric model was carried out with the experimentation of previous work in literature (Salmón et al., 2018).Comparison of the experimental and

simulation work is presented in figure 3. It is shown that there is good agreement between the experimental data and the results gained by the model.

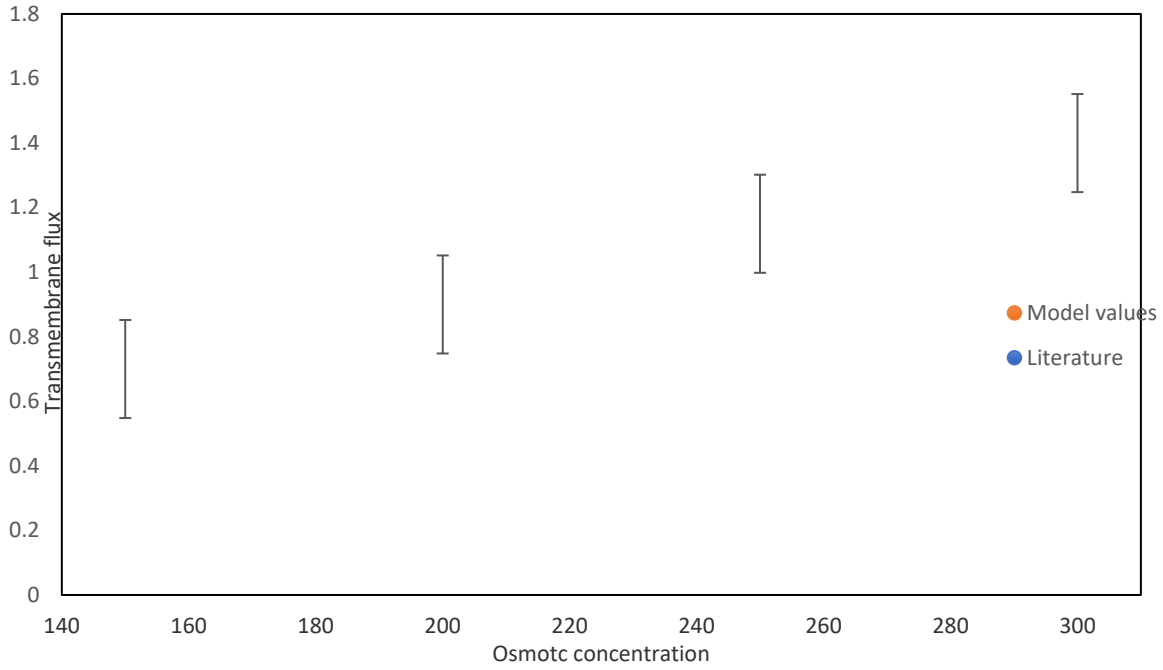

Figure 3. Comparison of model results with experimental data

In post processing the effect of concentration and flow rates of feed and osmotic solution on transmembrane flux was studied.

4. 2 Concentration of feed

With the increase or decrease of concentration of feed no effects on transmembrane flux was observed as shown in figure 4. This is because the driving force is activity coefficient that is solely dependent on osmotic concentration. There is little decrease in transmembrane flux with increase of feed concentration but that is very small and it will be considered as negligible.

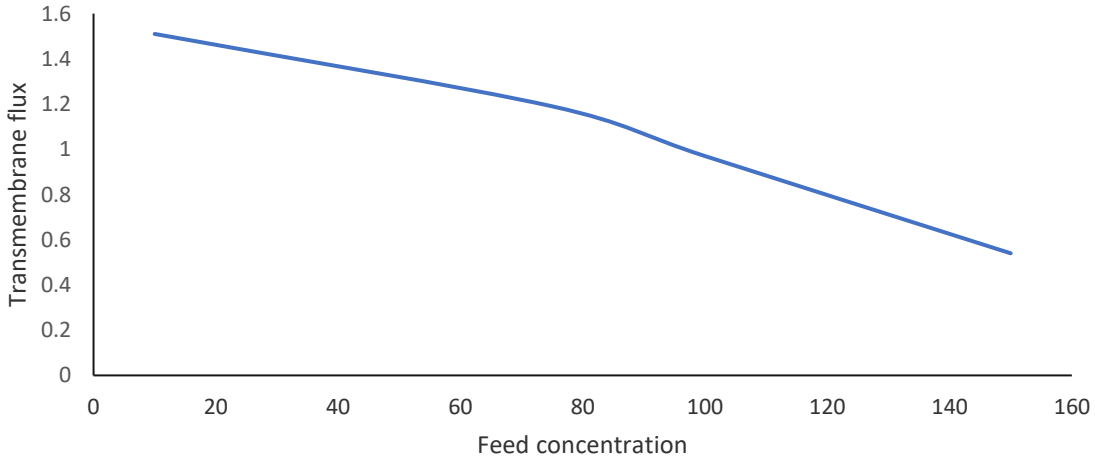

Figure 4. Effect of feed concentration(Na_2So_4) on transmembrane flux

4.3 Concentration of osmotic solution

The transmembrane flux is affected by the change of osmotic concentration as shown in figure 5. It increases with increase of osmotic concentration while it decreases with decrease of osmotic concentration. The great transmembrane flux ensures more transport of water between tube and shell side and as a result maximum crystals are obtained.

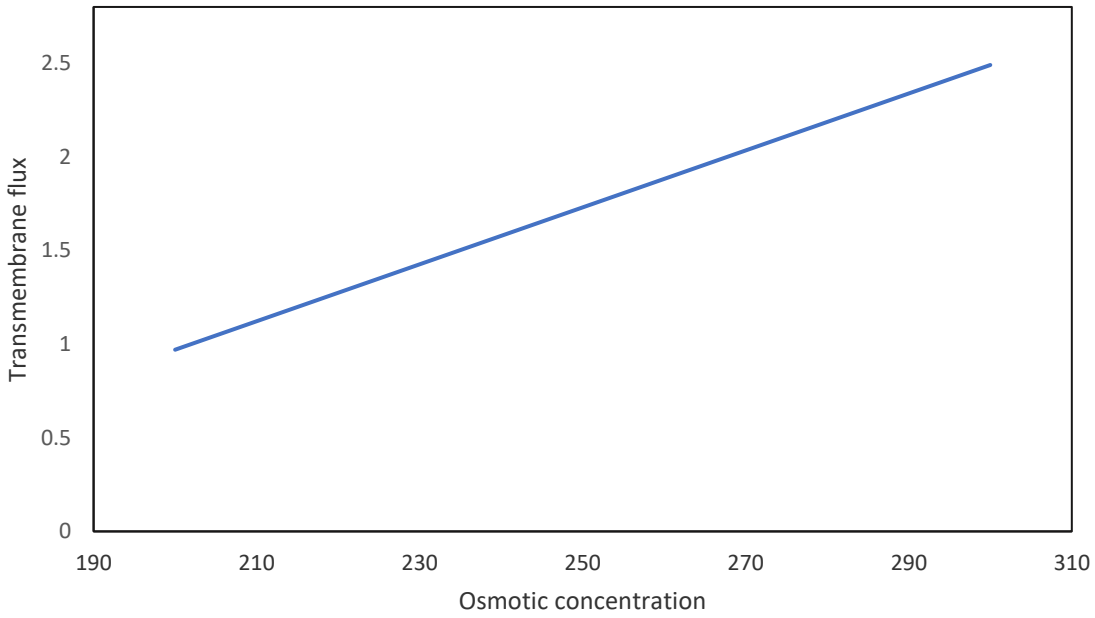

Figure 5. Effect of Osmotic concentration (NaCl) on transmembrane flux

4.4 flow rate of feed

There is no appreciable effect of increase or decrease of flow rate of feed on transmembrane flux as shown in figure 6

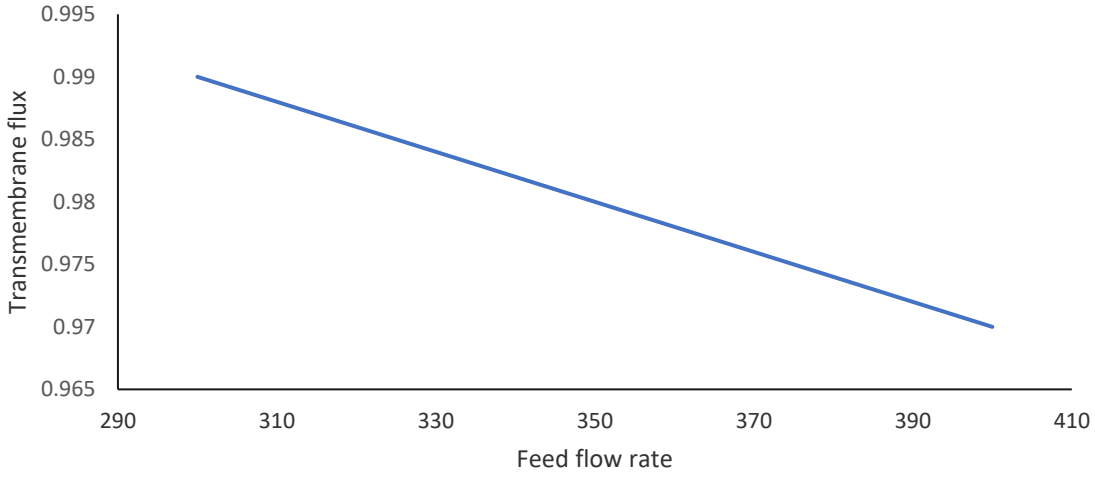

Figure 6. Effect of feed flow rate on transmembrane flux

4.5 Flow rate of osmotic solution

The transmembrane flux is not affected by change in flow rate of osmotic solution. As shown in figure 7.

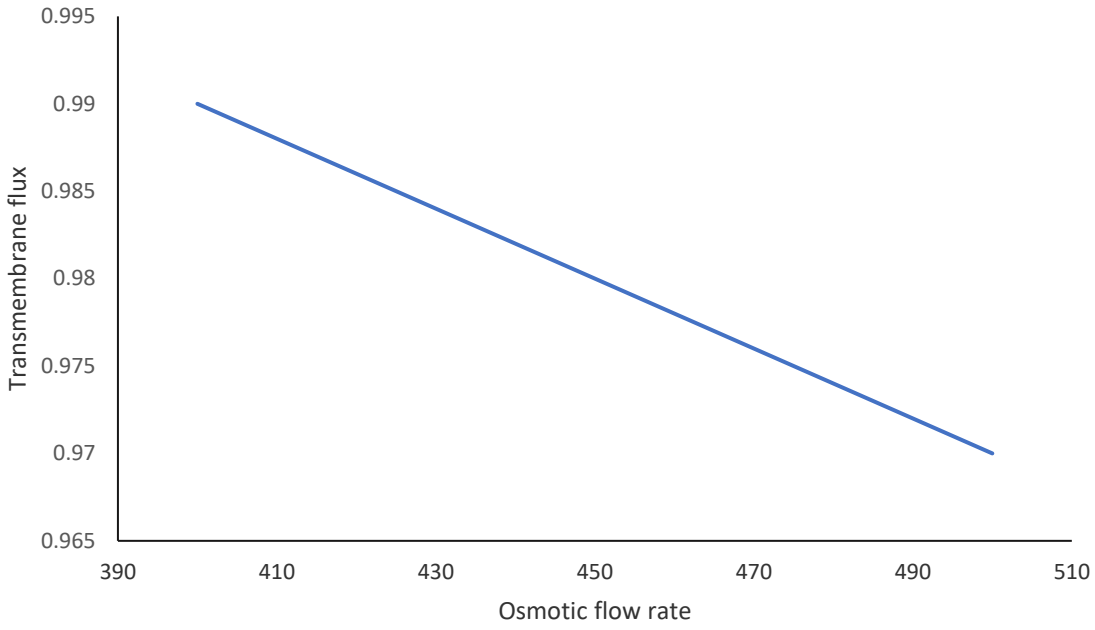

Figure 7. Effect of osmotic flow rate on transmembrane flux

The surface concentration of water in tube, membrane and shell is shown in figure 8 while the graph of overall concentration is shown in figure 9.

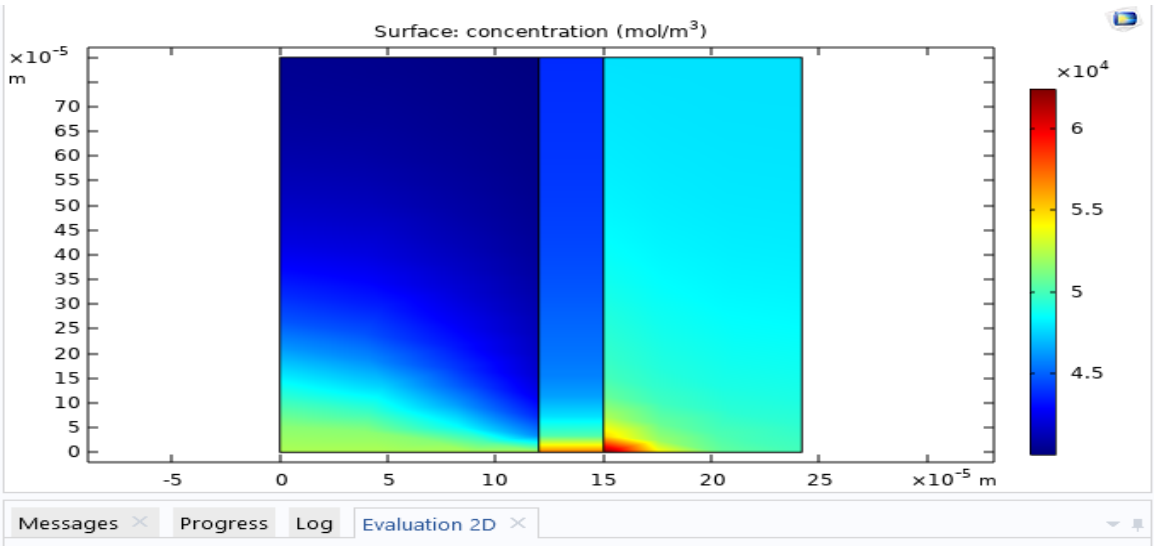

Figure 8. Surface concentration (Image from comsol multiphysics 5.5)

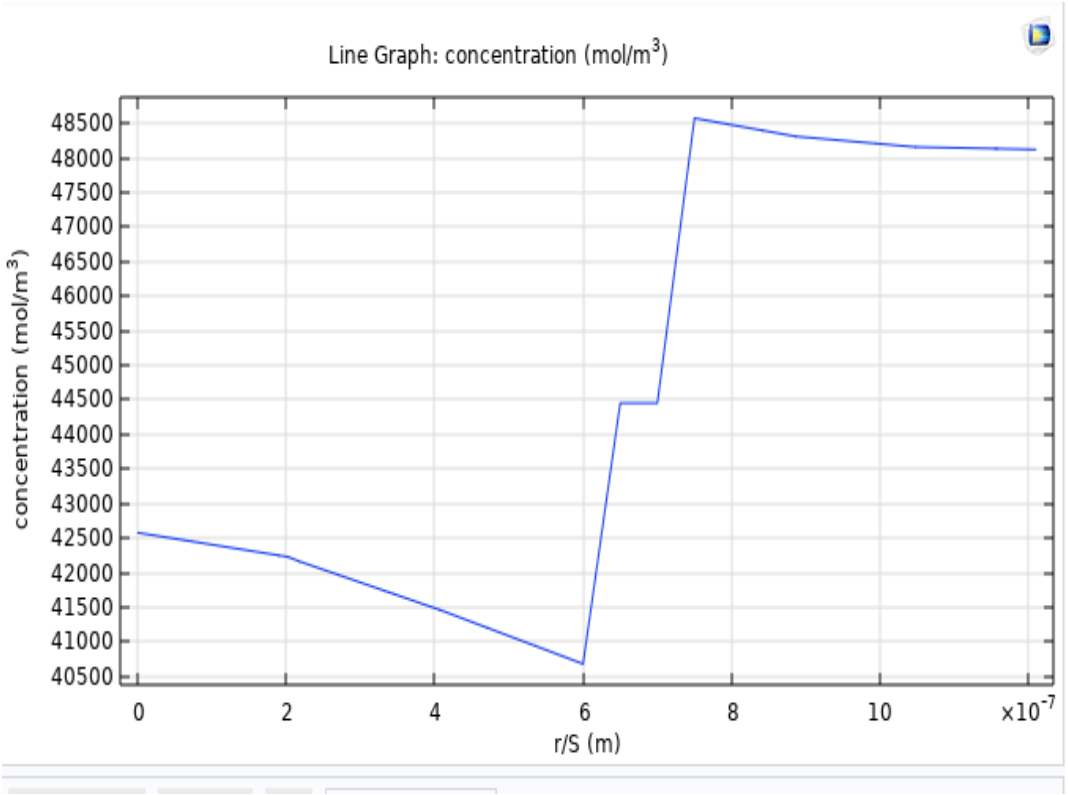

Figure 9. Overall concentration gradient

Conclusions

A great threat to aquatic life is possessed by industrial waste water containing inorganic salts like Na_2So_4. For the survival of aquatic life and utilization of Na_2So_4, its recovery from industrial waste water is must. Due its easy scale up and low energy consumption, membrane distillation crystallization is one the best method for recovery of Na_2So_4 from water expelled by industries as waste. In the contemporary research, a membrane contactor whose fibres were hollow was used to simulate membrane distillation crystallization process. Numerical model is applied to recovery of inorganic soluble salts from aqueous solution with Sodium chloride as osmotic agent in (HFMC). To address the transfer of solute from fiber 's one side (aqueous phase) to fiber 's other side (osmotic phase), convection-diffusion based mass transfer Navier Stokes equations is implemented. The equations are solved numerically in the COMSOL Multiphysics$_{TM}$ software. The transmembrane flux increased with increase of osmotic concentration while increase or decrease of feed concentration and has no appreciable effect. The result were in good agreement with literature

6 References

Ahmad, N. A., Goh, P. S., Yogarathinam, L. T., Zulhairun, A. K., & Ismail, A. F. (2020). Current advances in membrane technologies for produced water desalination. *Desalination, 493*, 114643. https://doi.org/https://doi.org/10.1016/j.desal.2020.114643

Alkaisi, A., Mossad, R., & Sharifian-Barforoush, A. (2017). A Review of the Water Desalination Systems Integrated with Renewable Energy. *Energy Procedia*, *110*, 268-274. https://doi.org/https://doi.org/10.1016/j.egypro.2017.03.138

Alwatban, A., Alshwairekh, A., Alqsair, U., Alghafis, A., & Oztekin, A. (2019). Desalination and Water Treatment Effect of membrane properties and operational parameters on systems for seawater desalination using computational fluid dynamics simulations. *Desalination and water treatment*, *161*, 92-107. https://doi.org/10.5004/dwt.2019.24275

Elimelech, M., & Phillip, W. A. (2011). The Future of Seawater Desalination: Energy, Technology, and the Environment. *Science*, *333*(6043), 712. https://doi.org/10.1126/science.1200488

Fuller, E. N., Schettler, P. D., & Giddings, J. C. (1966). NEW METHOD FOR PREDICTION OF BINARY GAS-PHASE DIFFUSION COEFFICIENTS. *Industrial & Engineering Chemistry*, *58*(5), 18-27. https://doi.org/10.1021/ie50677a007

Marjani, A., & Shirazian, S. (2011). Simulation of heavy metal extraction in membrane contactors using computational fluid dynamics. *Desalination*, *281*, 422-428. https://doi.org/https://doi.org/10.1016/j.desal.2011.08.032

Muhammad, A., Younas, M., & Rezakazemi, M. (2017). Quasi-dynamic modeling of dispersion-free extraction of aroma compounds using hollow fiber membrane contactor. *Chemical Engineering Research and Design*, *127*, 52-61. https://doi.org/https://doi.org/10.1016/j.cherd.2017.09.007

Muhammad, A., Younas, M., & Rezakazemi, M. (2018). CFD simulation of copper(II) extraction with TFA in non-dispersive hollow fiber membrane contactors. *Environmental Science and Pollution Research*, *25*(12), 12053-12063. https://doi.org/10.1007/s11356-018-1282-1

Nemerow, N. L. (2007). *Industrial waste treatment [contemporary practice and vision for the future]*. Elsevier/Butterworth-Heinemann.

Pajonk, A. S., Saurel, R., & Andrieu, J. (2003). Experimental study and modeling of effective NaCl diffusion coefficients values during Emmental cheese brining. *Journal of Food Engineering*, *60*(3), 307-313. https://doi.org/https://doi.org/10.1016/S0260-8774(03)00052-9

Qin, L., Liu, Q., Meng, Q., Fan, Z., He, J., Liu, T., Shen, C., & Zhang, G. (2017). Anoxic oscillating MBR for photosynthetic bacteria harvesting and high salinity wastewater treatment. *Bioresour Technol*, *224*, 69-77. https://doi.org/10.1016/j.biortech.2016.10.067

Razavi, S. M. R., Rezakazemi, M., Albadarin, A. B., & Shirazian, S. (2016). Simulation of CO2 absorption by solution of ammonium ionic liquid in hollow-fiber contactors. *Chemical Engineering and Processing: Process Intensification*, *108*, 27-34. https://doi.org/https://doi.org/10.1016/j.cep.2016.07.001

Rezakazemi, M., Iravaninia, M., Shirazian, S., & Mohammadi, T. (2013). Transient computational fluid dynamics modeling of pervaporation separation of aromatic/aliphatic hydrocarbon mixtures using polymer composite membrane. *Polymer Engineering & Science*, *53*(7), 1494-1501. https://doi.org/https://doi.org/10.1002/pen.23410

Salmón, I. R., Simon, K., Clérin, C., & Luis, P. (2018). Salt Recovery from Wastewater Using Membrane Distillation–Crystallization. *Crystal Growth & Design*, *18*(12), 7275-7285. https://doi.org/10.1021/acs.cgd.8b00580

Shannon, M. A., Bohn, P. W., Elimelech, M., Georgiadis, J. G., Mariñas, B. J., & Mayes, A. M. (2008). Science and technology for water purification in the coming decades. *Nature*, *452*(7185), 301-310. https://doi.org/10.1038/nature06599

Upadhyaya, S., Singh, K., Chaurasia, S., Dohare, R., & Agarwal, M. (2015). Mathematical and CFD modeling of vacuum membrane distillation for desalination. *Desalination and Water Treatment*. https://doi.org/10.1080/19443994.2015.1048306

Younas, M., Druon-Bocquet, S., & Sanchez, J. (2010). Kinetic and dynamic study of liquid–liquid extraction of copper in a HFMC: Experimentation, modeling, and simulation. *AIChE Journal*, *56*(6), 1469-1480. https://doi.org/https://doi.org/10.1002/aic.12076